GSI

Diss. 2009 - 14
November

Radiobiological experiments for carbon ion prostate cancer therapy: Interplay of normal and tumor cells in co-culture and measurement of the oxygen enhancement ratio

Cläre von Neubeck

(Dissertation des Fachbereichs Biologie der Technischen Universität Darmstadt)

Gesellschaft für Schwerionenforschung mbH
Planckstraße 1 · D-64291 Darmstadt · Germany
Postfach 11 05 52 · D-64220 Darmstadt · Germany

GSI Helmholtzzentrum für Schwerionenforschung GmbH
Technische Universität Darmstadt

Radiobiological experiments for carbon ion prostate cancer therapy: Interplay of normal and tumor cells in co-culture and measurement of the oxygen enhancement ratio

Vom Fachbereich Biologie der Technischen Universität Darmstadt

zur

Erlangung des akademischen Grades

eines Doctor rerum naturalium

genehmigte Dissertation von

Dipl.-Ing. Biotechnologie Cläre von Neubeck
aus Frankfurt (Main)

1. Referent: Prof. Dr. Gerhard Thiel
2. Referent: Prof. Dr. Gerhard Kraft

Tag der Einreichung: 31.07.2009

Tag der mündlichen Prüfung: 28.09.2009

Darmstadt 2009
D17

Zusammenfassung

Co-Kultur Systeme sind häufig ein geeignetes Modell um die Reaktion von Geweben *in vitro* zu untersuchen, die bei einer Strahlentherapie notwendigerweise gleichzeitig als Ziel- und Nachbarvolumen exponiert werden. In dieser Arbeit wurde ein Co-Kultur Modell auf Basis von Rattenzellen eines Prostatakarzinoms (Dunning R-3327-AT-1) und des Dünndarmepithels entwickelt um die Bestrahlungssituation eines Prostatakarzinompatienten zu simulieren. Beide Zelllinien wurden in Mono-Kulturen auf ihre Strahlensensitivität gegenüber 250 kVp Röntgen sowie 270 MeV/u, 100 MeV/u und 11.4 MeV/u Kohlenstoffionen untersucht. Aus den Überlebensdaten wurden die Parameter des Linear-Quadratischen Modells, α und β, errechnet und die relative biologische Wirksamkeit (RBW) bestimmt, wobei die RBW_{α} der strahlenresistenteren Prostatakarzinomzellline im Gegensatz zur Dünndarmzelllinie größer war. Der Vergleich von RBW Werten errechnet mit dem *local effect model* (LEM) zeigte sehr gute Übereinstimmungen mit den gemessenen Werten. Die Daten aus Mono-Kulturen wurden verglichen mit Co-Kulturen unbestrahlter und bestrahlter Zellen (250 kVp Röntgen, 100 MeV/u und 11.4 MeV/u Kohlenstoffionen) beider Zelllinien. Die gemessene Synergie in den Co-Kulturen wurde auf bestrahlungsabhängige und -unabhängige Faktoren zurückgeführt. Um diese Effekte zu untersuchen wurde die Sekretion der inflammatorischen Zytokine TGFβ, TNFα und IL-2 gemessen. Es zeigte sich, dass deren Sekretion unabhängig von der Bestrahlung und der Co-Kultur war.

In der Tumortherapie stellen hypoxische Tumorareale aufgrund erhöhter Strahlenresistenz ein Problem dar. Um Zellen unter definierten Sauerstoffbedingungen zu kultivieren und zu bestrahlen wurde eine Kammer entwickelt, in der der Sauerstoffgehalt gezielt reguliert werden kann. In dieser Kammer wurden die Prostatakarzinomzellen unter oxischen und hypoxischen Bedingungen mit Kohlenstoffionen mit einem $\overline{LET}$ von 100 keV/μm bestrahlt. Der Sauerstoffverstärkungsfaktor (OER) wurde für Röntgenbestrahlungen mit OER = 2,35 und für Kohlenstoffionen mit OER = 1,5 bestimmt. Die Ergebnisse der Co-Kultur und der Experimente mit definiertem Sauerstoffgehalt wurden unter dem Gesichtspunkt der Prostatakarzinomtherapie diskutiert.

Summary

Co-culture models are helpful to examine cell to cell interactions *in vitro* and to assess the cross-communication between two particular cell populations. Co-culture systems partially reflect the complex *in vivo* situation: in this study an in vitro co-culture model of prostate cancer cells (Dunning R-3327-AT-1) and small intestine cells (intestinal epithelium cell line 6) of the rat was established to simulate the carbon ion treatment of prostate cancer patients at GSI. Both cell lines were characterized in mono-cultures for their radio-biological response against 250 kVp x-rays and carbon ions of 270 MeV/u, 100 MeV/u, and 11.4 MeV/u, respectively. The parameters of the linear quadratic model, α and β, for cell survival curves were determined as well as the relative biological effectiveness (RBE). The measured RBE values were compared to calculations of the *local effect model* (LEM) and were in agreement to the calculations. The RBE_{α} value increased stronger for the more radio-resistant prostate cancer cell line than for the epithelium cell line. The survival of unirradiated and irradiated cells from co-cultures (250 kVp x-rays; 100 MeV/u and 11.4 MeV/u carbon ions) was compared to mono-cultures under the same conditions. The measured effects were attributed to irradiation independent as well as to irradiation dependent factors. To study these effects, the inflammatory cytokines TGFβ, TNFα, and IL-2 were analyzed, but their secretion was independent of irradiation.
To study the problem of hypoxic cells in tumor treatment a hypoxia chamber was developed in which cells were grown under a defined oxygen status. Prostate cancer cells were irradiated with 250 kVp x-rays and carbon ions with a $\overline{LET}$ of 100 keV/μm under oxic and hypoxic conditions. The oxygen enhancement ratios for 10% survival were found to be OER = 2.35 for x-rays and OER = 1.5 for carbon ions. The results of the co-culture model and the experiments under defined oxygen status are discussed in relation to ongoing prostate cancer therapy.

Contents

1 Introduction

1.1 Objectives

The cancer treatment with heavy ions started at GSI in December 1997. Up to the end of July 2009, 440 patients with chordomas, chondrosarcomas, and adenocystic carcinomas were successfully treated. The five year tumor control rate increased from 30-40% after conventional treatment to values higher than 80% in all these cases [123, 122, 21]. In 2006 a study on locally advanced prostate cancer was started [97]. But for future developments in therapy the number of indications has to be increased and the treatment advantages have to be extended to other tumor types. There are still some unsolved problems in heavy ion radiation therapy. On the basis of prostate cancer, as an example, these unsolved problems can be explained. Prostate cancer patients were irradiated with a combination of intensity modulated radiotherapy (IMRT) at the *Universitätsklinikum Heidelberg* and with six fractions of carbon ion boost irradiation at GSI (active beam scanning). The IMRT delivers the photon dose in many small irradiation fields of different beam directions to achieve a three dimensional tumor conformal overlapping dose. The carbon ions are delivered in only two opposing fields without reducing the delivered dose in the tumor volume. Since the prostate is a deep-seated organ, both methods irradiate healthy tissue and including parts of the radio-sensitive organs like the rectum and bladder. Due to the greater precision carbon ion irradiation excludes more healthy tissue than the IMRT irradiation which protects the normal tissue sufficiently. For carbon ion therapy in Japan (passive beam control) side effects like inflammatory reactions in the co-irradiated organs are published [134, 66, 137] and reduce the maximal deliverable dose to the tumor. A better comprehension of the healthy tissue reaction alone and in combination with prostate cancer cells could help to reduce side effects, to medicate the inflammation or to enhance the deliverable dose to the tumor.

In a first reaction to these problems it was planned to establish an *in vitro* co-culture system of prostate cancer cells and normal cells of the surrounding tissue to simulate the patient treatment situation and to analyze tissue reactions.

The questions raised were:

- ➢ How is the survival of irradiated tumor cells influenced by **normal** cells (irradiated / unirradiated)?
- ➢ How is the survival of irradiated or unirradiated normal cells influenced by **tumor** cells (irradiated / unirradiated)?
- ➢ Which biochemical substances mediate the influence on the survival?
- ➢ Are there different reactions between cells irradiated with carbon ions or x-rays?

A common feature of prostate tumors is that they are poorly oxygenated tissue which is more radio-resistant [89]. Furthermore, hypoxia has been correlated with local tumor recurrences [131] and consequently with a poor prognosis [89]. Due to the oxygen effect the hypoxic tissue is more radio-resistant than well oxygenated tissue. By using high LET carbon ions the oxygen effect is reduced [52]. For carbon ion irradiation with mixed LET the oxygen effect is unclear. If it were possible to deactivate all hypoxic cells more efficiently, the poor prognosis in terms of local recurrences would be revised. Therefore, more biological data of hypoxic cells are needed to improve the treatment planning system.

The second intention of this thesis was to develop a measurement system for hypoxic cells which fulfills the following criteria:

- ➢ adjustable and defined oxygen status of the cells,
- ➢ measurable acute and chronic hypoxia, and
- ➢ suitable for photon and carbon ion irradiation.

With this system, the oxygen enhancement ratio for x-ray and carbon ion irradiation should be measured.

1.2 Physical properties of ionizing radiation and radio-biological fundamentals

The depth dose profiles of photons and carbon ions differ because of their physical properties (see figure 1.1). Concerning therapy conditions carbon ions have a better dose distribution than photons i.e. a better tumor conformity can be reached. Sparsely ionizing radiation like photons deposits its energy via photo effect, *Compton*-process, and pair production. The resulting secondary electrons of high energy photons are preferentially scattered forward. This shifts the maximum energy deposition profile of photons to higher

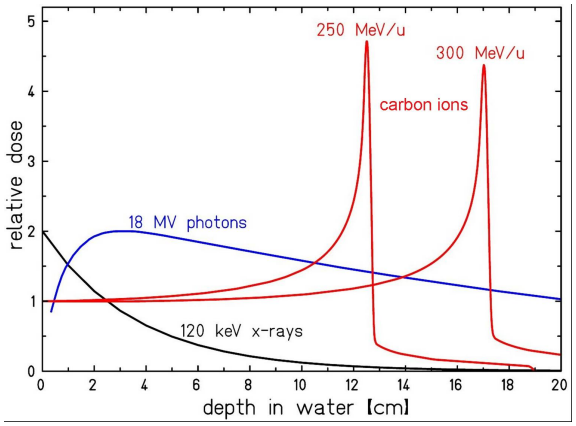

Figure 1.1: The relative dose distribution for x-rays, photons and carbon ions with depth in water. Courtesy of U. Weber.

depths, but after a few centimeters the depth dose profile decreases exponentially. In contrast, particle irradiation like protons or carbon ions exhibits an inverse depth dose profile. The energy deposition increases slowly with depth to a sharp maximum, the Bragg-peak. The deposited energy along the covered distance is defined as the linear energy transfer (LET).

$$LET = \frac{dE}{dx} \tag{1.1}$$

Equation 1.2 shows the relation between LET [keV/μm], dose D [Gy], fluence F [cm^{-2}], and density of the irradiated material ρ [cm^3/g]

$$D = 1.6 \cdot 10^{-9} \cdot F \cdot LET \cdot \rho^{-1}, \tag{1.2}$$

where the numeric factor accounts for the conversion of the units as given above. The biological effect of sparsely and densely ionized radiation differs. The relative biological effectiveness (RBE) allows a comparison between the two beam qualities. The RBE is the ratio of a standard radiation dose to a test radiation dose which induces the same biological effect (see Eq. 1.3).

$$RBE = \left.\frac{D_{\mathrm{x-ray}}}{D_{\mathrm{ion}}}\right|_{\mathrm{isoeffect}} \tag{1.3}$$

Figure 1.2 illustrates the RBE with two typical survival curves of sparsely (x-rays) and densely (carbon ions) ionizing radiation. The cellular survival after x-ray irradiation follows a shoulder curve which can be described with Eq. 1.4.

$$S = S_0 \cdot e^{-\alpha D - \beta D^2} \tag{1.4}$$

Here is S_0 and S the survival before and after the irradiation, respectively, α (Gy^{-1}) the initial slope, and β (Gy^{-2}) the curvature of the linear quadratic survival curve. The shouldered shape results from repairable damages in the low dose area (α value is dominant). The accumulation of lesions leads to irreparable complex damages for higher doses (β value is dominant). The ratio of α and β is characteristic for a cell line and is a parameter for radio-sensitivity. A pronounced shoulder corresponds to a high radio-resistance and a small α/β ratio.

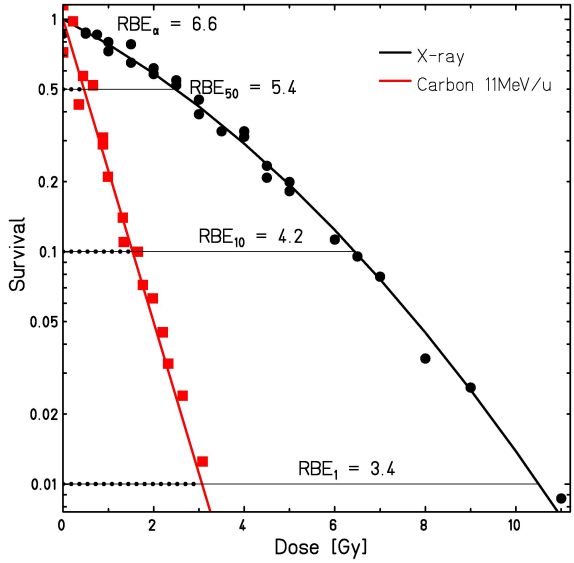

Figure 1.2: Relative biological effectiveness of 11.4 MeV/u carbon ions compared to 250 kVp x-ray irradiation, Courtesy of W. K.-Weyrather.

The cell survival after ion irradiation with high energy deposition values follows an exponential decline with increasing doses (LET > 100 keV/μm). The high LET of ions induces complex and mostly lethal damages in the cell. If the repair capacity of the cell is over strained, the term (βD^2) converges to zero. The cell inactivation or the mitotic death of cells after irradiation can be determined in a colony forming assay [104].

Figure 1.2 shows the RBE_α which is given by the ratio of the initials slop α in the limit of vanishing dose,

$$RBE_\alpha = \frac{\alpha_{\mathrm{ion}}}{\alpha_{\mathrm{x-ray}}}. \tag{1.5}$$

For cancer therapy with carbon ions at GSI the RBE is calculated with the local effect model (LEM; [120, 33]). The model includes three central ingredients which reveal the

RBE characteristics: a) the target size, e.g. size of the cell nucleus, b) track structure of the ions used, since the RBE is particle dependent, and c) x-ray survival curve of used cell type, since the RBE is cell type dependent. It is not possible to determine the RBE values for patient treatment. So the LEM calculation is needed for each voxel of the target volume. For the RBE calculation of patient treatment the data of photon radiotherapy are used to calculate the corresponding clinical data instead of cell RBE values. The physical optimization of the treatment plan is done with the treatment planning software TRiP98 [78]. The carbon ion beam is controlled with this optimized plan and scans over the tumor volume. For more details see Haberer *et al.* [50].

The beam absorption in the tissue leads to the production of radicals. Hall postulated that the radicals react with the surrounding molecules e.g. with the DNA. In the presence of oxygen the DNA radicals react with oxygen molecules to peroxides, and the lesion in the DNA is fixed. In the absence of oxygen (hypoxia) no fixation of the DNA damages with oxygen takes place. The free DNA ends could be realigned which, in consequence, increased the cell survival [52]. This theory is under discussion, and the real mechanism might be more complex. The damages in the DNA are of special interest since Munro identified the cell nucleus as the most sensitive target in the cell [93].

The cellular survival under hypoxic conditions is increased. The ratio of a dose under hypoxic to a dose under oxic conditions which induces the same biological effect is defined as the oxygen enhancement ratio (OER).

$$OER = \left.\frac{D_{\text{hypoxic}}}{D_{\text{oxic}}}\right|_{\text{isoeffect}} \tag{1.6}$$

In contrast to the RBE, the oxygen effect seems to enhance the survival by a constant factor independent from survival level. Depending on the cell line and the oxygen status the enhancement factor is in the range of one to three, whereas a tissue supply of $\leq 3\%$ oxygen is sufficient for the occurence of the full oxygen effect [52]. In radiotherapy the oxygen effect is of great importance since some tumors show large hypoxic areas, e.g. prostate tumors [89]. Due to the OER these hypoxic areas are more radio-resistant to sparsely ionizing radiation. The OER is LET dependent. The higher the LET the smaller is the enhancement factor and the OER converges to one. By the use of densely ionizing radiation like carbon ions the OER can be reduced. Therefore, particle therapy is well suited to effectively inactivate hypoxic cells. Furthermore, the cellular response to radiation depends on the exposure length to hypoxic conditions. It is reported that the radio-sensitivity of chronically hypoxic cells is reduced to 30% compared to acute hypoxic cells [89].

1.3 The prostate and its cancers

The prostate together with the testes, the epididymis, and the seminal vesicles form the inner genitals of the man. The prostate adjoins cranial to the bladder and dorsal to the rectum. The chestnut shaped and sized organ encloses the beginning of the urethra. The tubuloalveolar exocrine gland is composed of thirty to fifty single glands with excretory ducts into the urethra. The glands are surrounded by smooth muscle cells and connective tissue. The prostate is externally bordered by a connective tissue capsule and can be classified in histological zones: peripheral (70-75% of gland mass), central (25-30% of gland mass), periurethral, transition, and anterior fibro-muscular (no glands) zone. Prostate cancer develops in most cases in the peripheral zone [85, 91].
The prostate carcinoma is the most frequently occuring cancer for men in Germany and responsible for 10% of cancer related death per year. The risk of prostate cancer increases with age and 90% of the patients are older than 60. The important diagnostic procedures are digital rectal palpation, serum level of prostate specific antigen (PSA), sonography, and punch biopsy [113].
Prostate carcinomas can pathologically be divided into four categories: latent (undetected in life, autopsy), incidental (not detectable with clinical diagnostic, incidentally discovered, T1), occult (primary tumor not detected, metastases induced finding), and clinical prostate cancer (assured diagnosis, T2-T4). 95% of the tumors are adenocarcinomas whereas urothelial or squamous cell carcinomas as well as sarcomas appear rarely. The aggressiveness of prostate cancer is evaluated with Gleason scoring (factor 2-10). With this the differentiation pattern of the cell structures are judged [34]. In addition, different morphological growth patterns (cribriform, anaplastic, well and poorly differentiated glandular) can be found [10]. The tumor classification is performed according to the TNM system of the international union against cancer which differentiates between primary **T**umor, regional lymph **N**ode and distant **M**etastasis (see table 1.1). Prostate cancer metastasizes first into the lymph nodes of the pelvis minor and later, metastases can be found in the bones, liver, and lung. The therapeutical procedure depends on the tumor state. A *wait-and-see* strategy with controls is used in state *I* while in state *II*, a curative approach, (radiotherapy, hormone-therapy) or surgery can be chosen. For state *III* no therapeutically guideline exists (all therapy forms except chemotherapy), and in state *IV* a systemic therapy of hormone-, chemo- and pain-therapy is suggested [34].
However, the method of cancer treatment has to comply with the general condition and the expected life span of the patient, the severity of the illness, and the expected side effects of the treatment. For radiotherapy two methods are used. Method one, the brachytherapy applies irradiant materials directly into the prostate while the IMRT, the second method

Table 1.1: Prostate cancer classification according to the international union against cancer, excerpt of TMN system [34]

State	Category	Definition
	TX	primary tumor not rateable
	T0	no indication for primary tumor
I - II	T1a-c	incidentally detected tumor
II	T2	tumor only in prostate (one lope T2a, both lopes T2b)
III	T3	tumor with capsular penetration (external expansion T3a, seminal vesicle infiltration T3b)
. IV	T4	tumor is fixed and/or infiltrating other structures
	NX	regional lymph node not rateable
	N0	no lymph node metastases
	N1	regional lymph node metastases
	MX	distant metastases not rateable
	M0	no distant metastases
	M1	distant metastases (other lymph nodes M1a, bones M1b, rest of the body M1c)

irradiates externally in three dimensional conformal manner. The primary side effects in both cases are impotence, incontinence, and intestinal disorders [113].

1.3.1 Dunning prostate cancer cell system

The original adenocarcinoma was discovered by Dunning in the dorsal lope of the prostate of a male Copenhagen rat (*rattus norvegicus*) in 1961 and was named R-3327. Parts of the tumor were supplied to other institutes, and over the years several sub-lines were developed with different characteristics. The genealogy of the R-3327 rat prostate cancer is presented in reference [64]. In this thesis the sub-line R-3327-AT-1 (RAT-1) is used which occurred at John Hopkins Oncology Center in 1976. RAT-1 cells form *in vivo* a fast growing, androgen- and estrogen-insensitive, and anaplastic tumor with a low metastatic ability [65]. Anaplasia is characterized by the loss of structural and functional differentiation of normal cells [34] and is histological graded with five (Gleason) [20]. *In vitro* the cell doubling time is 32.5 $\pm$ 3.7 h and the plating efficiency (PE) is 16.7 $\pm$ 0.9%. The mean chromosome number was determined with 60 $\pm$ 7 [65]. The normal rat karyotype for *rattus norvegicus* is 42 (2n) which means that RAT-1 cells have an aneuloid chromosome

number. Aneuploidy (condition under which a cell has missing or extra chromosomes) can occur with two principle mechanisms: chromosome loss and non-disjunction. A complete chromosome can get lost if the kinetochore of the chromosome is not attached to the spindle fiber. During anaphase the chromosome is therefore not moved to the poles of the dividing cell nucleus. The membrane formation in the end of the meiosis excludes the chromosome from the daughter cells, and the formation of a micronucleus is possible. Non-disjunction describes the failure in division of the sister chromatids in the beginning of the anaphase. Thereby, a hyperploid (1n + x) and a hypoploid (1n - x) daughter cell develops.
The RAT-1 cells grow *in vivo* to larger tumors whereas the smaller tumors are significantly less hypoxic. But even large tumors do not form a central necrosis. The better oxygenated tumors show an enhanced response to radiation when the cells were irradiated with a single dose of 30 Gy of 4 MV x-rays [12]. Furthermore, RAT-1 cell tumors are known to be moderately radio-resistant [101].

1.4 The intestine and radiation side effects

The upper intestine is comprised by the mouth, pharynx, esophagus, and stomach. The lower gastrointestinal tract consists of the small intestine which has three parts (duodenum, jejunum, ileum). The large intestine has three parts as well: cecum with appendix, colon (ascending, transverse, descending colon, sigmoid flexure), and rectum. The general structure of the intestinal wall is from outwards to inwards composed of a serosa, a longitudinal muscle layer, a circular muscle layer, a sub-mucosa, and a mucosa. The mucosa of the small intestine is folded and covered with finger shaped and 1 mm high villi. The villi surface is comprised out of absorbing epithelium cells [30]. The intestinal epithelial cells (IEC) have three essential functions: a) nutrient uptake, b) immunological defense, and c) forming a barrier. The barrier are the cells themselves through tight junction sealing (zonula occludens) and mucus (glycocalyx) secretion [19]. The IECs desquamate at the villus tips [102] and are replaced by undifferentiated stem cells from the proliferous zone within the crypts [99]. A complete cell exchange corresponds to the functional lifetime of a epithelial cell which is e.g. *in vivo* for murine differentiated epithelial cells five to ten days [121].
Independent from the type of radiotherapy, in prostate cancer treatment the surrounding normal tissue (intestine, bladder, urethra) is partly co-irradiated and shows dose dependent side effects. Tissues with a high proliferating rate such as intestinal mucosa are most sensitive to ionizing radiation and have the greatest risk of injury. The radiation-induced gastrointestinal syndrome is an acute reaction to radiation and is characterized through a

massive depletion of intestinal epithelium cells, disorders of fluids, and solute transports. The rate of apoptosis in murine epithelial crypt cells after irradiation was found to be higher than that in the villi and showed a saturated dose response at approximately 1 Gy of photons [127, 121]. These results are supported by a report of beginning changes in the human intestinal epithelium after irradiation with 1-2 Gy of photons [34]. Long-term complications in the intestine can be the manifestation of progressive vasculitis, enteritis, and fibrosis [127]. Prostate cancer treatment with carbon ions at the heavy ion medical accelerator in Chiba, Japan (passive beam control) [134], delivered a total dose of 66.0 Gy (RBE, Japan) in 20 fractions over five weeks. The patients developed side effects with grade *I* (17.3%) and grade *II* (2.7%) complications in the rectum. In a second study the dose was reduced to 57.6 Gy (RBE, Japan) in 16 fractions over 4 weeks. The side effects could be limited with this method to grade *I* (10.3%) and grade *II* (1.1%) complications in the rectum.

1.4.1 Intestinal epithelium cell line 6

The intestinal epithelial cell line 6 (IEC-6) originated from the intestinal crypt cells of a rat, as judged by morphological and immunological criteria. As described by Quaroni *et al.* the cells are non-tumorigenic and retain the undifferentiated character of intestinal epithelial stem cells [106]. For the cell line a stable karyotype of 42 chromosomes, a constant population doubling time of 20 h (19-22h) which tends to decrease with age, and a PE of 2.3% were determined. The life span of the cells is limited to 30-40 passages while the morphology is stable [106]. The IEC-6 cells are used for a wide range of experiments and are well characterized in literature. Wroblewski *et al.* analyzed the radiation effect *in vivo* in rats and *in vitro* with IEC-6 cells. They concluded that the observed effects in crypt cells *in vivo* were identical to the effects in the IEC-6 cell line [147]. This conclusion makes the IEC-6 cell line suitable for side effect investigation. In addition, IEC-6 cells are a common model for normal human intestinal epithelial biology [138].

1.5 Cytokines

Inflammatory cytokines can be divided into two groups according to their involvement in the inflammatory response: cytokines promoting acute versus chronic inflammation. Important cytokines for the acute reaction are interleukin (IL)-1, IL-6, IL-8, IL-11, and **TNF**α. The chronic inflammation can be subdivided into cytokines mediating humoral responses (IL-4, IL-5, IL-6, IL-7, IL-13) and cytokines which mediate cellular responses

(IL-1, **IL-2**, IL-3, IL-4, IL-7, IL-9, IL-10, IL-12, interferons, **TGF**β, **TNF**α, TNFβ). Most cytokines are multifunctional and pleiotropic which means that they elicit their effect locally or systemically in an autocrine or paracrine manner [35]. In this thesis the cytokines IL-2, TNFα, and TGFβ were analyzed. The decision to analyze TGFβ, TNFα, and IL-2 was motivated by the results of the co-culture survival experiments and the published effects of the cytokines on prostate and intestinal epithelium tissue. Under subsection 4.3.4 the decision is discussed in detail. In the following the current knowledge about the three cytokines will be presented in general and in context to the used cell lines (rat anaplastic prostate cancer cells, rat intestinal epithelium crypt cells) in particular.

TGFβ signaling pathway

Independent of the induced regulatory effect the TGFβ signaling pathway is conserved from flies to humans. The three isoforms of TGFβ (1-3, 25 kDa homodimer) are synthesized as pro-hormones in the cell and are converted into bioactive molecules in the extracellular matrix [98, 25]. The effect of TGFβ-1 and TGFβ-3 is mediated through the receptors RI (53 kDa) and RII (70 kDa). Both are transmembrane serine/threonine kinase receptors at the cell membrane that induce a phosphorylation after TGFβ binding [7, 145]. TGFβ-2 needs the interaction with betaglycan, which is formally called RIII, to be delivered to RII [25]. The primary intracellular effectors of TGFβ signals are SMAD-2 and SMAD-3 which displace the activation via interactions with SMAD-4 and nucleoporins from the membrane into the nucleus. In the cytosol SMAD-proteins activate caspase-1, an apoptosis initiation factor, while in the nucleus the activation of several transcription factors is triggered [112, 25].

TGFβ activation

TGFβ is stored in its latent form in extracellular reservoirs in an abundant manner and needs to be activated. Ionizing radiation induces the formation of reactive oxygen species (ROS). It could be shown that ROS are responsible for the dose dependent activation of TGFβ after irradiation [2]. The inhibition of active TGFβ leads to inhibition of autophosphorylation of the nuclear protein kinase ATM (ataxia telangiectasia mutated). ATM is one of the first and central proteins to respond to DNA damage. The absence of TGFβ-ATM interactions increased the radio-sensitivity of e.g. epithelial cells [2].

TGFβ signaling in prostate tissue

Growth factors which affect the prostate can be divided into three categories: positive

growth factors stimulate proliferation and growth; negative growth factors inhibit growth and promote apoptosis while angiogenic factors stimulate vascular formation. It is controversial as to which category TGFβ belongs. Reynolds and Kyprianou suggest the category negative growth factor since TGFβ is released from the stromal cells in the prostate in a paracrine manner and induce in the prostatic epithelial cells growth inhibition and apoptosis [112]. In contrast, Tomlinson *et al.* reported that the inhibitory effect of TGFβ-1 depends on the differentiation status of the target cells. Undifferentiated cells in the prostate periphery (distal to urethra) are stimulated in their proliferation while the highly differentiated cells in the center (proximal to urethra) of the organ are inhibited [133]. Lee *et al.* consider TGFβ-1 to be a pleiotropic growth factor that inhibits proliferation and induces cell death in normal prostatic epithelial and stromal cells from rodents and humans. Furthermore, they reported that a low concentration of TGFβ-1 increases proliferation of prostatic cells [83]. According to Wikström *et al.* TGFβ inhibits the proliferation of epithelial cells and induces apoptosis in a normal rat prostate [145].
The expression of TGFβ in prostate tumors tends to be increased. The inhibitory growth effect of TGFβ is mediated via the TGFβRII. With ongoing tumor progression the expression of TGFβRII is decreased which might enhance the aggressive potential of the tumor [112]. The Dunning R3327 rat prostatic adenocarcinoma cell system seems to acquire a resistance to TGFβ mediated growth inhibition with tumor progression [145]. But the RAT-1 cell line was found *in vivo* and *in vitro* to express in both cases elevated TGFβ-1, TGFβRI and TGFβRII mRNA levels compared to normal dorsal prostate tissue [145].

TGFβ signaling in intestine tissue

In *in vivo* intestine the highest TGFβ mRNA levels can be found in the crypt cells. Here TGFβ promotes intestinal epithelial restitution and inhibition of proliferation after intestinal wounding e.g. enhanced cell death after radiotherapy. Restitution is *in vivo* independent of proliferation and involves the migration of viable epithelial cell from the edges of the injured area to cover the exposed area. These effects can be studied in a wound healing model based on IEC-6 cell monolayer. The TGFβ expression in the IEC-6 cell line is regulated by an autocrine mechanism, and TGFβ prevents the down regulation of extracellular matrix transcripts which are needed for restitution [102]. Furthermore, TGFβ inhibits the DNA synthesis in IEC-6 cells [149] and has only small effects on epithelial differentiation [99]. The production of TGFβ is enhanced by IL-2 which also promotes cell migration *in vitro*. Podolsky concluded that cytokines expressed in the intestinal mucosa promote epithelial restitution after mucosa injury through increased production of activated TGFβ-1 in epithelial cells [102].

TNFα signaling pathway

The pro-inflammatory cytokine TNFα (17 kDa) is mostly produced by T-lymphocytes and macrophages in a membrane-bound or in a soluble form. The effect of TNFα is mediated via two receptor complexes (TNFRI and TNFRII) [68]. In the following the receptor complex binds to the proteins TNF receptor associated death domain which activates the TNF receptor associated factor 2. From here three pathways are possible. Two of them activate the nuclear factor NF-κB which promotes survival factors such as bcl-2, an anti-apoptotic protein. The third pathway, phosphorylates activator protein-1, stimulates apoptosis [115].

TNFα signaling in prostate tissue

The effect of TNFα on cell survival and proliferation differs from *in vivo* to *in vitro* studies, while the species plays an important role as well. In a prostate cancer patient study it was observed that the TNFα level increased with severity of illness [6]. The expression of TNFα and both receptors are increased in epithelial cells of prostate cancer [115], too. But the cell proliferation in prostate cancer is enhanced since the pro-apoptotic way of TNFα is inhibited by p21 and the signal regulating kinase ASK1 [115]. In humans prostate cancer cell line LNCaP increased the numbers of apoptotic cells after treatment with 40 ng/ml TNFα which is in contrast to the *in vivo* results [73]. *In vivo* experiments on a rat Dunning sub-line, intra-tumor injections of TNFα resulted in a slower tumor growth in comparison to untreated control animals [125]. However, *in vitro* experiments with the same cell line and TNFα treatment had no significant effect on colony formation [135], which means no effect on cell survival or growth. The Dunning sub-line RAT-1, which is used in this thesis, was not involved in this study. It is expected that TNFα can have a positive or negative effect on RAT-1 cell proliferation.

TNFα signaling in intestine tissue

The intestinal mucosa produces and secrets TNFα [102]. Under inflammatory conditions the density of mucosa cells increases significantly and produces TNFα, IL-2 and IL-6 [149]. IEC-6 cells are part of the intestinal mucosa. The IEC-6 cells are able to secret TNFα which was demonstrated with lipopolysaccharides stimulation (LPS) [87]. The effect of TNFα on IEC-6 cells has been studied by Zachrisson *et al.*. The DNA synthesis of IEC-6 cells was enhanced in a dose-dependent manner after treatment with 0.57 x 10^{-9}- 10^{-11} M TNFα. This was associated with increased cell proliferation [149]. Higher proliferation activity was exhibited by IEC-6 cells after TNFα or IL-1β stimulation was compared to untreated controls. Both cytokines together suppressed IEC-6 cell prolifera-

tion by an unknown mechanism [90].

IL-2 signaling pathway

Il-2 (14-17 kDa) is the major growth factor for activated T-lymphocytes [79]. Beside activated T-lymphocytes, other normal and tumor cells are found to express and secret IL-2 as well [110]. The receptor complex (IL-2R) consists of a β- and a γ-chain and has an intermediate affinity to IL-2. Therefore, the cells react only on higher IL-2 concentrations. Through binding of an α-chain to the β- and γ-chains, a receptor with high affinity to IL-2 is formed [68]. The IL-2 effect is mainly mediated through tyrosine kinases which stimulates gene expression [79]. IL-2 seems to mediate the cell cycle progression in tumor cells via the CDK inhibitor p27 [110].

IL-2 signaling in prostate tissue

In a prostate cancer patient study it was reported that stage *II* and *III* tumors have slightly increased IL-2 levels. In stage *IV* tumors the IL-2 levels decrease dramatically due to the degradation of the immune system [6]. Royuela *et al.* analyzed the presence of IL-2 and its receptor in human prostate cancer and preliminary stages. A highly increased expression of IL-2 and its receptor was found in cells of prostate cancer compared to normal prostate tissue [114]. In general, the receptor IL-2R α-chain has been found to be overexpressed in all prostate cancer stages which corresponds to increased proliferation, drug resistance, transforming activities, and anti-apoptotic protein expression [79]. In human prostate cancer cell lines a correlation between androgen-sensitivity and growth in response to IL-2 was found: androgen-sensitive cell lines showed enhanced proliferation while androgen-insensitive cells were not effected [57]. There are several studies showing *in vivo* an inhibitory growth effect of IL-2 to the Dunning prostate cancer system in general and to the androgen-insensitive RAT-1 in particular [54, 53, 55, 70, 71]. For a combined treatment of IL-2 and irradiation (6 MV x-rays, total dose of 18 Gy in 3 fraction), tumor growth was more efficiently reduced than by irradiation alone [71]. These results demonstrate that conclusions based on observations made in patients or human cell lines are not transferable to the Dunning system.

IL-2 signaling in intestine tissue

The IEC-6 cell line of the rat is a model for normal human intestinal epithelium [138]. The cell line has a functional IL-2 receptor [102] and is able to secret IL-2 which was shown with LPS stimulation [87]. In addition, IL-2 enhances the proliferation of IEC-6 cells [126]. IL-2 treatment combined with radiation (4 Gy, fast neutron or 4, 8, 12 Gy γ

rays) increased the proliferation of irradiated IEC-6 cells and induced enhanced expression of IL2-R β-chain [37, 38].

Summary

It is confirmed by published data that both used cell lines (RAT-1 cells and IEC-6 cells) have functional TGFβ receptors and are able to secret TGFβ. Moreover, the IEC-6 cells express IL-2 and TNFα as well as the corresponding receptors. The three chosen cytokines should cover acute and chronic inflammatory response which are expected to be observed after irradiation.

2 Materials and methods

2.1 Cell lines and culture conditions

2.1.1 Dunning R-3327-AT-1

In this work the sub-line R-3327-AT-1 (RAT-1) of the Dunning prostate cancer cell system was used. The cell line was obtained from ATCC (No. JHU-29) in passage 31 (P31), propagated, and stored in liquid nitrogen (P35). The cells were cultured in Roswell Park Memorial Institute medium (RPMI) supplemented with 10% FCS and 100 U/ml penicillin/100 μg/ml streptomycin (all Biochrom AG, Berlin, Germany) in 95% humidified air at 37 °C and 5% CO_2. The passage was done weekly with 5 x 10^5 cells in 75 cm^2 culture flasks with 15 ml culture medium. Therefore, the cell layer was flushed with 1.5 ml of trypsin-EDTA-solution (0.05% trypsin, 0.1% EDTA, Pan, Aidenbach, Germany) and incubated with 3.0 ml fresh trypsin-EDTA-solution for 4 min in the incubator. The trypsin reaction was stopped by adding 10 ml culture medium. The cells were separated and counted with an electronic particle size analyzer (Z2 Coulter Counter, Beckmann Coulter, Krefeld, Germany) within the limits 9-26 μm before the cells were reseeded in desired dilutions or numbers.

2.1.2 Intestinal epithelium cell line 6

The intestinal epithelium cell line 6 (IEC-6) was isolated from a male rat (*rattus norvegicus*) and was established by Quaroni *et al.*. They suggested that IEC-6 cells are undifferentiated small intestine crypt cells. The cells were obtained from ATCC (No. CRL-1592) in passage (P) 13, were propagated, and long term stored in several vessels in liquid nitrogen (P15). For cultivation the cells were grown in Dulbecco´s modified Eagle medium (DMEM) supplemented with 10% FCS, 50 U/ml penicillin/50 μg/ml streptomycin (all Biochrom AG, Berlin, Germany), and 4.5 μg/ml insulin from bovine pancreas (Sigma Aldrich, Germany) in 95% humidified air at 37 °C and 10% CO_2. The cells were passaged weekly with 3-4 x 10^5 cells in 75 cm^2 culture flasks with 15 ml culture medium. Therefore, the cell layer was flushed with 1.5 ml of trypsin-EDTA-solution (0.25% trypsin, 0.02% EDTA, Pan, Aidenbach, Germany) and incubated with 3 ml fresh trypsin-EDTA-solution for 7 min in the incubator. The trypsin reaction was stopped by adding 10 ml

culture medium. The cells were separated and counted with an electronic particle size analyzer (Z2 Coulter Counter, Beckmann Coulter, Krefeld, Germany) within the limits 9-18 μm before the cells were reseeded in desired dilutions or numbers.
To isolate clones from the IEC-6 population, the cells were seeded in 96-well plates with a cell density of one cell/well in 200 μl medium. The fresh culture medium was mixed with one-third of "old" culture medium from a passage to enhance the growth conditions of the cells. A medium filtration was not performed, since no viable IEC-6 cells detach and float in the medium. After one week every well of a 96-well plate was controlled for colonies. Only from wells with definitely one colony were the cells trypsinized and transferred into 12.5 cm^2 culture flasks for continuing cultivation. The clones were propagated, the chromosome number was determined, and the clones were stored in liquid nitrogen. After defrosting, the clones were weekly passaged. The total cell number of the passage was determined, added to the total cell number of the week before, and plotted against the passage number. The slop of the linear fit could be considered as a "doubling time" and allows a comparison of growth rates.

2.1.3 Co-culture

For co-culture experiments both cell lines had to grow in the same cell culture medium. Therefore, the growth of IEC-6 cells and RAT-1 cells was tested in both culture mediums. The comparative cell cycle analysis of RAT-1 cells and IEC-6 cells in DMEM medium as well as in RPMI medium did not show an effect on both cell lines through the inverted medium (see figure 2.1). The PE of RAT-1 cells in normal medium (RPMI) was tested to be 38.6% while the PE in inverted medium (DMEM) was reduced to 28.2%. In contrast to the decreased RAT-1 cell PE, the IEC-6 cells were not influenced by the medium. In normal medium (DMEM) as well as in inverted medium (RPMI) the PE was constant with 63.5% and 62.4%, respectively. For co-culture experiments IEC-6 cells and RAT-1 cells were cultivated in RPMI medium supplemented with 10% FCS and 100 U/ml penicillin/100 μg/ml streptomycin in 95% humidified air at 37 °C and 5% CO_2. The co-culture were trypsinized with a trypsin-EDTA-solution (0.25% trypsin, 0.02% EDTA) and were counted within the limits 9-26 μm with an electronic particle size analyzer.
The co-culture survival experiments were carried out with two different set-ups. In the first experimental approach the cells were seeded 24 h prior to the experiment in 25 cm^2 culture flasks (45 flasks/cell line). Therefore, the PE (see subsection 2.1.6) and the cell doubling time was estimated, and an appropriate cell number was seeded. The doubling time has to be integrated into the calculation since the cells double every 24 h (see figures 3.1 and 3.5). On the day of the experiment the cells were irradiated and afterward,

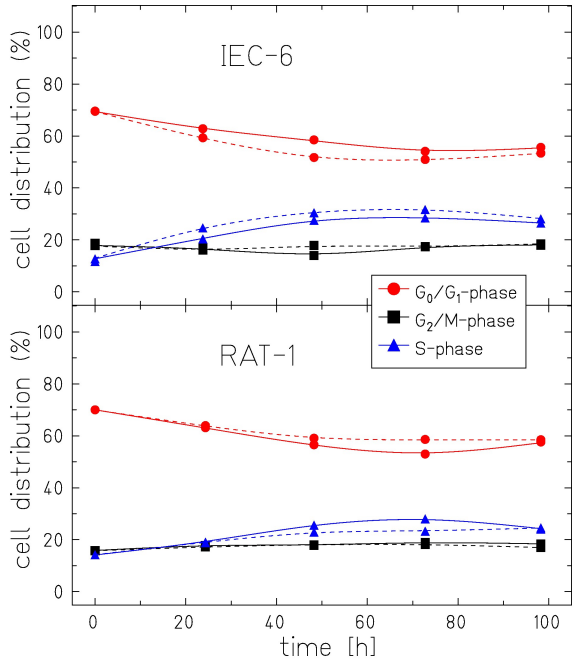

Figure 2.1: Cell cycle distribution of RAT-1 cells and IEC-6 cells in normal and inverted medium. Solid lines: RPMI medium, normal for RAT-1 cells, dashed lines: DMEM medium, normal for IEC-6 cells

unirradiated cells were added. In the second approach, the cells were irradiated or mock-irradiated in mono-cultures, trypsinized, and seeded together. In both experimental set-ups the cells were seeded seven times in 25 cm^2 culture flasks for the clonogenic survival assay (see subsection 2.1.6). Figure 2.2 shows the seeding scheme. The unirradiated cells are depicted in dark blue and dark green, while the irradiated cells are shown in light blue and light green. Mono-cultures of unirradiated and irradiated cells served as controls. These samples are shown in the color combination blue or green with white. The combination of irradiated and unirradiated cells of one cell line was not tested since the resulting colonies can not be distinguished in irradiated or control cells. Instead of full survival curves only three survival levels of RAT-1 cells were chosen (80%, 50%, and 15%) corresponding to a dose of 1, 3, and 6 Gy of x-rays. The survival of IEC-6 cells, which results after x-ray irradiation with these doses, was determined to be 73%, 38%, and 6%. The x-ray doses were converted with the aid of RBE to carbon ion doses. Table 2.1 gives an overview of the chosen survival levels as well as the corresponding absorbed doses and energies.

For data analysis the survival of mono-cultures was normalized on the PE for mono-cultures (PE_{mono}). The co-culture data points were normalized on the co-culture PE (PE_{co}) of unirradiated IEC-6 cells and RAT-1 cells. When several experiments were performed to one data point the mean values with their standard deviation were determined. If only one experiment was performed, an error estimation was carried out as described under

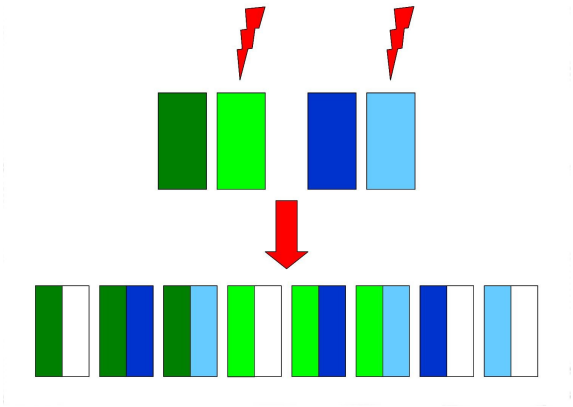

Figure 2.2: Seeding scheme for co-culture. RAT-1 cells are displayed in blue and IEC-6 cells in green. Dark colors represent unirradiated cells while light colors show irradiated cells. The mono-cultures (controls) are indicated with white fields.

Table 2.1: The table shows doses and beam energies used in co-culture experiments.

Survival levels [%]		**Dose [Gy]**		
RAT-1	**IEC-6**	**250 kVp x-rays**	**^{12}C 100 MeV/u**	**^{12}C 11.4 MeV/u**
80	73	1.0	0.6	0.17
50	38	3.0	1.7	0.53
15	6	6.0	4.1	1.46

subsection 2.7.1. To analyze the possible co-culture effect the normalized co-culture survival was divided by the normalized mono-culture survival.

For cytokine experiments (see section 2.3) the cells were irradiated with 0 Gy and 6 Gy of x-rays or 1.46 Gy (11.4 MeV/u) of carbon ions. After irradiation the cells were trypsinized, seeded with variable cell numbers, and cultivated in a 6-well plate/insert system (Insert: PET membrane with 3.0 μm pore diameter, Greiner Bio-One GmbH, Germany). The insert membrane is porous and allows the cell communication with soluble factors via the medium. In this system different growth behavior between the plate and the insert are possible. Therefore, both seeding possibilities were tested for a sample pair: plat/RAT-1 cells + insert/IEC-6 cells and inverse. The x-ray irradiation was performed twice and the cells were seeded with lower or higher cell numbers to clarify if the cell numbers influence the cytokine production. The ratio of seeded RAT-1 cells to IEC-6 cells was ten to seven like the seeded cell numbers in colony forming assays (see subsection 2.1.6). At certain points during the experiment the cell culture supernatant was harvested for cytokine measurements and centrifuged at 4 °C for 3 min at 300 *g*. The supernatant was stored long-term at -20 °C. In parallel, the total cell numbers were determined in the well and in the insert. For analysis, the measured cytokine amount in the

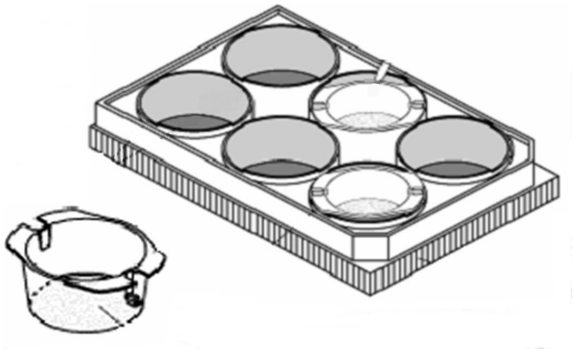

Figure 2.3: Schematic drawing of 6-well plate/ insert system used in co-culture experiments. Left panel: insert, right panel: 6-well plate with two inserts, Illustration: BD Biosciences, San Jose, CA, USA; modified

supernatant were correlated to the cell numbers.
In a clonogenic survival assay (see subsection 2.1.6) the cells have partial direct cell to cell contact. With the 6-well plate/insert system the direct cell to cell contact in co-culture was excluded and the cytokines could only be mediated via cell culture medium. To measure if the direct cell to cell contacts are important for the cytokine secretion in co-culture, the cells were seeded together in 6-well plates and the supernatants were handled as mentioned above. In a mixed suspension of both cell lines, a separated cell number for each cell line can not be determined which is needed for data analysis. In a particle size analyzer the cell histograms are congruent so that only the total cell number was detected. To circumvent this problem one cell line was stained with the vital membrane labeling fluorescent dye PKH67 (see subsection 2.4.2). In the flow cytometer the percentage distribution of the two populations (stained / unstained) were analyzed. In combination with the total cell number of both cell lines the cell number of each cell line could be determined and correlated to the cytokine amount.

2.1.4 Cryopreservation

For order to preserve the cells long-term cells were stored in liquid nitrogen at -196 °C. Therefore, the cells were trypsinized and pelleted by centrifugation for 10 min at 4 °C with 107 *g*. The medium supernatant was discarded, and the cells were resuspended in cooled culture medium containing 20% FCS and 10% dimethyl sulfoxide (DMSO, Applichem, Darmstadt, Germany) beside the normal medium components. 2 ml suspension with 1-2 x 10^6/ml cells was transferred into cryotubes. The samples were frozen to -80 °C in precooled isopropanol vessels (Nalgene Cryo 1 °C Freezing Container, VWR, Germany) in a controlled manner. After 24 h the tubes were transferred into liquid nitrogen.
For cultivation, the cells in the tubes were rapidly defrosted by shaking in a water bath

at 37 °C. The cell suspension was transferred into a tube with 10 ml 4 °C pre-cooled cell culture medium. To remove the DMSO the cells were pelleted by centrifugation for 10 min at 4 °C at 107 *g*. The medium supernatant was completely removed, the pellet separated, and the cells reseeded in 15 ml normal culture medium pre-warmed to 37 °C in 75 cm^2 culture flasks.

2.1.5 Growth curves

The cell doubling time t_D was determined in growth curves. A growth curve is subdivided in three phases of growth. In the initial lag-phase the cells attach after seeding and enter the exponential phase when the cells proliferate with a constant cell doubling time. Finally, the cells reduce their proliferation when the growth area becomes limited and enter the stationary phase (overview in reference [1]). In the experiments 1-5 x 10^4 cells were seeded in a culture flask with 12.5 cm^2 or 25 cm^2 growth area. Over several days the total cell number was determined in duplicates. In the exponential phase of the growth curve the cell doubling time was determined with the GSI in house program *gd* (©M. Krämer, 2003).

2.1.6 Clonogenic survival assay

To determine the cell survival rate after irradiation a clonogenic survival assay was performed. After treatment the cells were trypsinized, separated, and counted before the cells were reseeded in 25 cm^2 culture flasks. In addition, before counting RAT-1 cells needed a centrifugation over 8 min at 521 *g* to remove trypsin from the cell suspension. The inoculum (I) for cell seeding was calculated according to the following Eq.

$$I_{\mathrm{ml}} = \frac{N_C}{(N_{ml} \cdot S \cdot PE)}, \tag{2.1}$$

whereas N_C is the colony number/culture flask which should grow, N_{ml} is the cell number/ml in the cell suspension, S the reduced survival after irradiation, and PE the expected plating efficiency. The PE describes the percentage of cells which are able to proliferate and form colonies with more than 50 daughter cells within a certain time interval. Since the PE depends on the cell handling and the general status of the cells it has to be determined in every experiment. For RAT-1 cell assays N_C was 100 and the samples were reseeded in triplicates. In IEC-6 cell experiments N_C was 70 so that the cells have to

be reseeded in quadruplicates to achieve comparable colony statistics to RAT-1 cell experiments. In co-culture experiments with IEC-6 cells and RAT-1 cells both N_C-values remained constant but the flask number was increased to septuplicate with the objective of increased statistic and detection of even small co-culture effects. RAT-1 cells and IEC-6 cells were incubated for 11 days. After incubation the grown colonies were fixed and stained. The staining procedure started by discarding the medium. The grown colonies were fixed with 2 ml of 70% ethanol for 15 min at room temperature. The ethanol was aspirated, and the colonies were stained with 3 ml threefold methylene blue (see annex) for 8 min (RAT-1 cells) or 15 min (IEC-6 cells). The staining solution was discarded, the culture flasks were washed with 3 ml purified water to remove surplus staining reagent, and the samples were air dried under the fume hood. The stained colonies were counted under a stereomicroscope. In the following Eq. the obtained PE is calculated whereas N_R means the average of the resulting colony number/sample. In this case the sample is an unirradiated control and the survival is assumed with one.

$$PE = \frac{N_R}{(I_{\text{ml}} \cdot N_{ml})} \tag{2.2}$$

The survival of the irradiated cell samples has to be calculated according to the following Eq. and has to be normalized on the PE.

$$S = \frac{N_R}{(I_{\text{ml}} \cdot N_{ml} \cdot PE)} \tag{2.3}$$

2.1.7 X-Gal staining

X–Gal staining was used with IEC-6 cells for the detection of the enzyme β-galactosidase (β-gal) which is discussed to be a general indicator for cell senescence [28, 67]. Lee *et al.* demonstrated that senescence-associated β-galactosidase (SA-β-gal) corresponds to lysosomal β-gal [82] which is consistent with the observation that senescent cells increased the number of lysosomes [80]. Lysosomal β-gal has its maximal enzymatic activity between pH 4 and 4.5 and clearly lower activity at pH 6 [92]. The unusually high activity of β-gal in non-optimal pH is typical of senescent cells [46]. The indole derivative 5-bromo-4-chloro-3-indolyl-β-D-galactoside (X-Gal) is an artificial substrate of the enzyme β-gal. When β-gal cleaved the X-Gal a soluble and colorless indoxyl monomer is produced. Two indoxyl monomers form a dimer which is oxidized on air. The resultant halogenated indigo is a very stable and insoluble cyan compound [17]. For the staining 1 x 10^5 cells in 2 ml culture medium were seeded in Petri dishes with a diameter of 3 cm 48 h before the experiment. On the day of the experiment the medium was discarded and the cell

layer was rinsed three times with 1 ml PBS^{-}. The cell layer was fixed with 1 ml of a 3% formaldehyde solution for 5 min at room temperature. To remove formaldehyde surplus the cells were washed three times with 1 ml PBS^{-}. The staining was performed with 3 ml of X-Gal staining solution (see annex) for 18 h at 37 °C. Afterward, the staining solution was removed, and the cell layer was rinsed three times with 1 ml PBS^{-}. The analysis of the air dried samples was performed under a stereomicroscope at which X-Gal positive (blue-green colored cells) and negative cells were counted.

2.2 Chromosome preparation

Chromosome preparations were performed with IEC-6 cells and RAT-1 cells according to standard techniques [61]. Therefore, 1 x 10^6 cells were seeded 48 h before the experiment in 75 cm^2 culture flasks with 10 ml culture medium. On the experiment day 10 μl colcemid/ml medium (Roche Deutschland Holding GmbH, Germany) was added to the cells. Colcemid arrests the cells in mitosis by blocking the chromosome division through the spindle apparatus. After 4 h of incubation the cells were trysinized and harvested. The cell suspension was pelleted by centrifugation for 6 min at 204 *g*. The supernatant was discarded, and the pellet resuspended by knocking. 5 ml pre-warmed 0.075 M potassium chloride (KCl, Merck KGaA, Darmstadt, Germany) solution was added to the tube for a duration of 8 min which induced chromosome swelling. The cells were again pelleted by centrifuging for 8 min at 204 *g*. The supernatant was discarded. The pellet was resuspended by knocking, and 10 ml of fixative was added to the cells for a duration of 8 min. The fixative is composed of 3 parts methanol and 1 part pure acetic acid. The cells were incubated 30 min in fixative before the cells were pelleted by centrifuging over 10 min at 293 *g*. The fixative was discarded, the pellet resuspended by knocking, and the cells were washed with 10 ml fixative. After an additional centrifugation step at 293 *g* for 10 min the cells were resuspended in 1 ml fixative. The prepared suspension was dropped on wet slides (purified water). After 24 h of air drying the slides were stained for 10 min in a 10% Giemsa solution (Merck KGaA, Darmstadt, Germany) diluted with Soerensen buffer (pH 6.8, see annex) or were stained with the multicolor fluorescence in situ hybridization technique (see subsection 2.2.1). To remove surplus Giemsa solution the slides were washed in purified water and dried with compressed air. For permanent conservation the slides were sealed with Eukitt (Kindler GmbH & Co, Freiburg, Germany) and covered with a thin cover slip. For each sample the mitotic index was analyzed in 6000 nuclei, and the number of chromosomes per metaphase was determined in 300 metaphases.

2.2.1 Multicolor fluorescence in situ hybridization

The multicolor fluorescence in situ hybridization (mFISH) presents all chromosomes of a metaphase simultaneously in a single hybridization. Thereby, five different fluorochromes or a combination of the fluorochromes bind to the DNA and allow the analysis and identification of inter-chromosomal exchanges which is not possible with Giemsa staining (see subsection 2.2). Here the method was used to analyze the aneuploid IEC-6 cell metaphases. The mFISH kits are available for human and mouse chromosomes but not for rat chromosomes. An attempt was made to analyze the rat's chromosomes with a 21xMouse mFISH Probe Kit for mouse (MetaSystems, Altlussheim, Germany). The chromosome samples were prepared as described under subsection 2.2. The mFISH procedure was done according to the XCyte Lab Manual (manufacturer's instructions) including the RNAse pretreatment prior to the pepsin pretreatment but without post fixation after pepsin treatment. The cells was incubated with probe cocktail three days at 37 °C and prepared till the first detection step. After air drying the samples were counterstained with DAPI/Antifade (4',6-diamidino-2-phenylindole, B-tect GmbH, Hannover, Germany), covered with a slide, and stored protected from light at 4 °C. All concentrations of used solutions were consistent with the protocol of the manufacturer. The stained metaphases were analyzed with a motorized and computer-controlled fluorescent microscope equipped with a monochrome CCD-camera. The metaphases were excited with UV-light (DAPI-channel) and were selected manually under a 100x objective. With the software Ikaros & Isis version 5.0 (MetaSystems, Altlussheim, Germany) the automatic filter change and sample exposition as well as image recording and processing were controlled. Since mice have 21 and rats 22 different chromosomes the allocation of the chromosomes has to be done manually for analysis.

2.3 Detection of pro-inflammatory cytokines

To detect the pro-inflammatory cytokines TGFβ, TNF α, and IL-2, different Sandwich Enzyme-Linked ImmunoSorbent Assay (ELISA) detection kits from R&D Systems GmbH (Heidelberg, Germany) were used. In a Sandwich ELISA an antigen specific capture antibody is immobilized to the surface of a 96-well plate over night at room temperature. The sample with an unknown amount of antigen was added for binding to the first antibody. A second antibody was added and formed a complex with the antigen. The second antibody was coupled with a streptavidin-horse-radish-peroxidase-complex. The enzyme-complex produces through binding to an enzymatic substrate a visible signal which indicates the quantity of antigen in the sample. The detection of TGFβ, TNFα, and IL-2

was carried out in the cell culture supernatants of irradiated and unirradiated co-culture or mono-culture samples of IEC-6 cells and RAT-1 cells. The procedure was carried out according to the manufacturer's instructions. All antibody and solution concentrations were consistent with guidelines. The optical density was determined in a micro plate reader (BioTek EL808, BioTek Instruments GmbH, Bad Friedrichshall, Germany) at 450 nm. The wavelength correction was done with 570 nm. The data analysis was carried out with EXCEL®.

2.4 Flow cytometry

2.4.1 Cell cycle analysis

For cell cycle analysis the cells were trypsinized, separated, and counted. A minimum of 1 x 10^5 to a maximum of 1 x 10^6 cells were centrifuged 8 min with 521 *g* at room temperature. The supernatant was removed, and the pellet was resuspended in the reflux. The cells were washed twice with 1 ml PBS^- (centrifugation 521 *g*, 8 min) and resuspended in 1 ml ice cold 70% ethanol under vortexing for cell fixation. The prepared samples could be stored for four weeks at -20 °C. Alternatively, the ethanol could be removed after 1 h of fixation by centrifugation (521 *g*, 8 min). The cells were stained protected from light at room temperature for a minimum of 30 min with 1 μg/ml DAPI in PBS^- before measuring. The samples were measured and analyzed with the flow cytometer PAS III (Partec, Münster, Germany) and the Windows™ based softwares FloMax® (Partec, Münster, Germany) and MultiCycle (Phoenix Flow Systems, San Diego, CA, USA).
The cell cycle of eukaryotic cells is subdivided in four phases (see figure 2.4). During the M-phase, the chromosomes are condensed and therefore visible under a microscope. The M-phase contains the mitosis (division of the sister chromatids) and the cytokinesis (cell division). The mitosis itself is subdivided into the prophase, prometaphase, metaphase (early mitosis), anaphase, and telophase (late mitosis). The M-phase is followed by the interphase. The interphase contains the G_1-, S-, and G_2-phase. In G_1-phase the cells grow and duplicate their organelles. In the following S-phase the DNA is duplicated. The final dimension reach the cells in G_2-phase before the cells enter the mitosis again. Some cells left the cell cycle and stop dividing. This resting phase is called G_0-phase (overview in reference [1]). Because of the similar DNA content a differentiation of the sub-phases of the M-phase, a discrimination of M-phase and G_2-phase as well as a differentiation of G_0-phase and G_1-phase is not possible by using a flow cytometer for the cell cycle analysis.

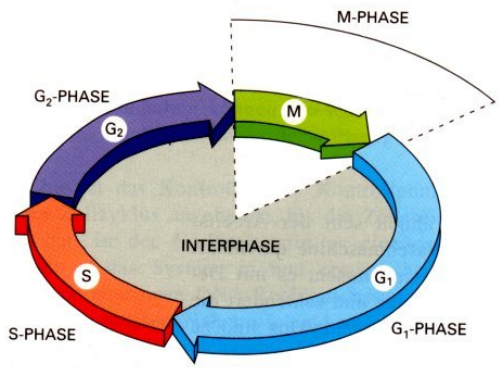

Figure 2.4: Cell cycle phases of an eukaryotic cell [1], modified

2.4.2 Fluorescence membrane labeling with PKH67 and analysis

PKH67 (Sigma Aldrich, St. Louis, WO, USA) is a green fluorescent labeling dye which integrates with its long aliphatic carbon tail into lipid regions of the cell membrane of intact cells. The dye has an extinction maximum at 490 nm and an emission maximum at 502 nm. The cell staining was performed with small changes, which are mentioned below, according to the manufacturer's instructions. The irradiated or unirradiated cells were trypsinized, separated, and counted. The needed cell number was transferred into a polypropylene tube, and the cells were pelleted at 400 *g* for 5 min. The supernatant was discarded, the cells were resuspended in 5 ml PBS^{-}, and centrifuged at 400 *g* for 5 min. The PBS^{-} was discarded, the reflux reduced to under 25 μl by pipetting, and the cells were resuspended in 1 ml Diluent C. In a separate tube 2 μl or 8 μl PKH67 staining reagent per 1 x 10^7 cells were mixed with 0.5 ml Diluent C. All following steps were done under conditions protected from light. The staining solution (PKH67 + Diluent C) was pipetted into the cell suspension. The suspension was mixed well by pipetting and incubated for 5 min at room temperature. During this time the PKH67 integrates into the cell membrane. The reaction was stopped by the addition of 2 ml FCS for 1 min followed by a centrifugation at 400 *g* for 5 min. The supernatant was discarded, and the cells were resuspended in 10 ml culture medium. The medium wash step was repeated three times before the cells were counted and reseeded in desired dilutions. The cells were grown protected from light for several days. At various points in time the cells were trypsinized, counted, and prepared for flow cytometer analysis. Therefore, the cells were pelleted at 521 *g* for 8 min. The supernatant (cell culture medium) was discarded. The cells were fixed 15 min in 2% paraformaldehyde (PFA) or 15 min in 70% ethanol. The fixative was removed by centrifuging at 521 *g* for 8 min. The cells were washed once with 5 ml PBS^{-}, centrifuged at 521 *g* for 8 min, and resuspended in 2 ml PBS^{-}. The auto-fluorescence of

the non stained cells was high enough and a counter staining against e.g. the DNA was not needed. The stained samples were measured with the argon laser (488 nm) of the flow cytometer PAS III (Partec, Münster, Germany). The data analysis were done with the Windows™ based software FloMax® (Partec, Münster, Germany) and and MultiCycle (Phoenix Flow Systems, San Diego, CA, USA) and the GSI in house program *gd* (©M. Krämer, 2003).
The PKH67 staining was performed with different dye concentrations (2 μl or 8 μl PKH67/ 1 x 10^7 cells), and the stained cells were measured alive in the flow cytometer. Figure 2.5 demonstrates that 2 μl PKH67 was adequate to stain the cells and allow a differentiation between stained and unstained cells (black curve, cross symbol). The amount of dye in the cell membrane is reduced with every cell division. Therefore, the number of less or unstained cells increased in a PKH67 stained samples with time. For an observation period of four days the dye concentration of 2 μl PKH67/ 1 x 10^7 cells was not high enough to distinguish between the stained and unstained cells (cyan curves, cross symbol). The enhanced PKH67 concentration (8 μl PKH67/ 1 x 10^7 cells) was more sufficient in that way that after four days the two populations were still dividable by their fluorescence (cyan and black curves, open circle).
For some applications, e.g. long-term storage, it is advantageous to fix the samples and prolong the time interval in which the sample could be measured with reproducible results. Two solutions are tested for the fixation: ethanol and PFA. In figure 2.5 is displayed that through the ethanol fixation (green curves, open or closed circle) the homogeneous peak of stained samples (black curve, open circle) is destroyed while the signal of fixed and unstained samples (black curve, closed circle) was shifted to lower signal intensities. The PFA fixation (red curves, open or closed circle) had very small influences on the staining (black curves, open circle, minimal peak shift) and should be the preferred agent. The great differences between the living IEC-6 cells (black curve, closed circle) and the PFA fixed cells (red curve, closed circle) results from an iniquitous separation of the living IEC-6 cells. The PFA fixed samples could be stored over eight weeks at 4 °C without signal loss. Over all, the staining with PKH67 needs to be optimized for each cell line but the method openes interesting analysis options.

2.5 Hypoxia chamber

Because oxygenation within tumors plays an important role in the outcome after treatment the simulation of different oxygenation situations with cell cultures could help to understand the underling mechanism and to collect data for treatment planning systems. For this purpose a hypoxia chamber was established to irradiate cell cultures with x-rays

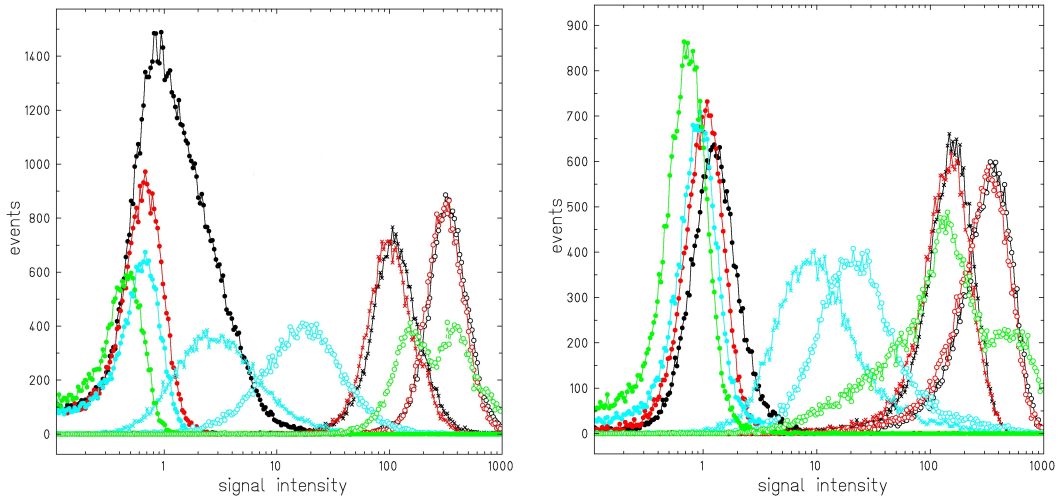

(a) IEC-6 cells (b) RAT-1 cells

Figure 2.5: PKH67 stained or unstained IEC-6 cells and RAT-1 cells. In black: living cells, in red: PFA fixed cells, in green: ethanol fixed cells, in cyan: growth for 96 h after treatment, PFA fixed, closed circle: unstained, cross: 2 μl PKH67/ 1 x 10^7 cells, open circle: 8 μl PKH67/ 1 x 10^7 cells

and heavy ions, especially carbon ions, under defined oxygen conditions. The hypoxia chamber and the sample ring were developed in the diploma thesis of C. Schicker which was supervised by W. K.-Weyrather and C. von Neubeck [117]. The results of the thesis were patented in references [118, 119]. Further details of the construction are reported in Schicker [117]

2.5.1 Construction

The hypoxia chamber was milled out of one piece of polyetheretherketone and has the external dimensions of 90 x 74 x 57 mm (length x width x height). The front wall is reduced to 1 mm thickness which is the so called *irradiation window*. On both side walls a female hose coupling was screwed which could be made penetrable by plugging a male coupling (both neoLab, Heidelberg, Germany). The coupling next to the irradiation window was used for the gas inlet and the other for the gas outlet. The top cover was made of transparent polymethyl methacrylate which allows position control of the sample. In the middle of the top cover and on the bottom of the chamber a chamfer was milled which fixes the cell samples in the correct position during the experiment (see subsection 2.5.2 and figure 2.6). With four screws and an additional O-ring (Dichtungstechnik Bensheim GmbH, Bensheim, Germany) around the top cover the chamber could be closed air tight.

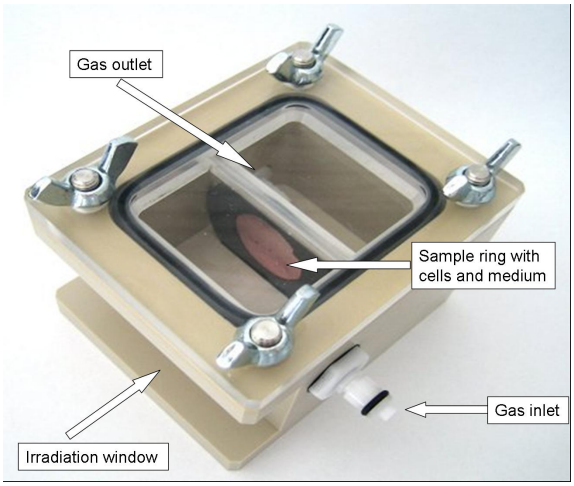

Figure 2.6: Hypoxia chamber with sample ring.

2.5.2 Cell samples and handling

For experiments in the hypoxia chamber the cells had to grow on a special foil. The bioFolie 25 (In Vitro Systems & Services, Göttingen, Germany) is permeable for gases such as CO_2 (2.2 μmol/cm^{2}h) and O_2 (6.3 μmol/cm^{2}h). Cell adhesion is possible on the hydrophilic side of the foil. For experiments the bioFolie 25 was cut into circles (∅ 44 mm), sterilized in 70% ethanol for 15 min, and air dried. With high viscous silicon paste (Baysilone, Bayer AG, Leverkusen) the foil was bond on a sample ring to form a "Petri dish". The sample ring was made of polyvinyl chloride, has a thickness of 3 mm, and a radial through boring which is closed with silicone paste or a little screw. 48 h prior to the experiment 3 x 10^4 RAT-1 cells in 1 ml culture medium were seeded on the foil-Petri dish. On the day of the experiment, a second foil was stuck with silicon paste on the ring to generate a sterile volume in-between the two foils. The sample ring was fixed in a retaining bracket with the radial through boring on top (see figur 2.7). The volume

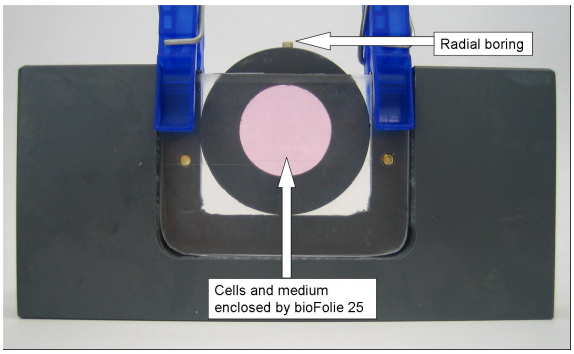

Figure 2.7: Retaining bracket with fixed sample ring.

created by the two foils was filled with 1.4 ml of fresh culture medium, and the through

boring was closed with silicone paste. The cell sample ring was inserted into the hypoxia chamber with the cell layer in direction of irradiation window (see subsection 2.5.1). For more details see reference [117]. The cell samples in the hypoxia chamber were aerated with pure N_2 for test measurements or 95% N_2/ 5% CO_2 (Linde AG, Pullach, Germany) for experiments. After irradiation the cell sample was removed from the chamber, and the cells were analyzed in a clonogenic survival assay. Therefore, the foil without cells was removed, the medium discarded, and the cell treated as described under subsection 2.1.6.

2.5.3 Gassing modalities

The cell samples in the chambers were aerated with different gas mixtures to reduce the oxygen in the gas phase and in the culture medium under controlled conditions. The partial O_2 pressure was measured with an optical O_2 micro sensor (Needle-Type Housing) and a measuring instrument Microx TX 3 (both PreSens, Regensburg, Germany). The gas flow was measured with a thermal mass flow meter calibrated for nitrogen (1000 ml/min N_2, red-y compact meter GCM, Vögtlin instruments AG, Aesch, Switzerland). Through the usage of nitrogen based gas mixtures a measurement error of 3% should be taken into account beside the instrumental error of 1% (total error 3.2%, error estimation Vögtlin instruments AG). The time interval to achieve hypoxic conditions (t_{hyp}) is dependent on the gas flux and was determined with five in-line connected hypoxia chambers. A pure nitrogen flow of 100 ml/min replaces the air in the chambers within 5.54 min. To simulate experimental conditions the chambers were loaded with sample rings which were filled with purified water. A flow of 100 ml/min, 150 ml/min, and 200 ml/min pure nitrogen corresponds to t_{hyp} values of 164.4 min, 150.2 min, and 86.2 min, respectively. The experimental protocol for the cell experiments were defined to be a 2 h gassing with 200 ml/min which take into account the device error of 3.2%, the chamber flushing time of 5.54 min, and the time to achieve hypoxia conditions in the chambers.

2.6 Cell irradiation procedure

All irradiation experiments were performed with asynchronous proliferating cell cultures in culture flask, Petri dishes or on bioFolie 25 for experiments in hypoxia chambers. In every experiment unirradiated control cells (0 Gy) for determining the PE were seeded, incubated, and handled under the same conditions like the irradiated samples.

X-ray irradiation

The x-ray irradiation was performed with the x-ray machine Isovolt DS1 (Seifert, Ahrens-

berg, Germany). The accelerating voltage was set to be 250 kVp with a cathode current of 16 mA. At the beam exit window a filter system of 7 mm beryllium, 1 mm aluminum, and 1 mm copper absorbed the long wave part of the radiation. The dose and the dose rate were detected by a dosimeter (SN4, PTW Freiburg, Germany). The irradiation was performed with a dose rate of 1.3 to 4.0 Gy/min at room temperature while the absorbed doses were between 0 to 27.0 Gy.

Carbon irradiation

The GSI's Universal Ion Linear Accelerator (UNILAC) accelerates the carbon ion up to 20% light velocity, and the following heavy ion synchrotron (SIS) enhances the acceleration to 90% light velocity. For experiments at UNILAC the cells were cultured in 3 cm Petri dishes and were irradiated in Petri dish compatible magazines. The stopping carbon ions had a primary energy of 11.4 MeV/u and 9.8 MeV/u on target with the corresponding LET of 170 keV/μm. The applied doses were in the range of 0 to 3.5 Gy. A detailed description of the irradiation procedure and dosimetry is given elsewhere [76]. After irradiation the Petri dishes were removed from the magazines under sterile conditions. In every Petri dish the inner border was cleaned with a sterile cotton bud. This has to be done since the Petri dish is irradiated in a vertical position, and a medium drop is formed at the bottom of the inner border. In the medium drop the ions stopped and do not hit the cells. With the wiping step all unirradiated cells are removed.

For irradiation at SIS facility the cells were cultured in 25 cm^2 culture flasks which were completely filled with culture medium and sealed with an additional *parafilm* strip (American National Can Group, San Diego, CA, USA). The cells were irradiated with intensity modulated raster scanning technique as described in detail elsewhere [50]. Monoenergetic fields with a primary energy of 100 MeV/u or 270 MeV/u were delivered (LET: 28 keV/μm and 13 keV/μm, respectively). These energies were reduced to energy levels of 93.2 MeV/u and 267 MeV/u on target (LET: 27.9 keV/μm and 13.7 keV/μm, respectively) due to the ion traversal through the detector system and the culture flask bottom in the beam line (1.3 mm water equivalent thickness). The applied doses were in the range of 0 to 8.0 Gy.

Samples in the hypoxia chamber were irradiated with a spread out Bragg peak (SOBP) of 1 cm thickness with a dose-averaged LET ($\overline{LET}$) of 100 keV/μm. The applied doses for oxic samples were 0 to 3.0 Gy and for hypoxic samples 0 to 5.4 Gy.

2.7 Statistical data analysis

2.7.1 Error estimation for survival experiments

The PE (see Eq. 2.2) of unirradiated control samples was determined in every survival experiment and it defines the 100% survival level for a specific experiment. All irradiated samples of this specific experiment have been normalized to this value according to Eq. 2.3. The ratio of sample numbers of unirradiated controls to irradiated samples was in all experiments described smaller or equal to 1:4.
In the following paragraph the error estimation for survival experiments is presented within two different cases and explained. In the first part, the error estimation for complete survival curves is presented while in the second part, the error calculation for isolated survival values or experiments, which are done once is shown. The error calculation for the survival experiments with multiple samples has been carried out as followed. The average survival $\overline{S}$ of the survival values S_1, S_2 ..., S_n corresponding to one dose was calculated as well as their standard deviation $\sigma_{\overline{S}}$ and their standard error of the mean $SEM_{\overline{S}}$ in which the number of samples is given by *n*.

$$\overline{S} = \frac{1}{n}\sum_{i=1}^{n} S_i \tag{2.4}$$

$$\sigma_{\overline{S}} = \sqrt{\frac{1}{n-1}\sum_{i=1}^{n}(S_i - \overline{S})^2} \tag{2.5}$$

$$SEM_{\overline{S}} = \frac{\sigma_{\overline{S}}}{\sqrt{n}} \tag{2.6}$$

From the linear-quadratic fit to the survival data the parameters α and β were determined with their averages $\overline{\alpha}$ and $\overline{\beta}$ as well as their standard deviations σ_α and σ_β.

$$\sigma_\alpha = \sqrt{\frac{1}{n-1}\sum_{i=1}^{n}(\alpha_i - \overline{\alpha})^2} \tag{2.7}$$

$$\sigma_\beta = \sqrt{\frac{1}{n-1}\sum_{i=1}^{n}(\beta_i - \overline{\beta})^2} \tag{2.8}$$

For the radio-resistance parameter α/β the relative error $\sigma_{\alpha/\beta}$ was performed according to Eq. 2.9.

$$\Delta\alpha/\beta = \frac{\sigma_{\alpha/\beta}}{\alpha/\beta} = \sqrt{\left(\frac{\sigma_\alpha}{\overline{\alpha}}\right)^2 + \left(\frac{\sigma_\beta}{\overline{\beta}}\right)^2} \tag{2.9}$$

The error estimation for survival experiments which were done once was developed [136]. The survival within the linear-quadratic model is given by Eq. 2.10, and E is the associated effect as defined in Eq. 2.11.

$$S = e^{-(\alpha D + \beta D^2)} \tag{2.10}$$

$$E = \alpha D + \beta D^2 \tag{2.11}$$

The error is on the one hand influenced by the fluctuation of the data points around the individual survival curve (E_S) and on the other hand changed by the variation of the ensemble of the curves ($E_{\alpha,\beta}$). The error contributions of E sum up to ΔE in Eq. 2.12.

$$\Delta E = \sqrt{\Delta E_S^2 + \Delta E_{\alpha,\beta}^2} \tag{2.12}$$

The first factor contributing to the error is caused by the fluctuation of survival levels around their corresponding linear-quadratic curve. The associated error ΔE_S is calculated as the standard deviation of the measured effect levels E_i of unirradiated samples.

$$\Delta E_S = \sqrt{\frac{1}{n-1}\sum_{i=1}^{n}(E_i - \overline{E})^2} \tag{2.13}$$

Inserting Eq. 2.11 in the definition of the standard deviation resulting in Eq. 2.14.

$$\Delta E_{\alpha,\beta} = \sqrt{\sigma_\alpha^2 D^2 - 2\sigma_{\alpha,\beta}^2 D^3 + \sigma_\beta^2 D^4} \tag{2.14}$$

The factors σ_α and σ_β were determined according to Eqs. 2.7 and 2.8 at which beam and energy dependent mean α and β values were determined to $\overline{\alpha}$ and $\overline{\beta}$. For the calculation of the curve fluctuation $E_{\alpha,\beta}$ it was assumed that α and β are inversely correlated. The values were joined in Eq. 2.15 to calculate the third parameter $\sigma_{\alpha,\beta}$.

$$\sigma_{\alpha,\beta} = \sqrt{-\frac{1}{n-1}\sum_{i=1}^{n}[(\alpha_i - \overline{\alpha})(\beta_i - \overline{\beta})]} \tag{2.15}$$

Table 2.2: The table shows the error percentage of survival for selected doses calculated with error propagation for x-rays and two carbon ion energies.

Cell line	Dose [Gy]	250 kVp x-ray	^{12}C 100 MeV/u	^{12}C 11.4 MeV/u
RAT-1	0	9.3	9.3	9.3
	1	10.6	10.2	9.4
	3	17.8	17.4	10.1
	6	41.3	64.1	14.6
IEC-6	0	12.0	12.0	12.0
	1	13.3	14.8	12.0
	3	19.3	27.4	12.5
	6	32.8	62.6	15.3

The upper and the lower error limits of the survival were calculated according to Eqs. 2.16 and 2.17. The error limits have almost equal distances to the mean survival. Henceforth, the error interval was regarded to be symmetric with respect to the mean survival values.

$$S = e^{-(E \pm \Delta E)} \tag{2.16}$$

$$\Delta S = \frac{S_{upper} - S_{lower}}{2} = \frac{e^{-(E-\Delta E)} - e^{-(E+\Delta E)}}{2} \tag{2.17}$$

In table 2.2 the error percentage of survival for selected doses is shown. Both cell lines show in principle similar error values. The values increased with increasing doses due to higher uncertainties and variances in the survival levels to higher doses. This biological effect is expressed by the term $\sigma_\beta^2 D^4$ in Eq. 2.14. Overall, the errors of 11.4 MeV/u irradiation are smaller than the other irradiation error since the β containing terms converge to zero.

2.7.2 Calculation of RBE

The effect of different beam qualities on cells can be compared with the relative biological effectiveness (RBE). The RBE value calculation for RAT-1 cells and IEC-6 cells differs since the radio-resistance of RAT-1 cells stays stable and the radio-resistance of IEC-6 cells against x-rays increases clearly with cultivation time as discussed in section 4.2. This causes changing α values for x-ray irradiation and higher doses for 10% survival

levels. It was not possible to detect this behavior also for carbon ions irradiation due to the limited amount of data. In the following, the calculation of errors for both cell lines is described.

RAT-1 cells

For every survival curve the parameters α and β as well as their average $\overline{\alpha}$ and $\overline{\beta}$ were determined for different energies and beams. Likewise, the standard deviation $\sigma_{\overline{\alpha}}$ and $\sigma_{\overline{\beta}}$ were calculated. The RBE_α was determined according to Eq. 1.5 and the relative error of RBE_α was done according to Eq. 2.18.

$$\Delta RBE_\alpha = \frac{\sigma RBE_\alpha}{RBE_\alpha} = \sqrt{\frac{{\sigma_\alpha}^2}{\overline{\alpha}}_{ion} + \frac{{\sigma_\alpha}^2}{\overline{\alpha}}_{x-ray}} \tag{2.18}$$

The RBE for 10% survival (RBE_{10}) was calculated according to the same formalism as used for RBE_α with the doses for 10% survival.

$$\Delta RBE_{D10} = \frac{\sigma RBE_{10}}{RBE_{10}} = \sqrt{\frac{{\sigma_{D10}}^2}{\overline{D10}}_{ion} + \frac{{\sigma_{D10}}^2}{\overline{D10}}_{x-ray}} \tag{2.19}$$

IEC-6 cells

For carbon ion survival curves the parameter α was determined with its means and standard deviations as described for RAT-1 cells. For x-ray survival curves the α values were plotted versus passage number and fitted by a line, see figure 2.8. The error of α was set to be the 68% confidence interval. At the mean passage number of the performed carbon ion experiments (17.67) the α value with its deviation was evaluated (0.354 ± 0.021). The RBE for 10% survival was calculated along the lines of RBE_α with the doses for 10% survival. The determined D_{10} at passage number 17.7 was 5.0 ± 0.13 Gy.

2.7.3 Analysis of chromosome samples

For each chromosome sample 300 metaphases were analyzed according to their chromosome numbers. Furthermore, the mitotic index in 6000 cells per sample was counted. From the received data a weighted mean m and a weighted standard deviation σ_m, for chromosome numbers or mitotic index, were calculated according to the following Eqs., where x is the data and w the weights with $\sum_i w_i = 1$.

$$m = \frac{\sum x_i w_i}{\sum w_i} \tag{2.20}$$

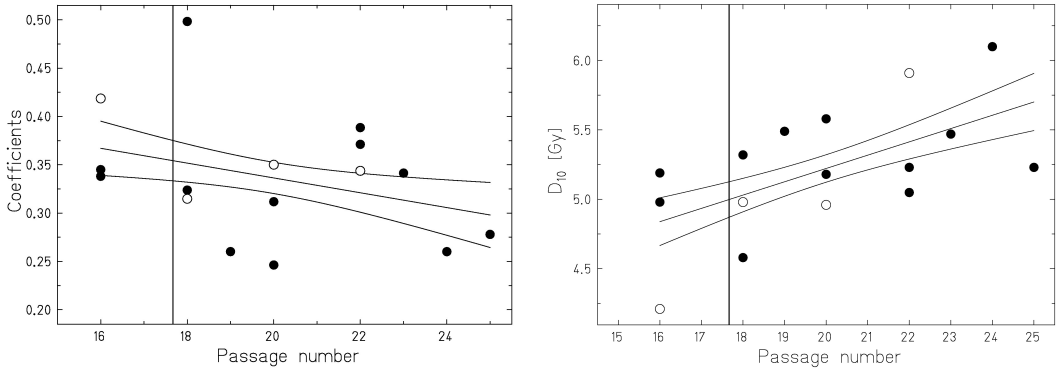

(a) α values (b) D_{10} values

Figure 2.8: α values and D_{10} of IEC-6 cell x-ray survival curves. The vertical line indicates the mean passage number of performed carbon ion experiments. Closed circles: serum batch I, open circles: serum batch II

$$\sigma_m = \sqrt{\frac{\sum x_i^2 w_i}{\sum w_i} - m^2} \tag{2.21}$$

3 Results

3.1 Characterization of rat adenocarcinoma cell line R-3327-AT-1

The adenocarcinoma cell line R-3327-AT-1 (RAT-1) is a fast growing, androgen- and estrogen-insensitive, and anaplastic tumor of the Dunning system ([65], see subsection 1.3.1). For experiments RAT-1 cells from the stock in P35 were defrosted and passaged once a week in RPMI medium with phenol red as pH indicator and the passage was numbered consecutively. The pH of the RPMI medium decreased between two passages which was optically detected by a color alteration from red-violet to light orange of the pH indicator. Figure 3.1 shows the cells three days and six days after seeding. A confluent cell layer could not be achieved since the cells start to grow in multilayer and pile up in cell clusters at 70% confluence. A separation of the cells was not possible after three days growth of clusters. The cell doubling time t_D was determined in growth curves and was calculated to be 21 ± 2 h in the exponential phase of the growth curve. The t_D remained stable over the whole passage period (see figure 3.1).

The cell cycle distribution of RAT-1 cells in P38 is presented in figure 3.2. The ex-

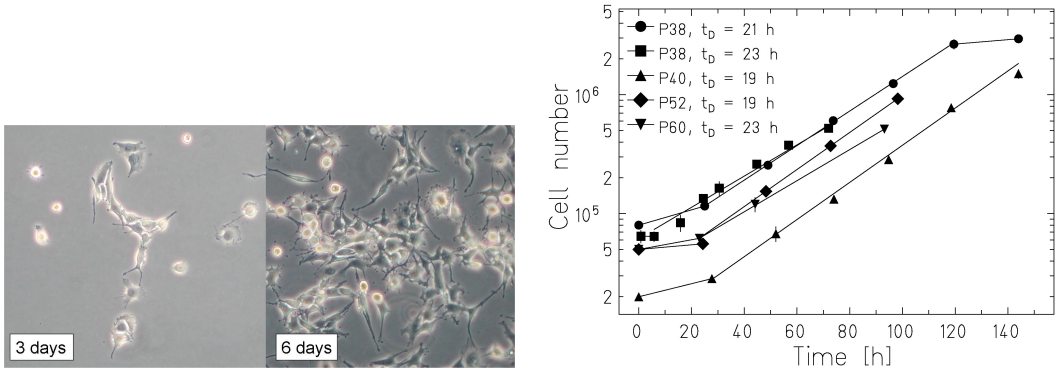

Figure 3.1: Left panel: RAT-1 cells three days and six days after seeding in culture flask. Magnification $\approx$ 20x **Right panel:** Growth curves of RAT-1 cells in culture flasks. The passage number P and the doubling time t_D is given for each curve.

periment was performed in duplicates over five days after mock irradiation and 250 kVp x-ray or 11.4 MeV/u carbon ion irradiation which reduced the cell survival to 10%. In the first twelve hours after irradiation a G_2-block was induced in the irradiated samples. The maximum of the G_2-block is between five and eight hours. The x-ray and the carbon ion irradiated cells accumulate to 41% in G_2-phase while in the control sample only 29% of

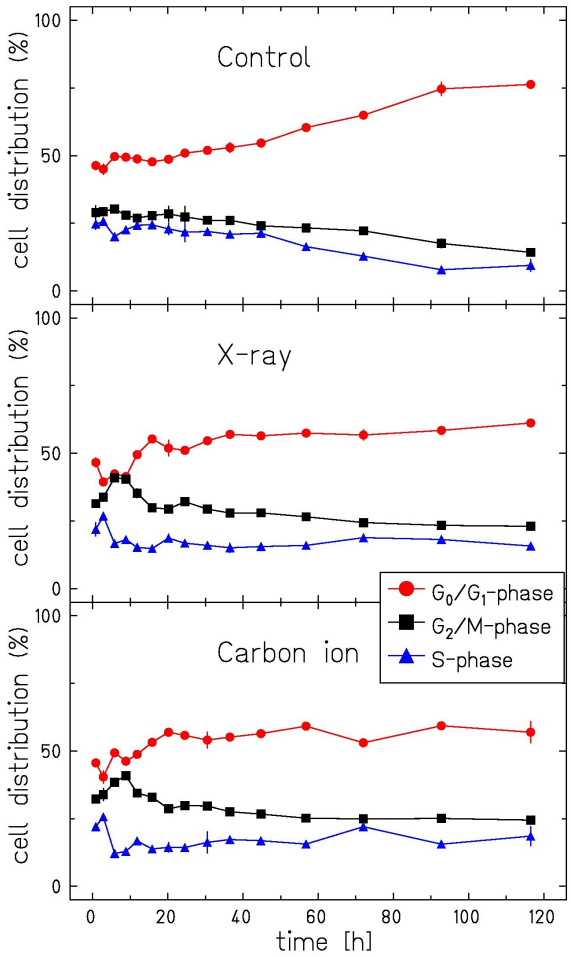

Figure 3.2: Cell cycle distribution of RAT-1 control cells and after 250 kVp x-ray or 11.4 MeV/u carbon ion irradiation to 10% survival level in P38.

the cells were enriched in G_2-phase. At later points in time the irradiated samples were not distinguishable from the control cells. At the end of the observation period 76% of the control cells accumulated in G_1-phase which indicates a limitation of growth area or nutrient in culture flask and an accompaning proliferation stop. 57% of the carbon ion irradiated cells and 61% of the x-ray irradiated cells were in G_1-phase after 120 h in culture. This indicates that the irradiated cultures did not reduce their proliferation since the cell numbers of growing cells were lower and no space or nutrient limitation took place.

Tumor cells often show variation in chromosome numbers (aneuploidy) and growth properties. To exclude possible large shifts of the chromosome distribution and/or a change in the mitotic index (MI) a chromosome analysis was performed with two individual cell batches from stock in P35 over several passages. Figure 3.4 shows the metaphase analysis of both cell batches where each small panel represents 300 metaphases of one passage. For illustration figure 3.3 shows two metaphases of RAT-1 cells. There was no detectable variation in the chromosome distribution, and small differences are due to statistical rea-

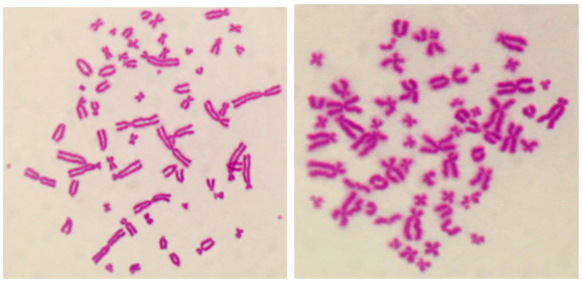

Figure 3.3: Metaphases of RAT-1 cells with 62 (left) and 64 (right) chromosomes, magnification ≈ 450x

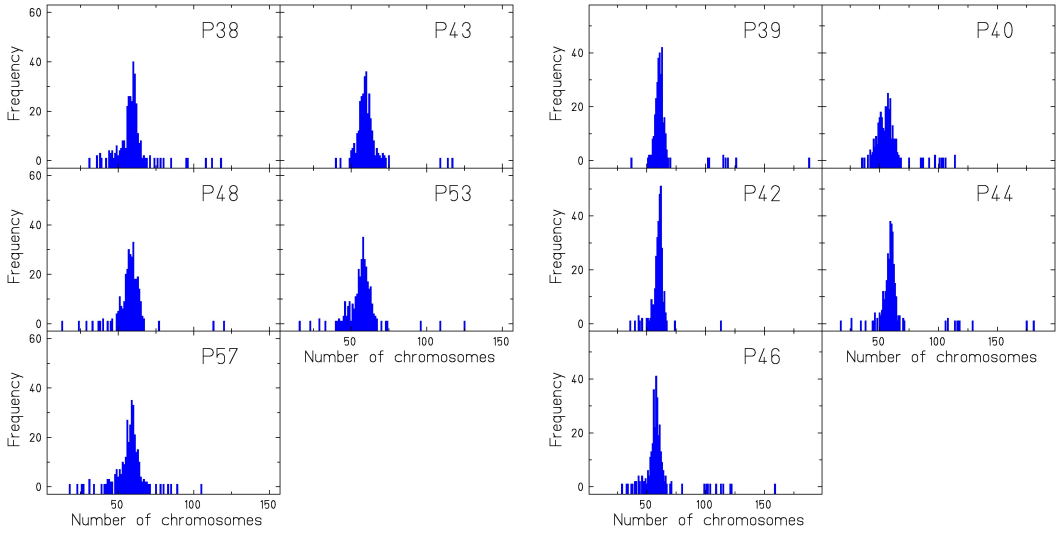

(a) RAT-1 cell batch 1 (b) RAT-1 cell batch 2

Figure 3.4: Histograms of karyotype distribution per metaphase in RAT-1 cells with time in culture. Every small panel is the analysis of 300 metaphases.

sons. For every passage a weighted average chromosome number was calculated. Out of these average chromosome numbers a mean chromosome number for RAT-1 cells was calculated to be 58.9 ± 9.5. Table 3.1 shows the average chromosome numbers beside the corresponding MI. The MI for a passage was determined in 6000 cells, and a weighted mean was calculated. As it can be seen the indexes do not vary essentially and the calculated mean MI was $11.7 \pm 1.1\%$. More details on calculations can be found in section 2.7.

Table 3.1: Analysis of two individual RAT-1 cell batches in different passages. The weighted chromosome number (WCN) with its weighted standard deviation (Δ WCN) was calculated in 300 cells and the mitotic index (MI) with its weighted standard deviation (Δ MI) was determined in 6000 cells.

Passage	**WCN**	**ΔWCN**	**MI** [%]	**ΔMI**
Cell batch 1				
P38	58.8	8.9	9.1	0.9
P43	59.9	7.1	13.2	0.2
P48	57.9	7.8	12.9	0.7
P53	56.8	8.6	13.1	0.8
P57	57.4	8.4	10.3	1.0
Cell batch 2				
P39	62.3	11.4	15.5	3.2
P40	56.4	10.6	6.0	1.3
P42	60.0	5.2	11.1	0.7
P44	60.4	14.5	13.3	0.5
P46	58.8	12.2	12.0	1.3

3.2 Characterization of intestinal epithelial cell line 6

The intestinal epithelial cell line 6 (IEC-6) of the rat is a common model for normal human intestinal epithelial biology [138] (see subsection 1.4.1). After defrosting the subcultivation of ICE-6 cells was done once a week. Figure 3.5 shows the cells three days and seven days after seeding in culture. The cells underlie contact inhibition and start to die and detach after one day growth in a confluent cell layer.
For cell line characterization the doubling time t_D was derived from growth curves. For an explanation of the method see subsection 2.1.5. The resulting graphs are plotted in figure 3.5 and t_D is given for every passage. With time in culture and with increasing passage number t_D decreased from 36 h to 17 h.

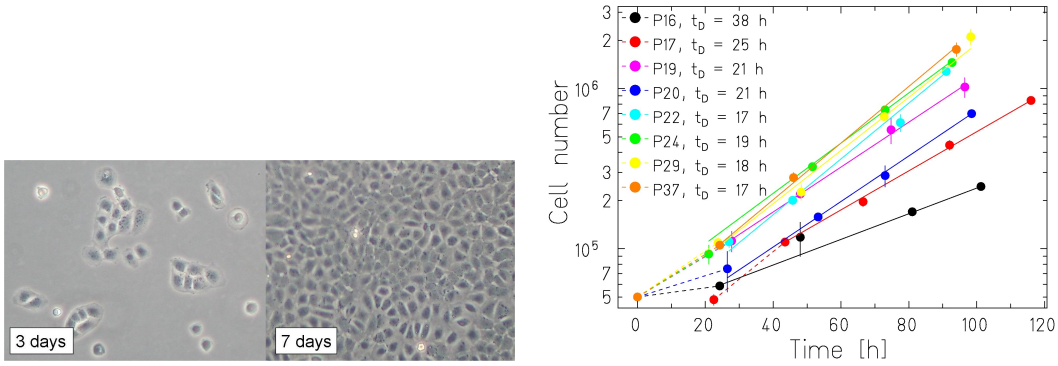

Figure 3.5: Left panel: IEC-6 cells three days and seven days after seeding in culture flasks. Magnification ≈ 20x, **Right panel:** Growth curves of IEC-6 cells in culture flasks. The passage number P and the doubling time t_D is given for each curve.

The cell line was further investigated with a cell cycle analysis. In every second passage (P16, P18, P20, P22, P24) cells were measured according to subsection 2.4.1. In figure 3.6 the cell cycle analysis of two different samples is shown. The upper two panels were prepared with cells in P16 while the lower two panels were cells in P20. It became obvious that the IEC-6 cell culture developed several sub-populations with age. The sub-populations seem not to have integer multiples of the normal DNA content. The peak analysis was not possible since too many sub-populations were present and their peaks overlapped.

Simultaneously the cell cycle distribution of IEC-6 cells in P17 was analyzed in duplicates over five days after mock irradiation and 250 kVp x-ray irradiation which reduced the survival rate to 10% (see figure 3.7). In the first twelve hours after irradiation a G_2-block is induced in the IEC-6 cells. The maximum of the G_2-block occurred after nine hours at which 38% of the irradiated cells accumulated compared to 22% in the control

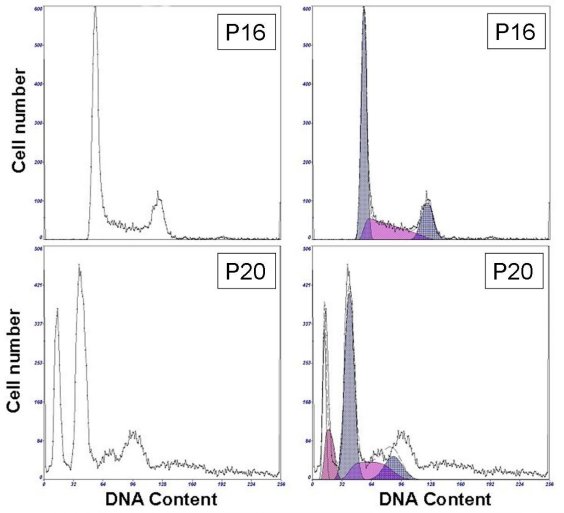

Figure 3.6: Cell cycle distribution of IEC-6 cells in P16 and P20

cells. At later pojnts in time the x-ray irradiated samples were not distinguishable from the control cells. At the end of the observation period 70%of the control cells compared to 60% of the x-ray irradiated cells accumulated in G_1-phase due to limitation of growth area or nutrient in culture flask and an accompaning proliferation stop. Further investigations to analyze the cell cycle were not made because of the developing sub-populations and the concomitant analysis problems.

The cell cycle analysis over several passages leads to the questions of chromosome stability and senescence of the IEC-6 cell line. For identification of senescent cells a X-Gal staining was performed as described in subsection 2.1.7. In sub-confluent IEC-6 cell samples no positive X-Gal staining was found from P16 to P24. In areas of confluent growth a light green staining was partially detected. The weak positive signal was probably induced by contact inhibition of the cells and was not scored.

A chromosome analysis was performed to identify possible sub-populations and to ensure that there were no cross contaminations with other species in the cell line. Figure 3.8 shows two examples of IEC-6 cell metaphases. In figure 3.9 the chromosome analysis of two individual IEC-6 cell batches over several passages is shown. Each small panel represents the analysis of 300 metaphases. The normal karyotype of rat cells (*rattus norvegicus*) is 2n = 42. A mean chromosome number of 42 could only be counted in very early passages (P15 to P18). At later points in time the weighted chromosome number (WCN) increased dramatically but differently in the two cell batches. Table 3.2 shows in detail the changing progression of cells with 42 chromosomes. In both cell batches the percentage of cells with 42 chromosomes decreased rapidly and the amount of cells with more than 42 chromosomes increased dramatically until nearly all cells showed an abnormal karyotype. After P20 a sub-population with 53 chromosomes appeared in both

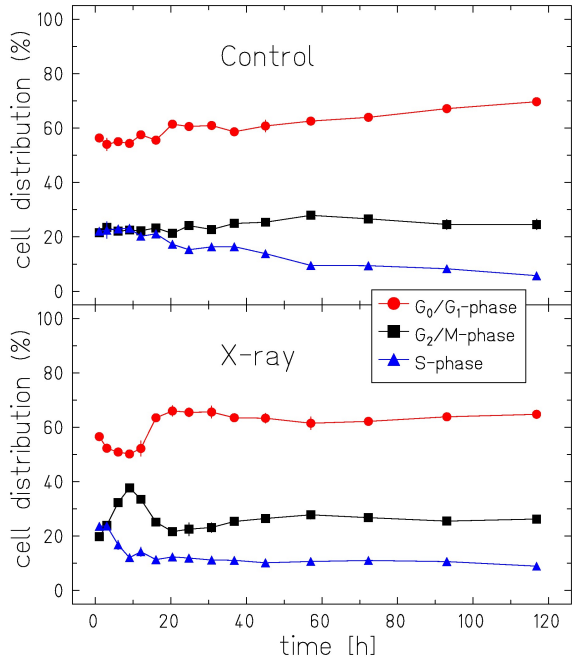

Figure 3.7: Cell cycle distribution of IEC-6 control cells and after 250 kVp x-ray irradiation to 10% survival level in P17, duplicates

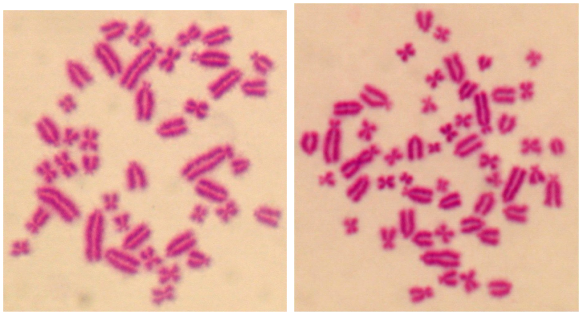

Figure 3.8: Metaphases of IEC-6 cells with 42 (left) and 54 (right) chromosomes, magnification ≈ 700x

batches which might indicate that this karyotype has a growth advantage. Tetraploid cells developed in both batches but with alternating frequency. Due to the weekly passage, a cell selection process takes place which could induce these statistical fluctuations. The cell line seems to have the tendency to develop tetraploid cells. Table 3.2 shows the corresponding mitotic indexes (MI) for the analyzed chromosome samples which increased slowly with culture time in parallel to the abnormal karyotypes. These results show a genetic alteration of the IEC-6 cell line which might have influences on the radio-resistance.

Table 3.2: Analysis of two individual IEC-6 cell batches according to their mitotic index (MI) and weighted chromosome numbers (WCN) with regard to metaphases with 42 chromosomes. For every passage the MI with its standard deviation (Δ MI) was determined in 6000 cells and the WCN with its weighted standard deviation (Δ WCN) was calculated in 300 IEC-6 cells. The last three columns name the percentage of metaphases with 42, less or more than 42 chromosomes at which N is 300.

Passage	**MI** [%]	**ΔMI**	**WCN**	**ΔWCN**	**%N =42**	**%N <42**	**%N >42**
Cell batch 1							
P15	6.5	0.8	42.2	6.9	37.7	32.3	30.0
P19	11.4	0.5	47.4	11.4	15.0	23.7	61.3
P26	8.7	0.8	46.9	7.2	3.3	12.3	84.3
P30	14.7	0.5	47.4	3.1	2.3	4.7	93.0
P34	18.3	0.7	49.6	3.7	1.0	2.0	97.0
Cell batch 2							
P16	6.5	1.1	41.8	3.3	29.3	42.3	28.3
P18	7.3	0.4	42.1	5.4	26.0	44.0	30.0
P20	10.4	0.2	45.7	6.7	17.7	23.7	58.7
P22	15.7	0.6	49.4	6.9	4.3	6.3	89.3
P24	10.9	0.4	63.6	20.0	0.7	2.0	97.3
P26	14.8	0.4	68.3	20.4	2.7	1.7	95.7

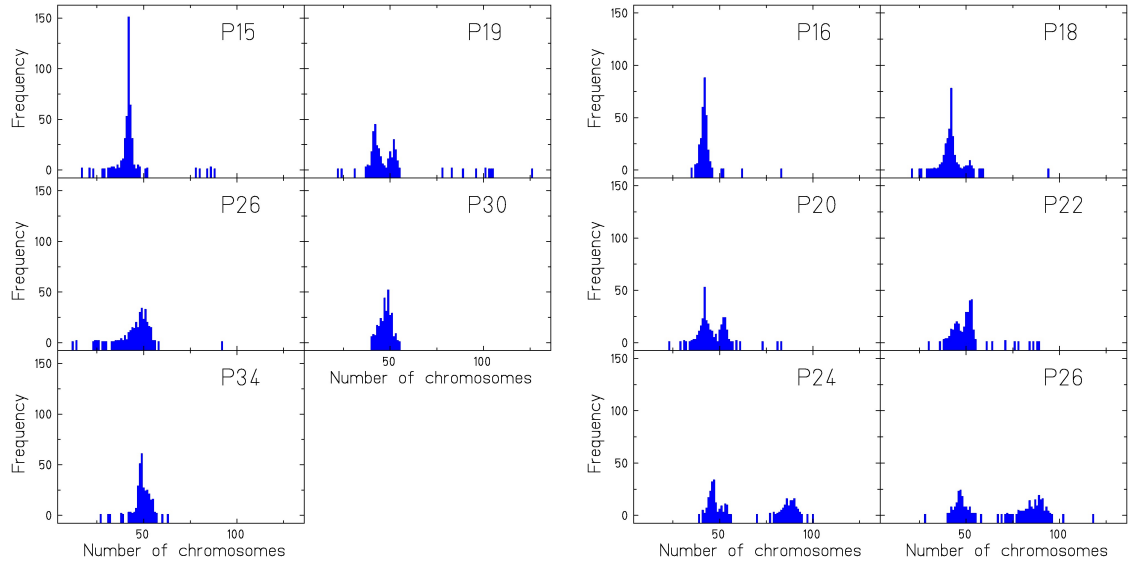

(a) IEC-6 cell batch 1

(b) IEC-6 cell batch 2

Figure 3.9: Histograms of karyotype distribution in metaphases of IEC-6 cells with time in culture indicated by passage number. Each small panel is the result of 300 analyzed metaphases.

3.3 Survival experiments

3.3.1 RAT-1 cells: radio-resistance against 250 kVp x-rays

To determine the radio-resistance of RAT-1 cells against 250 kVp x-ray irradiation the cells were seeded in culture flasks three days prior to the experiment, irradiated with doses between 0 to 10 Gy, and reseeded in culture flasks with expected 100 surviving cells for a colony forming assay. Figure 3.10 shows ethanol fixed and methylene blue stained colonies after eleven days of growth. The morphology of RAT-1 colonies differs even in control samples but in all cases the cells showed an intense blue color. The cell survival rate was calculated as described under subsection 2.1.6 and semi-logarithmically plotted against the dose. Figure 3.11 shows the cumulative x-ray curve (closed circles) of seven individual experiments. The mean α value was calculated to be 0.174 ± 0.052 Gy^{-1} while th mean β value was 0.026 ± 0.010 Gy^{-2} of the cumulative curve. The resulting α/β ratio was 6.8 ± 0.5 Gy which characterizes the cell line as moderately radio-resistant. The mean dose for 10% survival was 7.0 ± 1.4 Gy.

The colony forming assay for RAT-1 cells contained a centrifugation step before the cells were reseeded (see subsection 2.1.6). In figure 3.11 one experiment which was done without centrifugation is shown (curve with open circle). The comparison of the two curves shows that the cell survival rate decreased stepply for high doses when the cells were not centrifuged. This can be explained by the influence of the trypsin in the cell

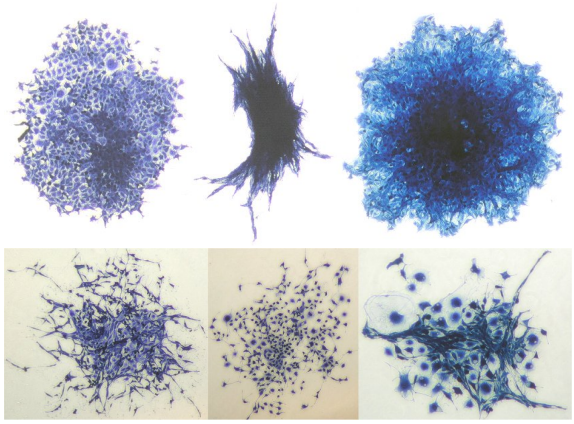

Figure 3.10: RAT-1 cell colonies: ethanol fixated and methylene blue stained, magnification ≈ 10-20x

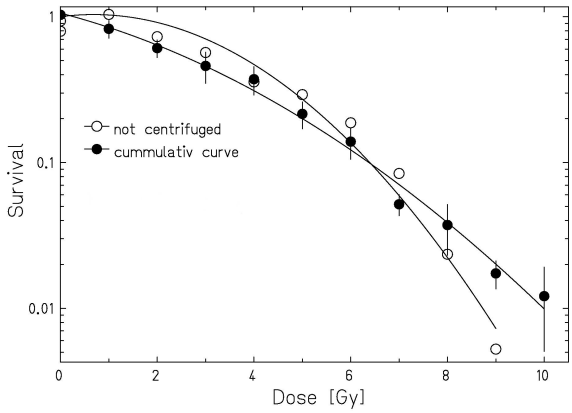

Figure 3.11: Survival curves of 250 kVp x-ray irradiated RAT-1 cell. Closed circle: experiment protocol with centrifugation, n=7, open circle: experiment protocol without centrifugation, n=1

suspension. For high irradiated cells a greater inoculum volume is needed to seed 100 expected surviving cells compared to lower irradiated cell samples. In consequence, a higher concentration of trypsin is retained in the medium for the colony forming assay. The higher trypsin content lead to additional cell death. Therefore, a centrifugation step was needed to remove the trypsin from the cell suspension and to detect only the reduced survival caused by irradiation.

3.3.2 RAT-1 cells: radio-resistance against carbon ions

For irradiation at SIS facility the cells were seeded in culture flasks while for irradiation at UNILAC facility Petri dishes were used for cell seeding. The cell preparation after irradiation was carried out similarly to x-ray experiments. Figure 3.12 shows the cell survival curves of four individual experiments after irradiation with carbon ions of 270 MeV/u, 100 MeV/u, and 11.4 MeV/u, respectively. Table 3.3 shows the corresponding fit pa-

Table 3.3: RAT-1 cells: α and β values as well as ratio α/β and D_{10} of carbon ion survival curves. The values are averages from four individual experiments with standard deviation.

Energy	α **[Gy^{-1}]**	$\Delta\alpha$ **[Gy^{-1}]**	β **[Gy^{-2}]**	$\Delta\beta$ **[Gy^{-2}]**	α/β **[Gy]**	$\Delta\alpha/\beta$ **[Gy]**	$\mathbf{D_{10}}$ **[Gy]**	$\Delta\mathbf{D_{10}}$ **[Gy]**
270 MeV/u	0.197	0.087	0.031	0.011	6.4	0.6	6.02	0.46
100 MeV/u	0.292	0.069	0.034	0.006	8.6	0.3	4.99	0.30
11.4 MeV/u	1.237	0.077					1.87	0.12

rameters of the linear quadratic model. The mean PE of RAT-1 cells were determined to be 0.446 with its standard deviation of 0.113 and its SEM of 0.026 out of all irradiation experiments (n=19).

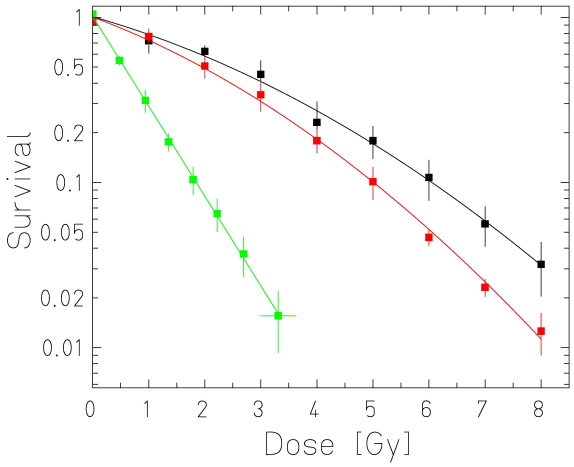

Figure 3.12: Survival curves of RAT-1 cells after carbon ion irradiation with different energies: 270 MeV/u (black), 100 MeV/u (red), and 11.4 MeV/u (green). The mean survival values with their standard deviation are given, n=4.

3.3.3 IEC-6 cells: radio-resistance against 250 kVp x-rays

To determine the radio-resistance of IEC-6 cells against 250 kVp x-ray irradiation the cells were seeded three days before the experiment in 25 cm^2 culture flasks, were irradiated with doses between 0 to 10 Gy, and reseeded in culture flasks with expected 70 surviving cells in a colony forming assay. After eleven days of growth the cells were fixed with ethanol, methylene blue stained, and the colonies were counted manually. The IEC-6 cell colonies showed a uniform morphology and were weakly blue colored (see figure 3.13). Figure 3.14 shows three and four independent x-ray curves, respectively, of two different IEC-6 cell batches (A1, A2). In the left panel IEC-6 cell batch A1 was irradiated in P19, P25, and P28 and in the right panel the IEC-6 cell batch A2 was irradiated

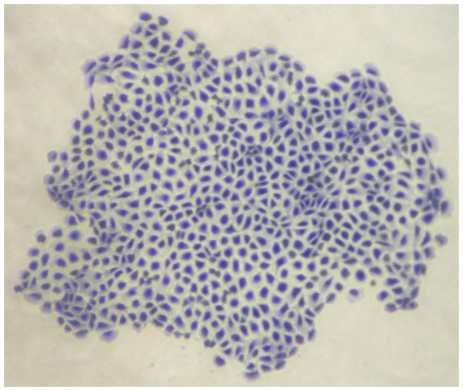

Figure 3.13: Colony of IEC-6 cells: ethanol fixated and methylene blue stained, magnification $\approx$ 20x

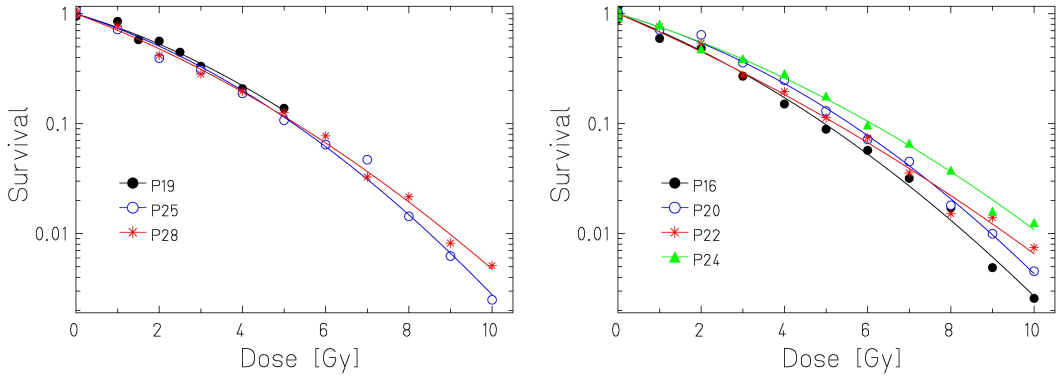

(a) IEC-6 cell batch A1

(b) IEC-6 cell batch A2

Figure 3.14: Survival curve of IEC-6 cells irradiated with 250 kVp x-rays

in P16, P20, P22, and P24. Cell batch A2 increased the radio-resistance with ongoing passage number, while cell batch A1 underwent no changes in radio-resistance. Because of the systematic shift, an average α and β values over all performed irradiation experiments was not calculated. Table 3.4 shows the α and β values of the individual experiments. The α and β values of cell batch A2 do not reflect the increasing radio-resistance. During the experimental phase of this work the cell culture serum was consumed so that new serum batches had to be tested for suitability. In the following the serum batches will be named as I, II, and III in which serum I is the consumed serum and serum II the new standard serum. To test the serum influence the IEC-6 cell batch A6 was split in three parts, and every part was cultivated eight weeks in culture medium with a specific serum. To control the serum effect on the PE, survival and the colony growth, an x-ray survival curve was performed every second week. Figure 3.15 shows the resulting curves. In serum I the IEC-6 cell batch A6 did not develop an increasing radio-resistance with time. In serum II the IEC-6 cells developed a pronounced radio-resistance while in serum III the IEC-6 cells increased their radio-resistance slightly. Interestingly, the cells in serum III did not

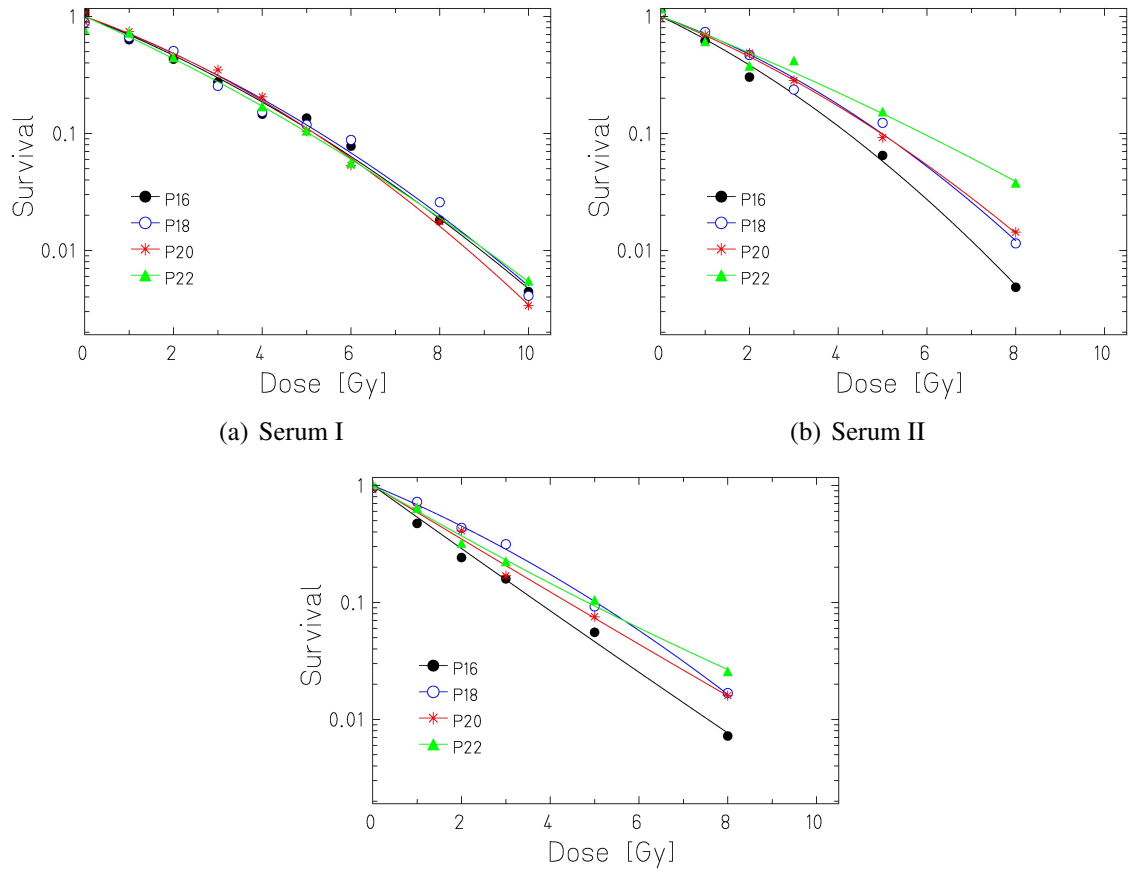

(a) Serum I

(b) Serum II

(c) Serum III

Figure 3.15: Serum test: 250 kVp x-ray survival curves of IEC-6 cell batch A6. The passage and the experiments were performed in culture medium with three different serums.

show shoulder curves. Table 3.4 presents the fit parameters for the x-ray survival curves. In conclusion, IEC-6 cells can, but do not necessarily, develop an increasing radio-resistance with age. A possible reason for this variance is the cell selection in the weekly passage (test hypothesis).

3.3.4 IEC-6 cells: radio-resistance against carbon ions

For carbon ion irradiation at SIS facility the IEC-6 cells were seeded in culture flasks, while for irradiation at UNILA facility Petri dishes were used for cell culturing. After irradiation the cells were trypsinized and reseeded in a colony forming assay with 70 expected surviving cells. The ethanol-fixed and methylene blue-stained colonies were counted and analyzed according to subsection 2.1.6. Figure 3.16 shows the average survival curves over four individual experiments for three different carbon ion energies 11.4 MeV/u, 100 MeV/u, and 270 MeV/u, each. The curves were performed in two beam

Table 3.4: The table presents the α and β values as well as ratio α/β and D_{10} of IEC-6 cell x-ray survival curves in dependency of cell batch and serum batch.

Cell batch	**Serum batch**	**P**	**PE**	α **[Gy^{-1}]**	$\Delta\alpha$ **[Gy^{-1}]**	β **[Gy^{-2}]**	$\Delta\beta$ **[Gy^{-2}]**	α/β **[Gy]**	$\Delta\alpha/\beta$ **[Gy]**	D_{10} **[Gy]**
A1	I	19	0.360	0.260	0.047	0.029	0.010	9.0	0.4	5.5
	I	25	0.481	0.278	0.048	0.031	0.005	9.0	0.2	5.2
	I	28	0.584	0.325	0.033	0.021	0.003	15.5	0.2	5.3
A2	I	16	0.245	0.338	0.042	0.025	0.005	13.5	0.2	5.0
	I	18	0.335	0.498	0.046	0.001	0.005	49.8	29.1	5.1
	I	20	0.451	0.246	0.026	0.030	0.003	8.2	0.1	5.6
	I	22	0.521	0.371	0.046	0.013	0.005	28.5	0.4	5.2
	I	23	0.616	0.341	0.029	0.014	0.003	23.7	0.2	5.5
	I	24	0.627	0.260	0.033	0.019	0.003	13.7	0.2	6.1
A6	I	16	0.248	0.345	0.051	0.019	0.005	18.2	0.3	5.2
	I	18	0.391	0.324	0.074	0.021	0.008	15.4	0.4	5.3
	I	20	0.414	0.312	0.033	0.026	0.003	12.0	0.2	5.2
	I	22	0.273	0.388	0.052	0.013	0.005	29.8	0.4	5.1
A6	II	16	0.207	0.419	0.094	0.030	0.011	14.0	0.4	4.2
	II	18	0.348	0.315	0.102	0.030	0.012	10.5	0.5	5.0
	II	20	0.433	0.350	0.032	0.023	0.004	15.2	0.2	5.0
	II	22	0.231	0.344	0.127	0.008	0.015	43.0	1.9	5.9
A6	III	16	0.277	0.625	0.104	0.002	0.012	312.5	6.0	3.6
	III	18	0.357	0.361	0.051	0.019	0.006	19.0	0.3	5.0
	III	20	0.463	0.530	0.090	0.002	0.011	265.0	5.5	4.3
	III	22	0.256	0.510	0.063	0.007	0.007	72.9	1.0	4.3

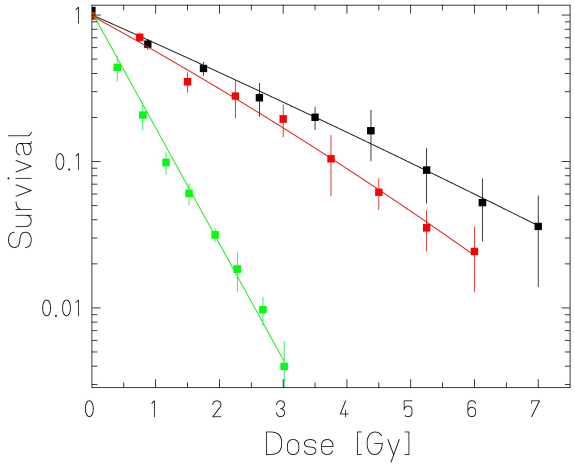

Figure 3.16: Survival of IEC-6 cells after track segment irradiation with 11.4 MeV/u (green), 100 MeV/u (red), and 270 MeV/u (black) carbon ions. The curves are the average over four individual experiments with standard deviation, each.

Table 3.5: IEC-6 cells: α and β values as well as ratio α/β and D_{10} of carbon ion survival curves. The values are averages from four independent experiments with standard deviation.

Energy	α **[Gy^{-1}]**	$\Delta\alpha$ **[Gy^{-1}]**	β **[Gy^{-2}]**	$\Delta\beta$ **[Gy^{-2}]**	α/β **[Gy]**	$\Delta\alpha/\beta$ **[Gy]**	$\mathbf{D_{10}}$ **[Gy]**	$\Delta\mathbf{D_{10}}$ **[Gy]**
270 MeV/u	0.439	0.038	0.008	0.008	54.9	1.0	4.95	0.74
100 MeV/u	0.551	0.144	0.007	0.040	78.7	5.7	4.19	1.14
11.4 MeV/u	1.804	0.064					1.25	0.09

times. The variances between curves of one beam time were very small but the differences between the beam times were only slightly more pronounced. The differences are significant at higher doses where the spread of colony numbers per culture flasks varies essentially. Independent of the irradiation modality in every colony forming assay a PE has to be determined. The calculated PE of fitted IEC-6 cell survival curves is presented in figure 3.17. The blue points display the PE which was determined in culture medium with serum I, the red points in medium with serum II, and the green points in medium with serum III. From the scattered plot, a strong influence of the serum on the PE can not be deduced. In all tested serums the IEC-6 cells increased their PE with the weekly passage. This effect seems to be limited since the PE passes into a plateau. A curve was not plotted due to insufficient data with higher passage numbers.

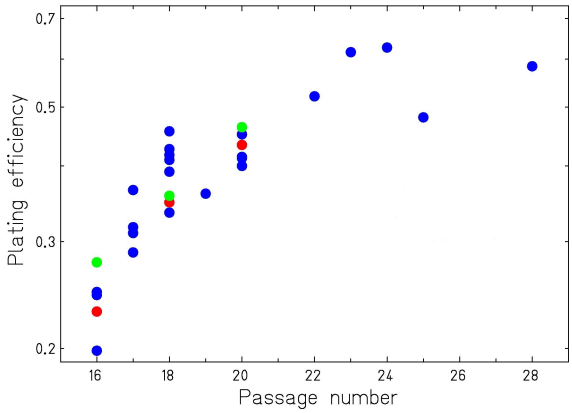

Figure 3.17: The PE of IEC-6 cells determined in culture medium with serum batch I (blue points), serum batch II (red points), and serum batch III (green points) is plotted against the passage number, which were done weakly.

3.3.5 Relative biological effectiveness (RBE)

The RBE was calculated according to section 1.2 and section 2.7. In figure 3.18 the RBEα and the RBE_{10} for IEC-6 cells and RAT-1 cells are plotted against the LET of the particle beam or against the residual range in water of the carbon ions. The physical parameters of the carbon beam are given in table 3.6. The RBE increases with increasing LET and decreasing residual range of the carbon ions. For high energy, representing the entrance channel, the RBE is close to one which means that the normal, tumor surrounding tissue is not further damaged through the use of carbon ions in comparison to photon irradiation. The RBEα of RAT-1 cells increased more pronounced than that of IEC-6 cells which is due to the steep survival curve after 11.4 MeV/u carbon ion irradiation. This indicates that carbon ions are well suited for the inactivation of the prostate cancer cell line.

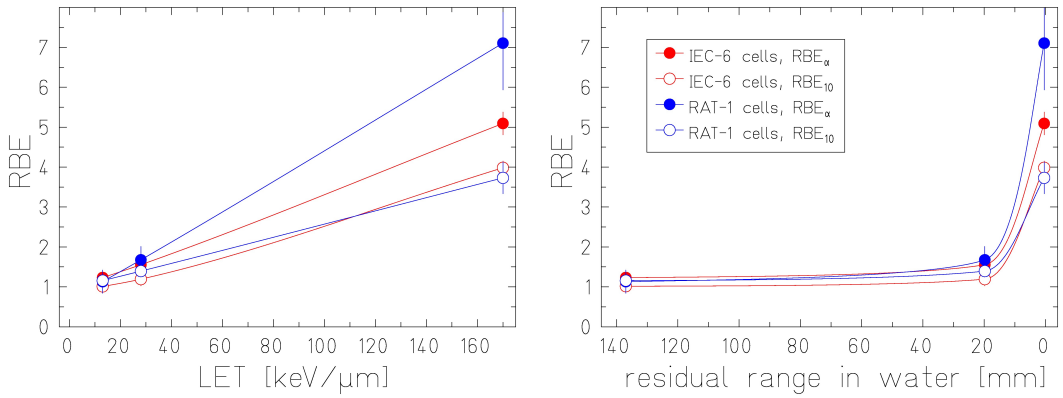

Figure 3.18: RBEα and RBE_{10} of IEC-6 cells and RAT-1 cells are plotted in the left panel against the LET and in the right panel against the residual range in water of the carbon ions. The RBE values are calculated out of the averages over four independent carbon experiments and seven (RAT-1 cells) and sixteen (IEC-6 cells) independent x-ray experiments, respectively.

Table 3.6: The table displays the physical beam parameters of the used carbon ion beams.

Energy [MeV/u]	LET [keV/μm]	Residual range in water [mm]	Correspondence to clinical application
270	13	137	entrance channel
100	28	19.8	close to tumor
11.4	170	0.41	tumor volume

3.4 Identification of sub-populations and clones in IEC-6 cell culture

3.4.1 Chromosome analysis with mFISH

The chromosome analysis in section 3.2 shows that the IEC-6 cells develop an aneuploid karyotype within a few weeks in culture. To identify the additional chromosomes a chromosome analysis with mFISH was done (see subsection 2.2.1). A complete mFISH kit for all chromosomes is only commercially available for human and mouse samples. Since the genetic relationship is close and the chromosome profile of mice (2n=40) is more similar to rats, a mouse mFISH was used on rat chromosomes. For the chromosome preparation IEC-6 cells in P22 were used to achieve a wide spectrum of karyotypes. It was expected to find sections of IEC-6 cell chromosomes stained like bands in which the chromosomes of the rat and the mouse match. The staining with TR, SpO, and DEAC went well, the hybridization with FITC-linked probes was diminished and nearly no labeling with Cy5 was found. In the first analysis step the chromosomes were manually arranged along their shape and size in the DAPI image. Based on the false colors, the arrangement was corrected in a second step. Figure 3.19 shows a mFISH stained metaphase with 52 chromosomes which is presented in the left panel in DAPI counter staining and in the right panel in false colors. The red circle demonstrates that chromosomes which are clearly of the same size and shape in DAPI staining were not necessarily displayed in the same false colors. In contrast, the green circle shows that chromosomes illustrated with the same false colors do not match in size and shape. It becomes obvious that a mouse mFISH is not suitable for the analysis of rat chromosomes. Due to missing mFISH alternatives or other high throughput methods the identification of the additional chromosomes was not followed up.

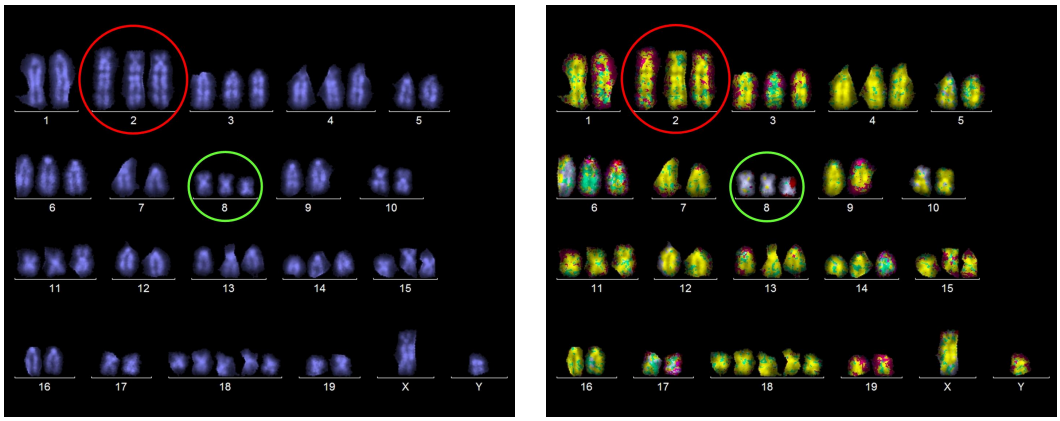

(a) Metaphase displayed in DAPI counter staining

(b) Metaphase displayed in false colors

Figure 3.19: Application of mouse mFISH on IEC-6 cells in P22. Shown is a metaphase with 52 chromosomes. Magnification ≈ 700x

3.4.2 Existence of radio-resistant IEC-6 sub-populations

The combination of increasing radio-resistance and PE, karyotype changes but decreasing doubling time suggests that a dominant sub-population of IEC-6 cells is responsible for these developments. Therefore, the IEC-6 cell batch A3 was sub-divided at P18 in three parts. One part was mock irradiated, one part was irradiated with 5 Gy of x-rays, and the last part was irradiated with 1.25 Gy of 11.4 MeV/u of stopping carbon ions. The irradiation did not only reduce the cell survival rate to 10% but also should deactivate especially the possible radio-sensitive sub-population. Two radiation qualities were tested because of the different damage characters which might generated other clones. After irradiation, the IEC-6 cells were trypsinizied and reseeded in culture flasks with a growth area of 75 cm ^{2}. In the weekly passage the total cell number was determined, added on the total cell number of the week before, and fitted against the passage number after irradiation (see figure 3.20). The plot allows a comparison of the growth rates and replaces the time consuming growth curves. Through the irradiation no changes in the growth characteristics of the IEC-6 cell cultures were observed. The lower cell number in the control samples at 21 days and 28 days after irradiation might be a mistake in the calculation of total cell number since later points in time show a good agreement with the x-ray and the carbon ion irradiated cell samples. The diminished slop of the curves after 40 days is not due to a limited growth area since the cell samples were reseeded weekly. It might be that the IEC-6 cell batch A3 underwent differentiation or senescence and slowed down its doubling time.

Every second week a chromosome preparation of all cultures was done to identify possible

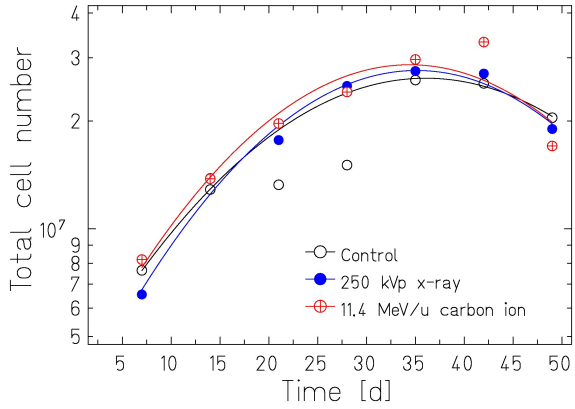

Figure 3.20: The total cell number of mock, 250 kVp x-ray, and 11.4 MeV/u carbon ion irradiated IEC-6 cells plotted against the time in days after irradiation.

developing sub-populations in the irradiated samples compared to the control cultures. Figure 3.21 presents the karyotypes of 300 analyzed metaphases for passage and sample. Independent of the radiation quality the reduction to 10% surviving cells did not induce the formation of different sub-populations compared to control cells. In all cases two sub-populations with similar mean chromosome numbers developed and the amount of tetraploid cells was low. The small variations between the cases are due to statistical reasons.

In figure 3.22 the weighted chromosome number (WCN) and the mitotic index (MI) are given for each passage and sample at which the data corresponds to the chromosome analysis in figure 3.21. As expected from the chromosome histograms the WCN increased all three samples with cultivation time. In parallel the MI increased with ongoing passage numbers as well. The slight decrease or stagnation of MI in P26/P8 might be due to reduced cell growth which was detected in figure 3.20 of the total cell numbers. In addition, figure 3.22 shows an overview over the existence of IEC-6 cells with the normal (*rattus norvegicus*) karyotype of 42, more than 42 or less than 42 chromosomes. The number of cells with the normal karyotype (2n=42) decreased with ongoing passage numbers. This process seems to be slower in unirradiated control cells compared to irradiated cells, whereas no differences between x-ray or carbon ion irradiation can be detected. At the end of the cultivation period, in all three cultures the percentage of cells with 42 chromosomes was below 5%. The IEC-6 cell batch A3 seemed to undergo differentiation or senescence. But with these results the observed increasing radio-resistance in cell batch A2 and A6 can not be explained.

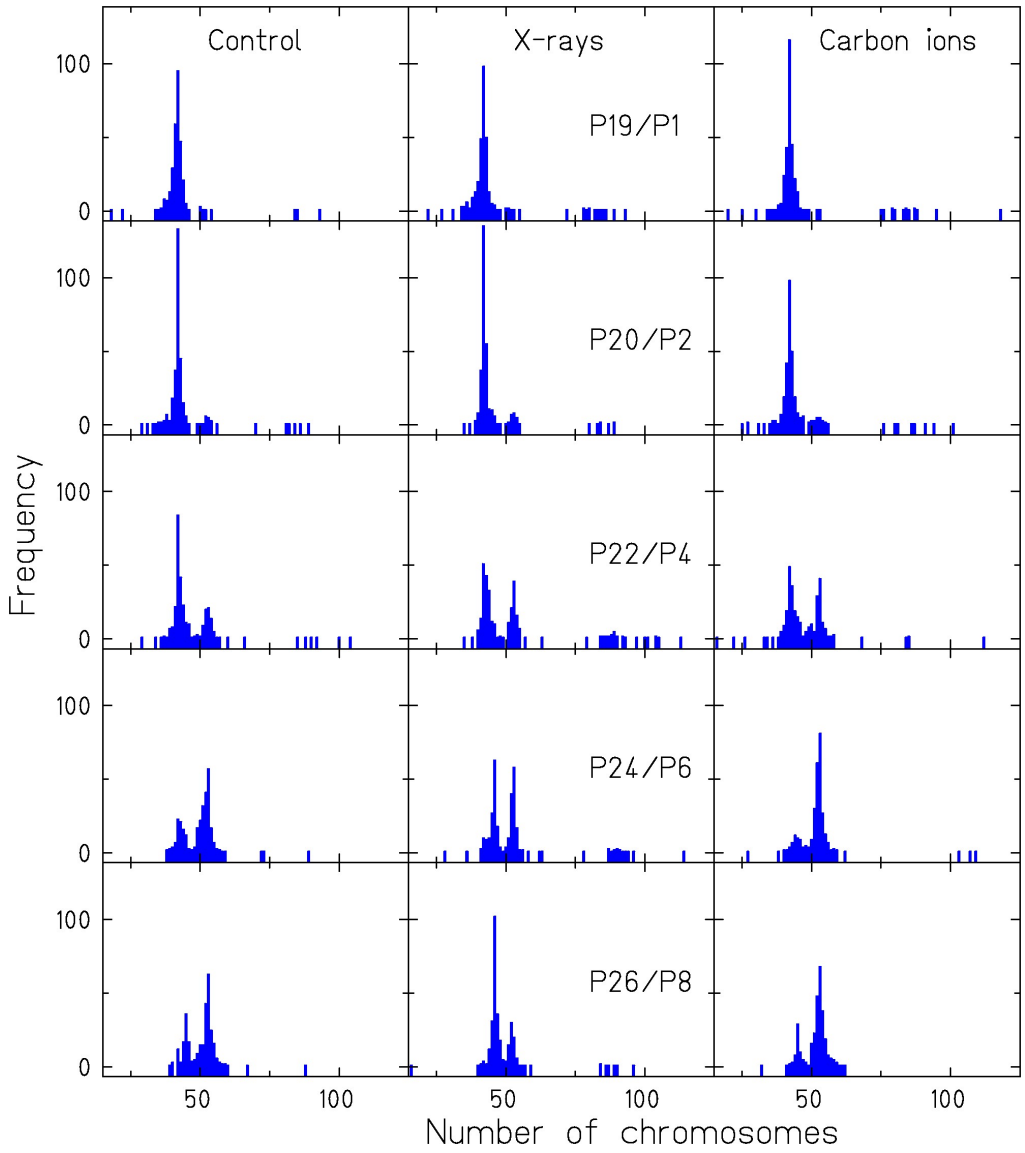

Figure 3.21: Karyotype histograms of IEC-6 control cells and after 250 kVp x-ray or 11.4 MeV/u carbon ion irradiation. Analysis was performed at several passages whereas the first P means the real passage and the second P means the passage after irradiation. Every small panel is the result of 300 analyzed metaphases/ passages and samples.

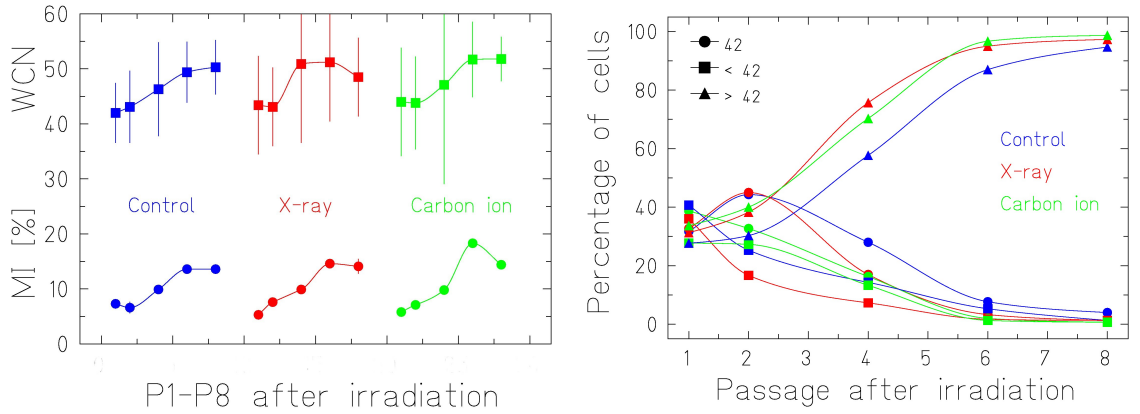

(a) WCN and MI [%] (b) 42, <42 or >42 chromosomes

Figure 3.22: Left panel: WCN (square) and MI (circle) of IEC-6 cells. Control cells, x-ray and carbon ion irradiated samples in passage P19/P1, P20/P2, P22/P4, P24/P6, and P26/P8. WCN was calculated in 300 IEC-6 cells and MI was determined in 6000 IEC-6 cells. Both values are given with their standard deviation. **Right panel:** Progression of IEC-6 control cells, x-ray and carbon ion irradiated cells with 42, less than 42, and more than 42 chromosomes.

3.4.3 Analysis of IEC-6 single cell colonies

The analysis of IEC-6 cells exposed to x-rays and carbon ions which reduced the survival rate to 10% could not clarify whether there are radio-resistant sub-populations or not. The isolation and analysis of IEC-6 clones should answer the question if there are single clones with a higher radio-resistance. The clones were isolated in P23 (cell batch A3) and P17 (cell batch A4) and were characterized for their karyotype and mitotic index. From cell batch A3 it was possible to isolate and propagate 16 clones from which twelve clones had 53 chromosomes, one clone with 44, 45, 54, or stable 91 chromosomes, respectively. From IEC-6 cell batch A4 ten clones could be cultured whereas four clones with 42 chromosomes, four clones with 43 chromosomes, and one clone with 45 or 88, respectively, were isolated. The IEC-6 culture age accompanied by the changes in chromosome profile was the crucial factor for the different karyotypes of the isolated clones. Six clones were analyzed over eight weeks concerning their karyotype, mitotic index, PE, radio-resistance, and growth rate. An overview over the isolation characteristics of the analyzed clones is given in table 3.7.

From the total cell numbers per passage a “doubling time” was determined. Figure 3.23 clearly shows that an increased chromosome number leads to a faster cell doubling. But clones with identical chromosome numbers and especially clones with normal karyotype did not show similar cell doubling times.
X-ray survival curve was performed in every second week to determine the PE and the radio-resistance and were plotted in figure 3.24. For none of the clones a changing radio-

Table 3.7: Overview over analyzed IEC-6 cell clones.

Clone code	Clone No.	Karyotype	MI [%]
1B3	1	45	8.02
1C3	2	53	5.56
IB3	3	42	11.74
ID3	4	42	3.62
2A3	5	53	14.09
4B2	6	44	9.43

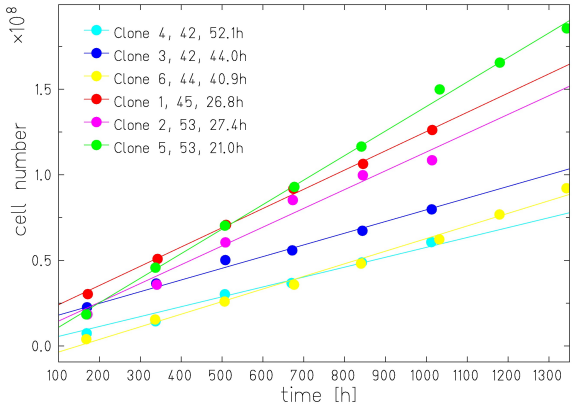

Figure 3.23: Cell growth of six IEC-6 clones: In every passage 4 x 10^5 cells were seeded. The total cell number of the harvest cells were determined and added on the total cell number of the week before. The slop of the linear fit could be considered to be a cell doubling time.

sensitivity with age is detectable out of the survival curve progression. By comparing the doses for 10% survival a slightly decreasing radio-resistance for clone 2 and a slowly increasing radio-resistance for clone 1, 5 and 6 were determined. The D_{10} stayed rather constant for clone 3 and 4. The small changes in radio-resistance were not recognizable in α and β values. The PE of clone 1-4 deviated while that of clone 5 strictly increased from 44% to 59% in four passages. Clone 6 showed no change in PE. The data are summarized in table 3.8.

In parallel to the x-ray curves, chromosome preparations were done to control the stability of the karyotype, the mitotic index, and to bring possible changes in radio-resistance into context. Compared to isolation characteristics of the analyzed clones, presented in table 3.7, escalated the MI of clone 2 from 5.6% to 12.0% but during the period of investigation the MI was stable. The huge differences in the MI values indicate that at the characterization point the cell culture of clone 2 was not in the exponential phase of growth, and the proliferation was reduced. The MI of clone 3 stayed stable, while the

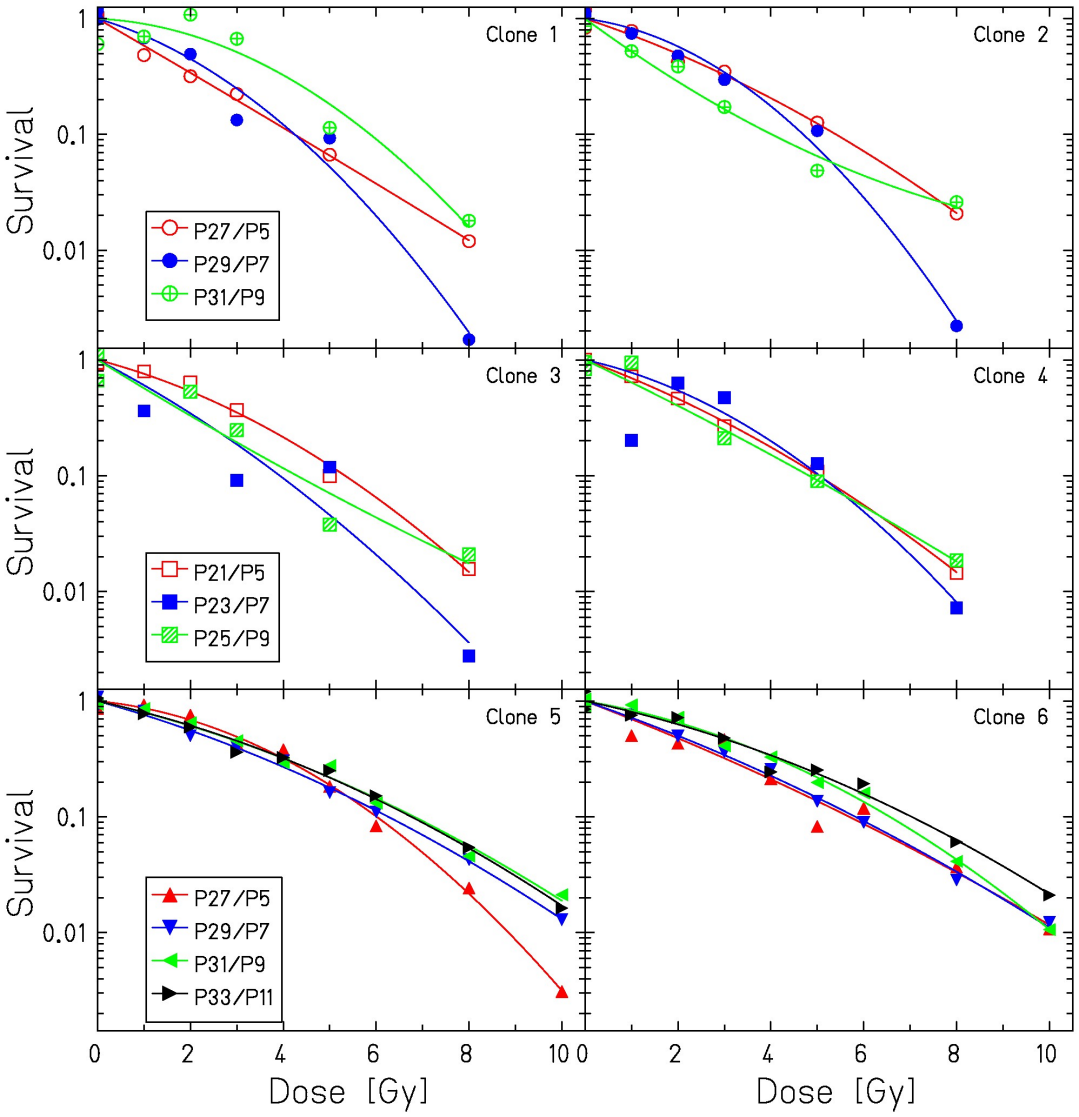

Figure 3.24: IEC-6 clones: survival curves after 250 kVp x-ray irradiation. The passage number indicates the real passage as well as the passage after isolation and is valid for both panels in a row.

Table 3.8: IEC-6 clones: PE, α/β ratio, and D_{10} of 250 kVp x-ray survival curves. The values are averages with their standard deviation as percentage. Clone 1-4: n=3, clone 5+6: n=4

Clone	**PE [%]**	**ΔPE [%]**	**α/β [Gy]**	**$\Delta\alpha/\beta$ [%]**	**D_{10}**	**ΔD_{10} [%]**
1	25.9	52.5	90.7	168.4	4.8	19.9
2	42.1	42.2	13.6	87.4	4.4	28.3
3	27.8	46.4	31.5	110.8	4.3	19.1
4	27.2	19.0	27.1	116.3	4.9	2.3
5	50.6	12.9	9.2	57.0	6.4	6.0
6	39.3	3.9	19.7	78.0	6.3	9.8

Table 3.9: IEC-6 clones: analysis of karyotype. The mitotic index (MI) was determined in 6000 cells with its standard deviation as a percentage (ΔMI [%]) and the weighted chromosome number (WCN) was calculated in 150 cells with its standard deviation as a percentage (ΔWCN [%]). Clone 1-4: n=3, clone 5+6: n=4

Clone	MI [%]	ΔMI [%]	WCN	ΔWCN [%]
1	10.5	24.7	46.0	0.9
2	12.0	6.6	52.2	3.3
3	10.6	9.9	44.2	2.6
4	8.4	20.9	45.6	5.8
5	10.8	18.6	55.1	0.9
6	8.1	39.1	45.7	0.4

MI of clone 1 and 4 increased. Clone 5 and 6 were isolated with a relatively high MI but directly after defrosting the MI was dramatically reduced to 8.5% and 4.0%. With ongoing passages both clones reached the MI of the isolation. It is possible that the growth was restricted by recovery from the frosting process. The MI could be determined in all samples with a deviation of 8.6%.
For the analysis, only clones were used which had stable chromosome numbers at the characterization point so that the determined values could be considered as 100% values. After six weeks in culture the karyotype of all clones except clone 2 had changed. Only clone 2 kept the original chromosome profile with slightly lower chromosome numbers. This could be due to sample preparation. The other clones increased their chromosome numbers. In conclusion, the majority of IEC-6 cells tended to increase their chromosome numbers and population doubling times. The cells change the MI and PE, also.

3.5 Co-culture

Clonogenic survival assays with co-cultured IEC-6 cells and RAT-1 cells were grown together in one culture flask. The colony forming assay protocol for both cell lines is identical so that no changes had to be done. The discrimination between the two cell types causes no problems since cell and colony morphology differs essentially as well as the staining properties with methylene blue. In the majority of cases the colonies have no direct cell to cell contact in the culture flask. The co-culture colony examples in figure 3.25 show that a cell line differentiation was still possible when colonies overlap or intermingle. RAT-1 cell colonies were not affected by co-culturing while the colony

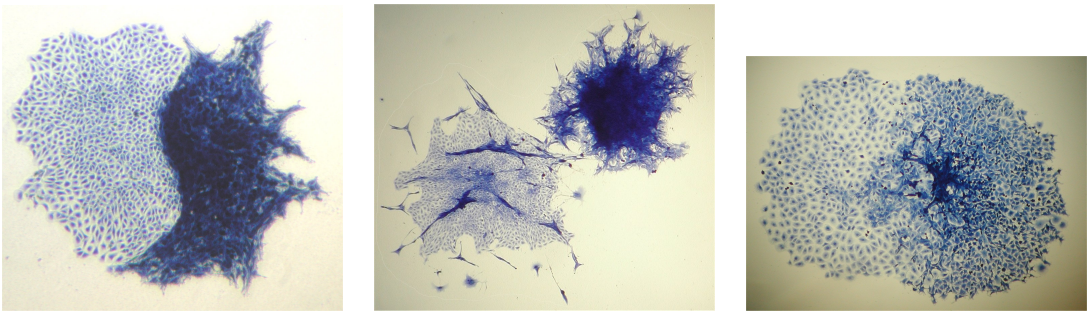

Figure 3.25: Co-culture colonies: in all panels are IEC-6 cells on the left side and RAT-1 cells on the right side, ethanol fixated and methylene blue stained, magnification ≈10x

Table 3.10: The table presents the number of performed experiments which were carried out with method P and method T as well as serum I and serum II. If not further specified, the cells were irradiated with 1, 3 or 6 Gy (RBE) of 250 kVp x-rays or carbon ions (100 MeV/u or 11.4 MeV/u).

Method	**Serum batch**	**250 kVp x-rays**	**100 MeV/u ^{12}C**	**11.4 MeV/u ^{12}C**
P	I	5	0	0
T	I	2, (only 3Gy)	2, (only 3Gy)	2, (only 3Gy)
T	II	5	1	1

size of IEC-6 cells increased, especially in the unirradiated controls, as found by visual examination.

3.5.1 Survival experiments

In the following paragraph, the question should be answered if co-culture conditions change the radio-sensitivity of the used cell lines RAT-1 and IEC-6. The survival experiments were performed with two different set-ups (method P and method T, see subsection 2.1.3) and two fetal calf serum batches (serum I and serum II). Table 3.10 shows an overview of the performed experiments. Independent experiments were summarized when serum and methods are identical. If only one experiment was performed, an error calculation was done as described under subsection 2.7.1 and the columns were marked with a cross. In the following all experimental data are plotted as a percentage to the corresponding average PE.

In general, the co-culture survival data did not show reproducible results for method P and method T as well as for serum I and serum II. In addition, method P seems to be more

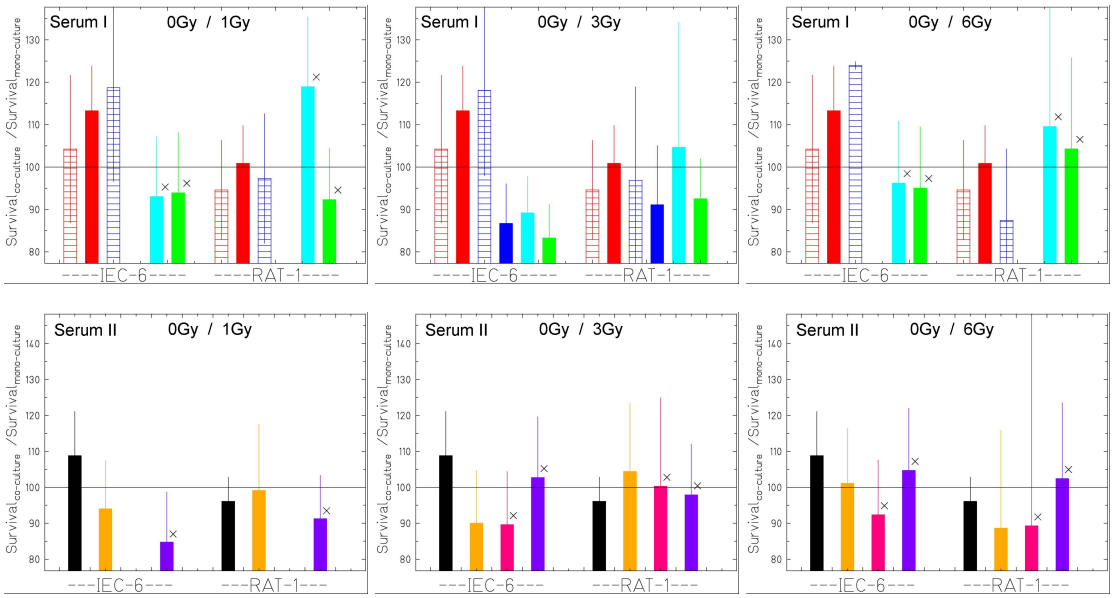

Figure 3.26: Co-culture serum I + II: 0 Gy IEC-6 cells + irradiated RAT-1 cells.
Stripped columns: method P, full columns: method T, cross: error calculation, no mark: mean values with standard deviation, **on top**: PE: red, 250 kVp x-ray: blue, ^{12}C 100 MeV/u: cyan, ^{12}C 11.4 MeV/u: green, **on bottom**: PE: black, 250 kVp x-ray: orange, ^{12}C 100 MeV/u: pink, ^{12}C 11.4 MeV/u: violet

subjected to errors and the results are therefore questionable. Overall, RAT-1 cells might not be as much influenced by co-culturing as the IEC-6 cells are. Nevertheless, for some co-culture combinations a trend could be extracted. First, independent of the serum the PE_{co} for IEC-6 cells is above 100%. This effect was especially noticeable with method T. With method P the effect was not so pronounced but still higher than the PE_{mono}. The PE_{co} for RAT-1 cells is not influenced by the co-culture with unirradiated IEC-6 cells. The PE_{co} is around or below 100%, independent of the serum or the method. Second, unirradiated IEC-6 cells have serum independent with method T no further benefit when the cells are combined with irradiated RAT-1 cells. Moreover, the survival rate was decreased for lower doses. The RAT-1 cells in this combination are unaffected except cells irradiated with 100 MeV/u and cultured in serum I (see figures 3.26). These cells slightly increased their survival rate with increasing dose. Third, in the inverse combination the unirradiated RAT-1 cells showed a LET- and dose-dependent benefit of the irradiated IEC-6 cells in serum II but RAT-1 cells grown in serum I did not show an influence. Irradiated IEC-6 cells in serum I showed a correlation between dose and survival for 100 MeV/u carbon ions but an inverse correlation for 11.4 MeV/u carbon ions. For carbon irradiated cells grown in serum II no clear tendency can be detected. For both serums the x-ray irradiation especially with 3 Gy seems to enhance survival (see figure 3.27). Fourth, when both cell lines are irradiated the RAT-1 cells showed no influence but the IEC-6 cells increased

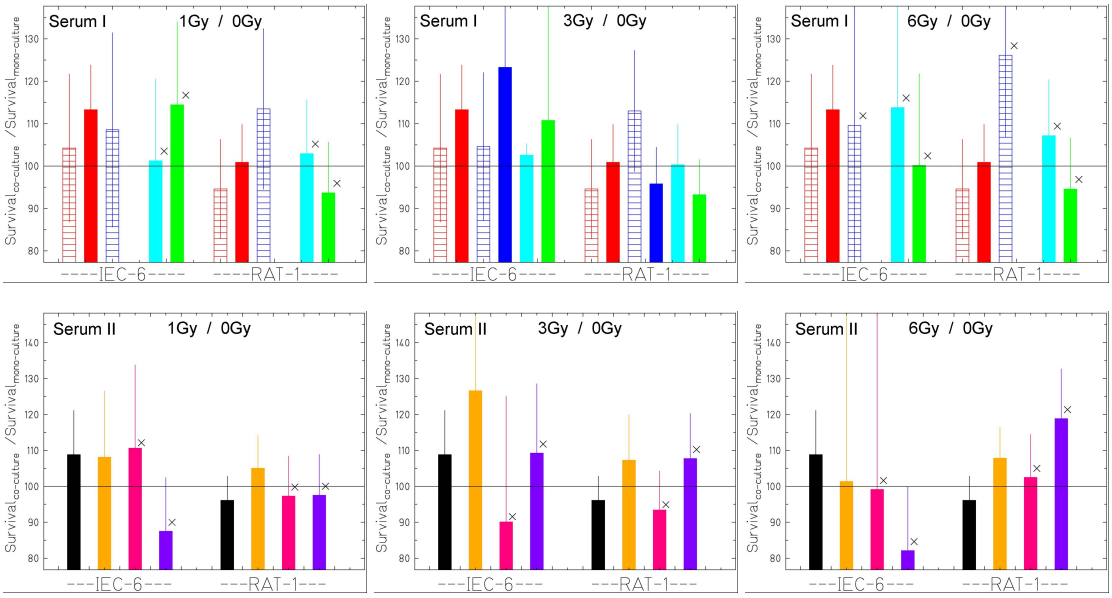

Figure 3.27: Co-culture serum I + II: irradiated IEC-6 cells + 0 Gy RAT-1 cells.
Stripped columns: method P, full columns: method T, cross: error calculation, no mark: mean values with standard deviation, **on top**: PE: red, 250 kVp x-ray: blue, ^{12}C 100 MeV/u: cyan, ^{12}C 11.4 MeV/u: green, **on bottom**: PE: black, 250 kVp x-ray: orange, ^{12}C 100 MeV/u: pink, ^{12}C 11.4 MeV/u: violet

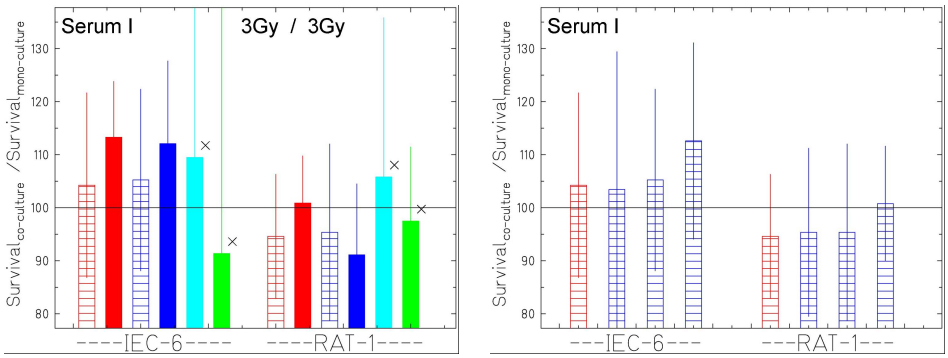

(a) Both cell lines 3 Gy (RBE) of x-ray or carbon ions

(b) Both cell lines 1, 3 or 6 Gy of x-rays

Figure 3.28: Co-culture serum batch I: irradiated IEC-6 cells + irradiated RAT-1 cells. Stripped columns: method P, full columns: method T, cross: error calculation, no mark: mean values with standard deviation, PE: red, 250 kVp x-ray: blue, ^{12}C 100 MeV/u: cyan, ^{12}C 11.4 MeV/u: green

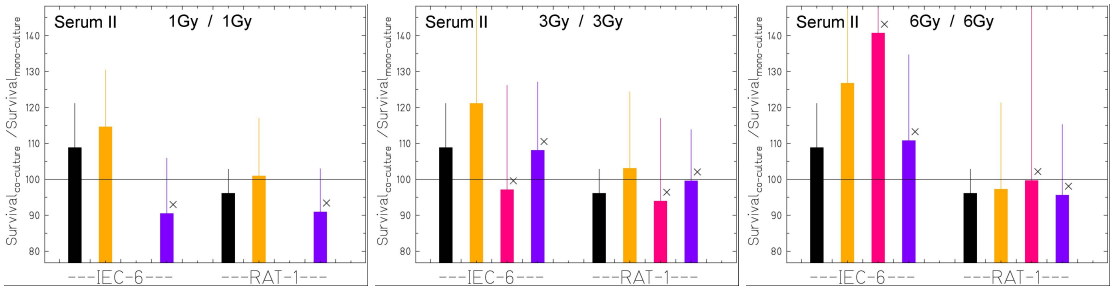

Figure 3.29: Co-culture serum II + method T: irradiated IEC-6 + irradiated RAT-1 cells. Cross: error calculation, no mark: mean values with standard deviation, PE: black, 250 kVp x-ray: orange, ^{12}C 100 MeV/u: pink, ^{12}C 11.4 MeV/u: violet

their survival rate in a dose-dependent manner in both serums. A LET dependency is not detected (see figure 3.28 and 3.29).

3.5.2 Cytokine measurements

The cytokine measurements in cell culture supernatants should explain the detected effects in co-culture survival experiments. Here the cells have almost no direct cell to cell contact so that the effect inducing substance should be a soluble factor which is mediated via the culture medium. Since the survival experiments are carried out in medium with serum the cytokine measurements are conducted in serum containing medium as well. Due to the limited accessibility of serum I the cytokine experiments could only be performed in medium with serum II. The 6-well plate/insert system was used for cytokine detecting experiments. Here one cell line was grown in the Petri dish and the second cell line in the insert. By the use of this system the direct cell to cell contacts are excluded. These contacts are important for cell to cell communication with molecules much smaller than cytokines. If the cytokine production is induced by small molecules, these direct cell to cell contacts would be important for the co-culture effect as well. To investigate the influence of the direct contact, the experiment was carried out with both cell lines growing in the same Petri dish.
The amount of measured cytokine in the cell culture supernatants has to be related to the number of cells. This allows a conclusion about the secreted cytokine amount per cell and a comparison of different experiments. When both cell lines were in one cell suspension, it was not possible to count the cell number of each population separately because of congruent cell histograms in the coulter counter, so that only the total cell number could be determined. This has been circumvented by fluorescent staining with PKH67 of one cell line involved. In a flow cytometer the percentage of stained cells to unstained cells could be determined, and the obtained percentage could be converted into real cell numbers with

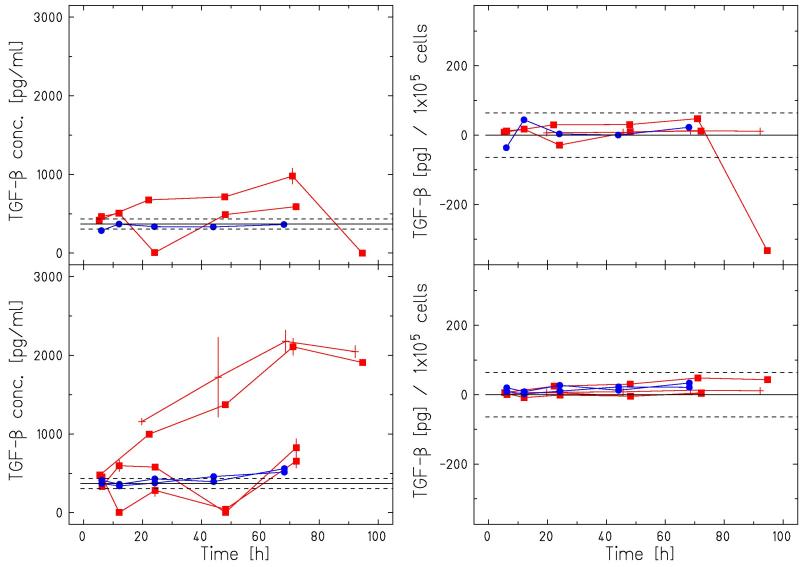

Figure 3.30: TGF-β measurements: Insert versus Petri dish. Mono-culture of 6 Gy (RBE) irradiated IEC-6 cells grown in inserts (on top) or Petri dishes (on bottom). 250 kVp x-ray experiment: red, 11.4 MeV/u carbon ion experiment: blue, cross: PKH67 stained cells, horizontal line: TGFβ content of the culture medium. **Left panels:** Total among of TGFβ in the sample adjusted for the serum level; **Right panels:** TGFβ content normalized to 1 x 10^5 cells.

the total cell number of the coulter counter result.

The cells were irradiated with 11.4 MeV/u carbon ions and 250 kVp of x-rays. The analyzed cytokines TGFβ, TNFα, and IL-2 were selected due to their inflammatory effects *in vivo* and *in vitro* (see section 1.5 and 4.3.4).

IEC-6 cells showed a noticeable increase in adhesion and growth in Petri dishes compared to inserts while RAT-1 cells were less affected by the growth support. Unirradiated IEC-6 cells increased their growth in Petri dishes by a factor of 1.62, irradiated IEC-6 cells by a factor of 1.26, and unirradiated RAT-1 cells as well as irradiated RAT-1 enhanced the growth by a factor of 1.09 and 1.05, respectively.

In the cell culture supernatants of all co-culture combinations and in the used cell culture medium with serum (without cells) no TNFα or IL-2 could be measured. The possible source of TNFα and IL-2 would have been the IEC-6 cells which are able to secret both cytokines which was shown with LPS-stimulation [87]. Obviously the co-culture conditions did not activate the same pathway as the LPS stimuli and did not induce TNFα or IL-2 secretion.

The cytokine experiments were carried out in serum containing medium. Serum is known to comprehend high amounts of TGFβ. Therefore, it was expected to detect high levels of TGFβ in the medium. The analysis of the TGFβ amount in serum containing medium (without cells) over the experiment period of maximum five days were determined to be stable 460 $\pm$ 18 pg/ml. This means that TGFβ is not degraded by incubation at 37°C and

that changes in the measured TGFβ amount are cell induced.
The TGFβ in the supernatants needs to be activated by incubation 5 parts supernatant with one part 1 N HCl (ELISA protocol, manufacturer's instruction). Without activation active TGFβ was only found in samples which were grown for four or more days and reached cell numbers above $\approx$ 3 x 10^5 cells. Under these conditions the medium pH changed to lower values indicated by color shift of pH indicator phenol red in the medium. It is assumed that through the cultivation time of four days and the increased cell numbers the accumulation of metabolites in the medium was enhanced. The increased amount of metabolites decreased the pH which induced a partial activation of TGFβ. The measured active TGFβ is therefore a reaction on the culture conditions and not on the co-culture or the irradiation.
The figures 3.30 and 3.31 show in the left panels the measured TGFβ amounts in cell culture supernatants and in the right panels the TGFβ amount adjusted to 1 x 10^5 cells. The measured TGFβ amounts suggest huge differences between the experiments in which the measured TGFβ levels increased with time all experiments. The adjustment of the TGFβ amount to 1 x 10^5 cells reveals that a more or less constant amount of TGFβ is produced by the cells. The detected differences were caused by the differing cell numbers seeded. Therefore, no differences between cells grown in Petri dishes or inserts and no differences between irradiated and unirradiated cells were detected. Furthermore, mono-culture or co-culture conditions had no influence on the TGFβ secretion. The PKH67 stained cells did not change their TGFβ secretion into the medium and co-cultures with direct cell to cell contact had no influence on the expression of TGFβ. To conclude neither TNFα nor IL-2 were measured and the detected TGFβ amount did not alter due to the co-culture so that the observed effects in the survival experiments are probably not caused by one of the analyzed cytokines.

It was remarkable that in some samples the time dependent secretion of TGFβ strongly fluctuated. It was not explainable by sample handling or performance of method why some measurement points depart from the remaining data or further, do not show a measurable TGFβ level at all. But, since the behavior appeared especially in experiments with low cell numbers the conclusion was made that the secreted TGFβ amount was close to or under the detection limit of the assay.

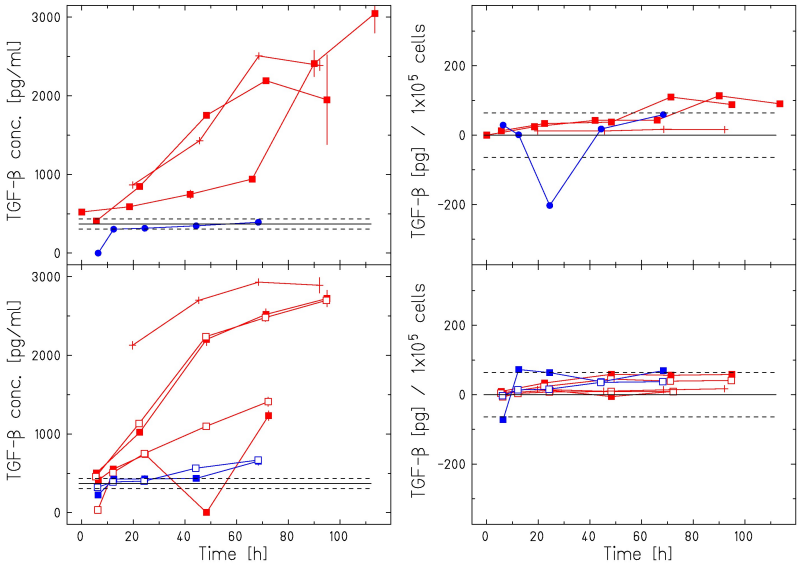

Figure 3.31: TGF-β measurements: mono-culture versus co-culture. **On top:** Mono-culture of 6 Gy (RBE) irradiated RAT-1 cells grown in Petri dishes. **On bottom:** Co-culture of 6 Gy (RBE) irradiated RAT-1 cells and IEC-6 cells. 250 kVp x-ray experiments: red, 11.4 MeV/u carbon ions: blue, open symbol: growth in inserts, closed symbol: growth in Petri dish, cross: PKH67 stained cell, horizontal lines: TGFβ content of the culture medium. **Left panels:** Total among of TGFβ in the sample adjusted for the serum level; **Right panels:** TGFβ content normalized to 1 x 10^5 cells.

3.6 Hypoxia chamber

For experiments under hypoxic and oxic conditions the RAT-1 cells were grown on bio-Folie 25 with 3 x 10^4 cells over 48 h. The gas mixture of 95% N_2 and 5% CO_2 flushed 2 h with 200 ml/min trough five in-line connected chambers at room temperature to achieve hypoxic conditions. The oxic cell cultures were kept outside the incubator for 2 h to simulate the gassing. After irradiation with 250 kVp x-rays or carbon ions with a $\overline{LET}$ of 100 keV/μm the cells were trypsinized and seeded in a colony forming assay. The survival was calculated according to Eq. 2.3 and plotted in figure 3.32. X-ray experiments were carried out six times while the carbon ion irradiation was conducted only once with hypoxic and twice with oxic cells due to lack of carbon ion beam times with suitable conditions. The error calculation as described under section 2.7 was not applied to the survival data of carbon ion irradiation under hypoxic since the amount of α and β values for carbon ion irradiation in hypoxia chamber was to low. It is suggested that the error of carbon ion experiments performed in the hypoxia chambers is comparable to that of x-ray irradiation experiments.

The cell survival after x-ray irradiation was a shouldered curve, as expected, while the survival after carbon ion irradiation follows an exponential decline. Therefore, for x-ray

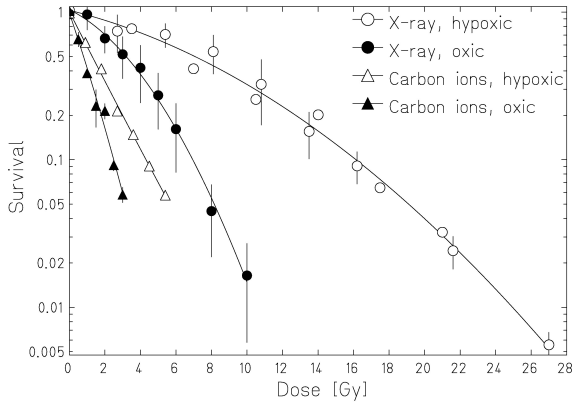

Figure 3.32: RAT-1 cell survival under hypoxic conditions compared to cell survival under oxic conditions. 250 kVp x-ray irradiation: mean survival values with standard deviation (n=6), Carbon ions irradiation with SOBP of $\overline{LET}$ 100 MeV/μm: oxic curve mean survival values with standard deviation (n=2), hypoxic curve n=1

irradiation α and β values could be calculated while for the carbon ion experiment only an α value was determined. In table 3.11 the α and β values were summarized for the experiments performed in the hypoxia chambers. The comparison of oxic survival curves of carbon ions and x-rays as well as hypoxic survival curves for carbon ions and x-rays identify carbon irradiation as more effective in cell inactivation. The deflection of the two oxic or hypoxic curves is the RBE, respectively. The RBE was calculated for hypoxic and for oxic conditions based on the cumulative curves according to Eq. 1.3. The cell survival under hypoxic conditions was enhanced compared to cell survival under oxic conditions. The difference between the two curves is defined as the OER. On the basis of the cumulative curves the OER values were determined according to Eq. 1.6. Table 3.11 shows the RBE and OER values beside the doses for a 10% survival rate which were needed for the calculation.

Table 3.11: Mean α and β values and D_{10} with the standard deviation for six independent 250 kVp x-ray experiments. For carbon experiments are the α value and the D_{10} given with the error of the linear fit. Blow the OER and RBE of experiments in hypoxia chamber are given. h: hypoxic, o: oxic

Exp.	α **[Gy^{-1}]**	$\Delta\alpha$ **[Gy^{-1}]**	β **[Gy^{-2}]**	$\Delta\beta$ **[Gy^{-2}]**	α/β **[Gy]**	$\Delta\alpha/\beta$ **[Gy]**	**D_{10} [Gy]**	**ΔD_{10} [Gy]**
X-ray h	0.068	0.035	0.005	0.001	15.9	0.78	16.0	0.78
X-ray o	0.144	0.054	0.030	0.006	6.6	1.07	6.7	0.82
Carbon h	0.548	0.049					4.2	0.38
Carbon o	0.819	0.219					2.8	0.75

$OER_{10,x\text{-}ray}$	**$\triangle$OER**	**$OER_{10,carbon}$**	**$RBE_{10,h}$**	**$RBE_{10,o}$**	**$RBE_{\alpha,h}$**	**$RBE_{\alpha,o}$**
2.35	0.13	1.5	3.8	2.4	8.0	5.7

4 Discussion and outlook

4.1 Cell lines

4.1.1 RAT-1 Dunning prostate adenocarcinoma cell line

The co-culture experiments should yield results relevant for therapy but also comparable to previous animal experiments performed by Dr. P. Peschke (German cancer research center, DKFZ). The cooperation with Dr. P. Peschke defined rats as the optimal model for animal experiments and thereby the cell system for this thesis. Peschke assesses the rat Dunning R-3327 system as an excellent model for human prostate cancer progression and the different cell lines allow a RBE determination related to differentiation level of the tumor [100]. The enzyme profile of the Dunning R-3327 system is close to humans, but not all cell lines of the system grow *in vitro*. The *in vivo* growth is limited to Fisher and Copenhagen rats [63, 65] which are both only available in the USA and therefore expensive compared to other rat strains. After tumor fragment implantation in the hind limp, the sub-line R-3327-AT-1 (RAT-1) grows reliable with a constant tumor doubling time [63]. Carbon ion irradiation of hind limb tumor bearing rats caused dose-dependent side effects like skin redness, dry and/ or wet sites, desquamation, necrosis, hair loss, and pigmentation abnormality [100]. Through the small irradiation field and the exact animal positioning side effects appeared only in the hind limb and not in the inner organs. Implantations of tumor fragments in the prostate are possible [150], but considerations to simulate the human prostate cancer irradiation with orthotropic implanted RAT-1 tumors in rats fail through technical problems e.g. organ motion. After an imaginary irradiation of orthotropic implanted RAT-1 tumors Peschke would suggest to find inflammatory side effects in the highly proliferating intestine [100].

As a part of this thesis the RAT-1 cells were characterized concerning their PE, doubling time, MI, and karyotype *in vitro* (see section 3.1). The PE was determined to be 44.6 $\pm$ 11.3% while the RAT-1 cells double in culture every 21 $\pm$ 2 h (see figure 3.1). The karyotype did not change during the culture period (58.9 $\pm$ 9.5) and the MI was constant (11.7 $\pm$ 1.1%) as presented in table 3.1 and in figure 3.4. *In vitro* data of RAT-1 cells are rare in comparison to *in vivo* data. Isaacs *et al.* characterized the RAT-1 cells with an *in vitro* growth time of 32.5 $\pm$ 3.7 h, a PE of 16.7 $\pm$ 0.9% and a chromosome profile with 60 $\pm$ 7 chromosomes [65]. The variations in PE and doubling time of this thesis in

comparison to Isaacs *et al.* are certainly due to the differing cell culture serums whereas the chromosome profile was identically. Furthermore, a cell doubling time of 13.1 h was reported in Corban-Wilhelm *et al.* which indicates a huge intra-cell line variation with regards to cell growth time [23].
After irradiation with x-rays or 11.4 MeV/u carbon ions the RAT-1 cells arrest in G_2/M-phase during the first 12 h but not in G_1-phase (see figure 3.2). In reference [43] the human prostate cancer cell line PC-3 accumulate in G_2/M-phase after irradiation with photons, too. The authors indicate a context of mutated p53 protein which is a crucial factor of the G_1/S-phase checkpoint arrest in response to DNA damage. The analysis of RAT-1 cells *in vivo* shows increased p53 levels in comparison to normal prostate tissue which suggests that p53 is not the reason for the missing G_1/S-phase checkpoint arrest *in vitro* [22].

4.1.2 Development of a co-culture system - a suitable cell line to RAT-1 cells is needed

To establish a co-culture system, a suitable cell line in combination to RAT-1 cells had to be found. The second cell line had to fulfill the following criteria: a) established rat cell line, b) male, c) normal tissue, d) biosafety level 1, e + f) adherent growth without or only with few additional growth factors, g) originated tissue normal prostate, bladder, urethra or intestine for the simulation of the effect in the entrance channel of prostate cancer irradiation with carbon ions, and h) contact to prostate cancer cells in the organism. The criteria are determined by the following reasons. The work with rat prostate cells defines the sex and the species of the second cell line. By the use of an established cell line the probability to achieve reproducible results with different cell batches should be enhanced in comparison to primary cells. The RAT-1 tumor cells should be combined with a normal cell line since the communication between the tumor and the surrounding tissue and not the communication between the tumor and its metastases should be analyzed. In addition, the GSI has only a statutory approval for cells with biosafety level 1 which excludes all cell lines with a higher biosafety level by law. Because the cells have to be irradiated in a vertical position at GSI the cells should grow adherent in culture vessels. Growth factors in the culture medium of the second cell line would complicate a co-culture since the effect of the growth factors on RAT-1 cells has to be tested. For prostate cancer irradiation at GSI the carbon ions are delivered in two opposing fields which include the hip bones and small parts of the radio-sensitive tissues intestine and bladder. The possible tissue origins of the second cell line could therefore be normal prostate, bladder, urethra and intestine with special regard to the rectum. Furthermore, all mentioned tissue types can have Intestinal epithelium cell line 6 (IEC-6 cells) had the highest intersection with the

criteria. This established cell line from the rat's small intestine is described as male and normal, has a biosafety level 1 categorization, grows adhered and only insulin dependent [106]. The combination of RAT-1 cells with IEC-6 cells simulates a state III-IV prostate tumor which spreads to other organs, here the intestine. The RAT-1 cells are anaplastic and therefore histological graded with the highest Gleason grad of 5. This supports the simulated *in vivo* situation of an aggressive tumor.

4.1.3 The IEC-6 cell line

The used IEC-6 cell batch underwent significant changes during its time in culture e.g. increasing PE (figure 3.17) and radio-resistance (figures 3.14 and 3.15), changes in karyotype (figure 3.9 and table 3.2), and decreasing doubling time (figure 3.5). Only in one cell batch an indication for a limited life span was detected. In all the other batches the cells grew without decreasing t_D. In contrast to these results, the IEC-6 cell line is described with a normal and stable rat karyotype (2n=42; *rattus norvegicus)*, a constant t_D of 20 h, a PE of 2.3% and a limited life span of 30-40 passages [106]. On inquiry, ATCC reported that the changes of the cell line were not known before. But ATCC referred to the potential of murine cells to spontaneously immortalize [4]. To avoid the selection of altered cells the usage of IEC-6 cells was limited to passage 15-20.
A closer look into IEC-6 related literature gives only one hint that age-dependent alterations of IEC-6 cells are known. The group around Jian-Ying Wang pointed out that there were no significant changes of biological functions and characterization from passage 15-20 [99, 139]. In reverse, this could mean that changes were observed at later passages but not investigated in closer specifications. Other authors which use the cell line within passage 15-20 refer to Wang's papers [88] or Wang is coauthor [108]. There are few publications which note the usage of IEC-6 cells before the 20th passage [129] or within passage 16-20 to minimize the passage effect [109] but without giving motivations or references. In the majority of papers IEC-6 cells were utilized as described in Quaroni *et al.* without commenting on a passage effect [106] (for examples see: passage 15-22 [9], passage 17-22 [62], passage 16-30 [48], passage 17-27 [47], passage 17-30 [132], and passage 20-26 [59]).

4.1.4 IEC-6 cell sub-populations and clones

To analyze the extra chromosomes in the IEC-6 cell metaphases staining techniques for rat cells were examined. Fluorescent staining products against rat chromosomes are rare

but some companies offer kits against single chromosomes (e.g. chromosome 12, Y, and X; Cambio Ltd, Cambridge, UK,). But without limiting the possible extra chromosomes the staining of a randomly chosen chromosome is of minor significance. Only one publication was found where a multicolor spectral karyotyping of rat chromosomes was described with self made flow-sorted chromosome-specific painting probes [15]. But this assay could not be applied to the existing microscope and software system at GSI. In the absence of a suitable whole genome wide staining kit the chromosome analysis was done with mouse mFISH probes on rat cells (see figure 3.19). It was expected that parts of the rat chromosomes are stained like a banding in the chromosome sections in which the chromosomes of rats and mice match. The resulting fluorescence signal of the mFISH staining did not allow a chromosome identification or differentiation. Comparable experiments were performed with rainbow cross-species fluorescence *in situ* hybridization with differentially labeled (Cy3, Cy5, FITC) gibbon chromosomes on human lymphocytes chromosomes which result in 90 bands [29]. Probably the biological relationship between mouse and rat is not high enough to achieve similar results like seen in gibbon and human mixed samples. Another approach to identify the extra chromosomes could be the G-banding technique with which the karyotype analysis in Danielpour *et al.* and Song *et al.* of rat epithelial cell lines has been done [128, 26]. The analysis requires experience and is usually done by specialized laboratories.

Beside the chromosome analysis of IEC-6 cell mass cultures, single clones were analyzed (see table 3.7). From two unirradiated cell batches clones were isolated and analyzed according to their radio-resistance, doubling time, and karyotype over eight passages. In the IEC-6 clone experiment no correlation between increasing chromosome numbers and increasing radio-resistance could be found. Both clones with 42 chromosomes had a stable radio-resistance (figure 3.24). Clones with higher chromosome numbers divided faster than clones with lower chromosome numbers. But clones with identical chromosome number did not show similar doubling times (figure 3.23).
The increasing growth rates of the IEC-6 cells could be interpreted as a first step into tumorigenesis. Insulin is an important growth factor of colonic epithelial cells and is mitogenic for tumor cell growth *in vitro* [44]. Giovannucci hypothesized that hyperinsulinema promotes colon carcinogenesis [44]. Following the general instruction of ATCC the culture medium of IEC-6 cells was enriched with insulin. It might be, that removal of insulin from the cell culture medium would slow down the process of decreasing cell doubling time. Co-culture experiments showed that IEC-6 cells survive and proliferate in an insulin-free medium. Whether a long-term cultivation in insulin-free medium over several weeks is possible and if the cell line alteration is suppressed, had to be tested.

In the course of the identification of radio-resistant sub-populations the survival of an IEC-6 cell batch was reduced through irradiation with x-rays or carbon ions to 10% (subsection 3.4.2). The irradiated IEC-6 cells were compared with unirradiated IEC-6 cells of the same cell batch and judged according to their doubling time (figure 3.20), karyotype (figure 3.21), and mitotic index (figure 3.22) over eight passages. In the long-term culturing differences were identified between irradiated and control samples. In irradiated cell samples the number of cells with more than 42 chromosomes developed faster in comparison to unirradiated IEC-6 cells of the same batch but in all three cases the growth rate and the MI decreased at the end of the observation period. These results indicate that through irradiation an early senescence could be induced. The X-Gal staining for senescence was performed in unirradiated cells of another cell batch (section 3.2). Here, no positive signal could be measured. But it is possible that through the heterogeneity of the cell line not all IEC-6 batches age in the same way, and it might be that positive stained cells could be found in irradiated cell samples.
It could be demonstrated that SA-β-gal is not required for senescence [82]. To investigate senescence in more detail the expression of hTERT (telomere shortening) as well as p53 and p16 (senescence pathway proteins) should be measured in IEC-6 cells [45].

After irradiation with 250 kVp x-rays, the IEC-6 cells stopped in G_2/M-phase for 12 h. At later points in time no differences to control samples were detected (see figure 3.7). Cell cycle experiments with carbon ion irradiated IEC-6 cells were not performed. Through the changes in karyotype with time in culture the DNA amount in the cells varies essentially. A differentiation of the sub-populations in cell cycle experiments was therefore not possible (see figure 3.6).
In general, the cell growth is controlled by several checkpoints in cell cycle progression. The G_1/S-phase checkpoint and the intra-S-phase checkpoint prevent the cells from unfaithful genome replication [77]. The cell arrest in G_1/S-phase checkpoint appears soon after damage induction through ionizing radiation [81]. The G_2/M-phase checkpoint is initiated to allow repair of DNA damages prior to mitosis [77]. It could be demonstrated that for initiating of checkpoint arrest in G_2/M-phase and for cell release from the checkpoint arrest a threshold of twenty double strand breaks exists [81]. Consequently, the incomplete repair of the cells generates chromosome aberrations.
After irradiation, the IEC-6 cells arrested in G_2/M-phase which indicate a genome replication without damage repair and a cell repair before entering mitosis. It is possible that the IEC-6 cell line has lost a functional G_1/S-phase checkpoint arrest. One of the most

important factors for cell cycle progression control, apoptosis, and DNA repair is p53 [86]. If the IEC-6 cells have lost functional p53, the cell line would accumulate DNA mutations which might contribute to genomic instabilities.
In a long-term cultivation of an IEC-6 cell batch, which was divided in three parts (x-ray or carbon ion irradiated and control cells), developed identical sub-populations (see subsection 3.4.2). This demonstrates that the whole IEC-6 cell population develops aneuploidy. Aneuploidy is associated with a defect in the mitotic spindle checkpoint and tumorigenesis. The spindle checkpoint can delay the mitotic progression by transiently inhibiting the anaphase-promoting complex in response to defective kinetochore-microtubule attachment [74]. If the attachment is faulty, the chromosomes would not be divided correctly to the daughter cells and an aneuploidy appears. To prove this hypothesis the spindle checkpoint proteins could be analyzed for transcription and function [74]. Instead of a conclusion the question is raised whether the IEC-6 cell line should continually be called "model for normal human intestinal epithelial biology".

4.1.5 Alternative cell lines to IEC-6 cells

The wide variability in PE, radio-resistance, and growth time of the IEC-6 cells is an uncertain element and a source of error in all performed experiments. Therefore, the search for alternative cell lines was extended. In general, cell lines of the urethra or bladder were not found. But the search identified two new cell lines from the group of David Danielpour. Out of the dorsal-lateral prostate of Lobund/Wistar rats Danielpour *et al.* established the cell line NRP-152 which are of epithelial origin [26]. The analysis of the karyotype identifies an aneuploidy with a mostly hypertriploid chromosomal distribution. In Song *et al.* the development of the epithelial cell line DP-153 from the dorsal prostate of Lobund/Wistar rats is reported [128]. The karyotype is aneuploid with most chromosomes in the diploid range. But trisomy (chromosome 7 and 12) and monosomy (chromosome 14, 15, and 18) were observed, too. Both cell lines are non-tumorigenic in athymic mice and epidermal growth factor, insulin, dexamethason, and cholera toxin are needed for optimal growths. The comparison of IEC-6 cells with the two prostate cell lines shows no benefit since DP-153 cells and NRP-152 cells have an aneuploid karyotype and are highly growth factor dependent. Two endothelial cell lines, YPEN-1 and YPEN-2, were isolated by Yamazaki *et al.* out of the prostate of a Copenhagen rat. The cells were immortalized by a hybrid virus [148]. Through the immortalization the cell lines were classified with biosafety level 2 and are not accredited at GSI. From the fetal rat small intestine Negrel *et al.* isolated the cell line IRD-98 which was eliminated because of the fetal origin and the expected differences to adult tissue [96].

Beside the IEC-6 cell line Quaroni *et al.* established one fibroblast cell line and three further epithelial cell lines from the rat intestine namely RIF and IEC-14 [106] as well as IEC-17 and IEC-18 [105]. IEC-14 and RIF are sparsely characterized whereas IEC-14 showed no growth inhibition, a life span over 100 passages, and soft agar growth which is clearly tumorigenic behavior. RIF cells were described as slowly growing (t_D= 25 h) with a poor PE (2.4%) [106]. Both cell lines seem to be not commercially available. IEC-17 cells were isolated from the duodenum while IEC-18 cells originated from the ileum. Both cell lines are non-tumorigenic in syngeneic animals, do not grow in soft agar, and have a diploid karyotype. For IEC-17 cells progressive morphological changes are published which seemed not to be spontaneous transformation but a differentiation to defined cell polarity [116]. This cell line alteration disqualified the IEC-17 cells for further investigations. Although, the IEC-18 cell line is not well documented in literature it could be an alternative to IEC-6 cells since their origin is closer to the rectum, they are commercially available (ATCC No. CRL-1589), and up to now no age-dependent changes were published.

4.1.6 Changing the cell system to human cells

The Dunning prostate cancer cell line system is unique. For human cell lines a comparable system is not available. The well documented human prostate cancer cell lines PC-3 (grade IV adenocarcinoma, epithelium, ATCC No.:CRL-1435, [72]), LNCaP (carcinoma, epithelium, ATCC No.: CRL-1740, [58]), and DU-145 (adenocarcinoma, epithelium, ATCC No.: HTB-81, [130]) offer interesting options due to their different cell characteristics. But they can not replace a tumor progression model like the Dunning system with more than ten cell lines [64]. Furthermore, the possibility to perform *in vivo* experiments under controlled conditions and compare the results to *in vitro* experiments is not given in a human system.
In co-culture the favorite origin for the second cell line is the normal prostate. The availability of normal human prostate cells is very limited as well as for rat cells. ATCC offer e.g. only cell lines with biosafety level 2 because of virus immortalization. Via Bio Whittaker the order of primary normal prostate cells with differing origin is possible (PrEC (epithelium), PrSMS (Smooth muscle cells), PrSC (stromal cells)). The variability between different donors of the primary cells could be high, and the co-culture system needed to be tested with every new cell batch. To conclude, a change of the species form rat to human is undesirable for co-culture experiments.

4.2 Mono-culture survival experiments

The pilot project for carbon ion therapy of prostate cancer patients was started with the goal to compare 30 patients treated with a combined IMRT and a carbon boost with 30 patients exposed to IMRT alone. The carbon ions for treatment were delivered with the raster scanning technique using a pencil beam that is guided over 3 x 10^5 voxel of the tumor volume. This technique guarantees an utmost tumor conform treatment, but needs in principle, for every voxel the appropriate RBE value. These values are calculated with the local effect model (LEM) which is based on physical parameters describing the beam quality and on the biological side the characterization of the cellular repair capacity. For the RBE calculations the cellular repair to ionizing radiation damages is assessed in x-ray experiments measuring clonogenic survival. There, the ratio α/β of the linear and the quadratic term of the dose response curve, respectively, can be used for the RBE calculations. Although, in therapy the α/β ratio has to be taken from the clinical situation i.e. from conventional therapy, it is interesting to compare the cellular data obtained in our measurements with the clinical data. In a very comprehensive research α/β ratios between 1.5 Gy and 6 Gy have been reported but quality weighted evaluations converged at a value of 2 Gy [13]. Therefore, an α/β ratio of 2 Gy is used in the biological treatment planning phase for prostate cancer at GSI [31]. The α/β ratio for conventional external beam radiation or low- and high-dose-rate brachytherapy is under discussion. Values between 1.5 Gy [95] and 3.1 Gy [140] are assumed.
The RAT-1 cell line is moderately radio-resistant against 250 kVp x-rays with an α/β ratio of 6.8 $\pm$ 0.5 Gy (figure 3.11). Experiments with irradiated RAT-1 cells *in vitro* can not be found in scientific literature, and in published *in vivo* irradiation experiments no α/β ratio was determined. Thus, it was not possible to compare the α/β ratio of RAT-1 cells to other cell lines *in vitro*. For six human prostate cancer cells an α/β ratio range was estimated to be between 1.09 to 6.29 Gy [16]. In all planning and treatment a high radio-resistance of prostate cancers is presumed. In contrast, the RAT-1 cells are only moderate radio-resistant.

The survival data of carbon ion irradiated RAT-1 cells was compared to calculations of LEM in its version II and IV (calculations performed by Thilo Elsässer, GSI, Biophysics group). LEM I calculated the biological effect according to the dose response of measured x-ray survival curves [120]. However, radical diffusion and the interaction of single strand breaks forming double strand breaks were first taken into account by LEM II [33]. The further version LEM III integrated a more realistic characterization of the radial dose distribution [32]. The latest version LEM IV considers in addition clustered DNA double strand breaks [31]. The LEM calculation for RAT-1 cell survival after carbon ion irra-

diation with different energies is based on the average $\overline{\alpha}$ and $\overline{\beta}$ values measured for 250 kVp x-ray irradiation (see subsection 3.3.1). In figure 4.1 the LEM calculations are plotted together with the measured survival curves. LEM IV calculations were in agreement with the experimental data while LEM II calculations were only suitable for 11.4 MeV/u carbon ion experiments.

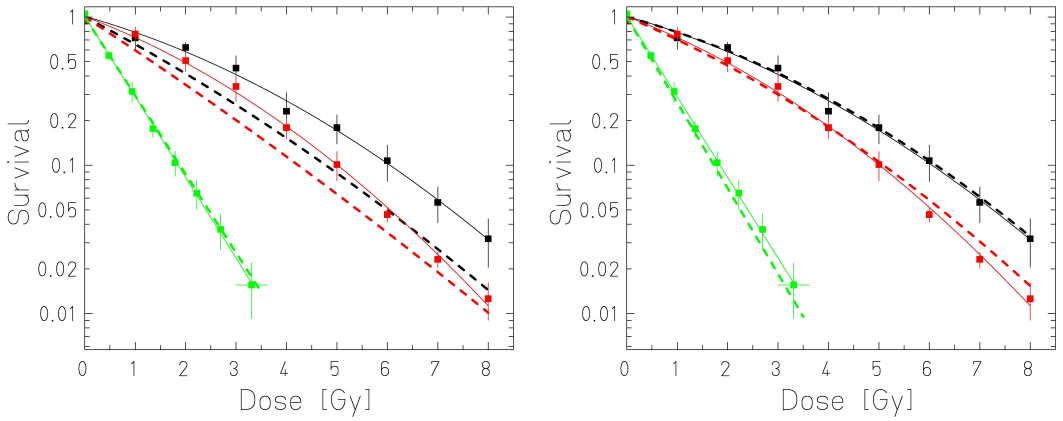

(a) Survival calculations with LEM II (b) Survival calculations with LEM IV

Figure 4.1: Survival curves of RAT-1 cells after carbon ion irradiation in solid lines compared to LEM calculations in dashed lines. The used carbon ion energies were 11.4 MeV/u (green), 100 MeV/u (red), and 270 MeV/u (black).

The radio-resistance of IEC-6 cells against 250 kVp x-rays changed with time in culture and differed between cell batches (figures 3.14 and 3.15). Because of this systematic change mean α and β values are not appropriated. Table 3.4 presents all α and β values for the performed x-ray experiments. The IEC-6 cells are more radio-sensitive in comparison to RAT-1 cells indicated by lower doses which were needed to reduce the cell survival to 10% (D_{10}). The D_{10} for RAT-1 cells was determined to be 7.0 $\pm$ 1.4 Gy while the D_{10} for IEC-6 cells fluctuate dependent on age between 5.0 and 6.0 Gy (see table 3.4). The IEC-6 cells were used by other authors in several irradiation experiments with x-rays or neutrons but α and β values or RBE values were not published. In the absence of other data the determined RBE values for IEC-6 cells were compared to an *in vivo* mouse study [39]. In the mouse study the RBE value of the intestine after carbon ion irradiation (SOBP, different LETs) and ^{137}Cr γ-ray irradiation were measured. The comparison of the RBE_{10} values for IEC-6 cells and the mouse intestine is plotted in figure 4.2. Essentially, the plotted RBE values against the LET did not differ. A steeper curve for the IEC-6 cells than for the *in vivo* mouse data is shown. This demonstrates that an *in vitro*/*in vivo* comparison of experimental data is possible.

The survival curves of IEC-6 cells after carbon ion irradiation were compared with cal-

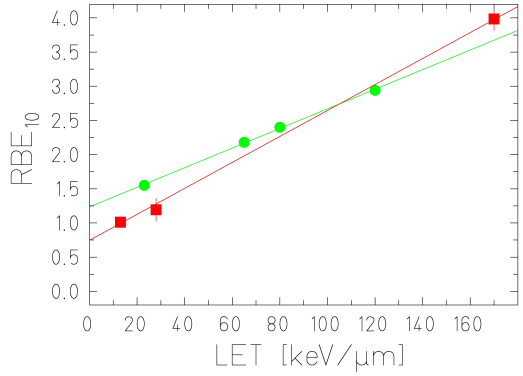

Figure 4.2: RBE_{10} of IEC-6 cells (red square) compared to *in vivo* RBE_{10} of the murine intestine (green circle). The RBE_{10} values for IEC-6 cells are average values of four independent carbon ion experiments and sixteen independent 250 kVp x-ray experiments while the data for murine intestine are published in [39].

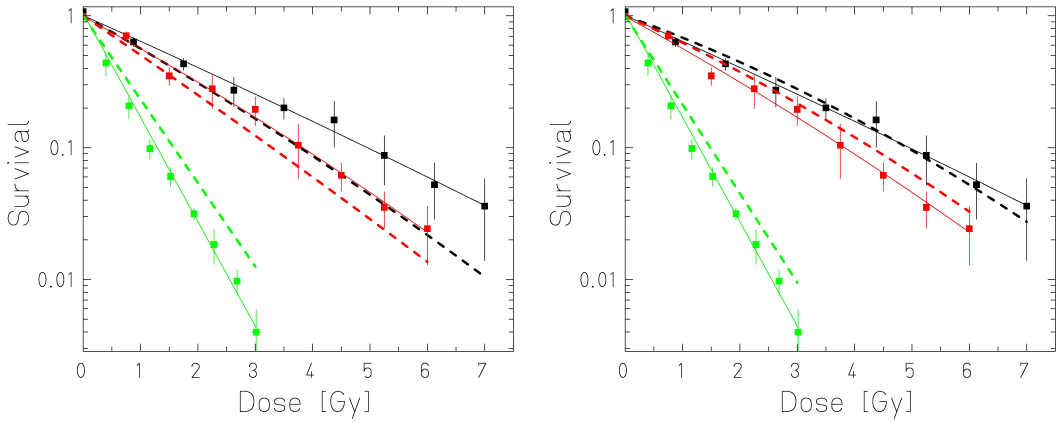

(a) Survival calculations with LEM II

(b) Survival calculations with LEM IV

Figure 4.3: Survival curves of IEC-6 cells after carbon ion irradiation in solid lines compared to LEM calculations in dashed lines. The used carbon ion energies were 11.4 MeV/u (green), 100 MeV/u (red), and 270 MeV/u (black).

culations of the LEM in version II and IV which were performed in advance by Thilo Elsässer (GSI, Biophysics group). For more details on LEM I-IV see two paragraphs above. The calculations are based on α and β values of IEC-6 cell x-ray curves. As mentioned previously mean α and β values could not be determined due to the changing radio-resistance of the cell line. To circumvent this problem, an estimation for "mean" α and β values was performed as described under section 2.7. The determined values were for α 0.35 $\pm$ 0.02 while β was 0.022 $\pm$ 0.003 (n=16). The comparison of the experimental IEC-6 cell data with LEM calculations shows that LEM IV predicted the IEC-6 cell survival rate more exactly than LEM II. Especially for 270 MeV/u carbon ions, which represent the energy in the entrance channel, the differences between LEM IV and the measured data are very small.

4.3 Co-culture experiments

4.3.1 Comparison of methods: cell pre-seeding versus trypsin treatment

The co-culture survival experiments of IEC-6 cells and RAT-1 cells were performed with two different set-ups. In the following both methods are discussed with regard to the protocol for a clonogenic survival assay and the cytokine secretion of the cells into the medium. In a clonogenic survival assay the cells needed to be trypsinized after irradiation and reseeded in defined numbers. Not all cells with high radiation damages do re-attach after the trypsin treatment and are excluded from the experiment. In irradiated tissue no elimination process took place so that these highly damaged cells exist. The motivation for method P, where cells are pre-seeded in suitable concentrations, was to analyze the communication between low, medium, high or not irradiated cells without excluding one of the sub-population. The pre-seeding was only possible for x-ray irradiation and not for carbon ion irradiation. At SIS facility the irradiation time span is limited and the irradiation time of the needed culture flasks with pre-seeded cells would have taken too long. Irradiation at UNILAC facility is only possible in Petri dishes with a diameter of 3 cm which corresponds to a growth area of approximately 7 cm^2. The amount of Petri dishes for a colony forming assay with comparable colony statistics as in culture flasks would have been too high. Beside the long irradiation procedure (3 h for a x-ray experiment) method P has additional disadvantages: a) the real number of irradiated cells is unknown, b) the irradiated cells were stained after twelve days of grow instead of eleven days, c) two PE values are needed for survival calculation, and d) the background of cells which start to grow after irradiation but do not achieve fifty daughter cells is very high. These uncertainties led to mistakes in the survival calculation and the experimental set-up was changed.

In method T the cells were trypsinized after irradiation and reseeded in culture flasks for the clonogenic survival assay. Method T reduced the x-ray irradiation time to 30 min whereas the number of cells in the culture flask was of little importance during the irradiation. Through the trypsination, all cells were seeded on the same day and could be stained after eleven days. The additional second PE was omitted. Furthermore, the background of cells was minimized, which attached but lost their mitotic ability after a few deviations. But the trypsin step might exclude highly damaged cell. A central disadvantage of method T is the medium exchange after irradiation. If the cells secret substances directly after irradiation into the medium, these substances can not have an influence on the other unirradiated cell line, and these substances will not be detected in a cytokine assay. That there are very fast reactions was demonstrated in co-culture experiment with unirradiated

and α-particle irradiated human prostate carcinoma cells DU-145 [142]. A bystander effect in the unirradiated cells could only be observed when the unirradiated cells were present in the medium of the irradiated cells during the irradiation. If the cells were combined 1 min after irradiation, the effect was not detected. The authors concluded that the mediating molecule has to be a short life radical other than nitric oxide. With method P as well as with method T fast reactions like described by Wang and Coderre [142] can not be detected but for the analysis of cytokine secretion and changing protein profiles method T is more qualified than method P.

4.3.2 Influence of serum on survival experiments and cytokine detection

The co-cultures survival experiments were performed in serum-containing medium and with two different serum batches (Biochrom AG, Berlin, Germany). Both cell culture serums influenced the PE and the survival as demonstrated in table 3.4 and figure 3.15. But the measured results with serum I could not be reproduced with serum II.
Cell culture serum could contain a variety of cytokines which are not identified and quantified by the producing companies. On inquiry, the Biochrom AG (Berlin, Germany) declare that all cytokines and growth factors which are able to penetrate the placenta could be found (mostly in low concentrations) in the fetal calf serum [11]. The different cytokine composition in the two serum batches caused the differing results in the co-cultures survival experiments.
Because of the cytokine amount in cell culture serum, the majority of published cytokine detecting experiments were performed in serum-free culture medium to obtain controllable and reproducible growth conditions. However, in this thesis the co-culture cytokine detecting experiments were performed on purpose in serum-containing medium to achieve identical conditions to the co-culture survival experiments. A comparative co-culture survival experiment over eleven days in serum-free medium was not performed since the lack of serum would lead to growth inhibition or even cell death.

4.3.3 Survival experiments

In the performed co-culture survival experiments the number of direct cell to cell contacts was rare and the communication via gap junctions (direct cell to cell contacts) could contribute only in a small percentage to the detected effects in survival. Therefore, the co-culture effect inducing molecule was suggested to be a soluble factor, which is mediated via the cell culture medium. It was assumed that more than one factor is responsible for the detected effects in co-culture. First, the PE_{Co} of IEC-6 cells was enhanced

which indicates an irradiation-independent factor (figure 3.26). Second, a positive survival effect for RAT-1 cells was only detected when IEC-6 cells were irradiated which indicates an irradiation-dependent factor (figure 3.27). Third, the IEC-6 cell survival was only enhanced when both cell lines were irradiated which indicates a second irradiation-dependent factor (figure 3.29).

The response of unirradiated cells to signals produced by neighboring irradiated cells is called the bystander effect. The used doses for irradiation (1, 3, and 6 Gy (RBE)) were therapy related and chosen dependent on the survival level. The irradiation doses were not in the typical bystander range which is below 1 Gy or above 15 Gy [103]. Nevertheless, the bystander effect will be discussed but without great detail. The effect is mediated by a factor released to the medium or involves direct cell to cell contact via gap junction whereas the communication via gap junctions is generally down regulated in tumor cells. In addition, gap junctions limit the signal molecule size to 1,000-1,500 Da, while soluble factors in the medium can have up to 10,000 kDa which includes cytokines. Bystander signaling has close parallels to inflammatory response which includes e.g. TGFβ, TNFα, IL-6, IL-8, ROS, and NO. Corresponding to the effect in the whole organism, the analyzed endpoints are termed the bystander response damaging (DNA damage, mutation, transformation, cell death) or protective (terminal differentiation, apoptosis, radio-adaptive response). The effect has no dose-response relationship and becomes saturated at very low doses (below 1 Gy) [103].

Cell lines used in this thesis, RAT-1 cells and IEC-6 cells, were not assayed in bystander experiments before. The general combination of prostate cancer cells with epithelial cells was also not studied. In addition, the originating tissue of the RAT-1 cells is unknown due to the anaplastic character of the cell line. Therefore, the result of this thesis can only be compared to other publications which combined general prostate cancer with other cells or epithelial cells with other cells.

The majority of publications which showed a bystander effect on PE or survival combined irradiated cells with unirradiated cells of the same cell line e.g. increasing PE of unirradiated human epithelial cells in co-culture with irradiated human epithelial cells after irradiation with carbon ions of differing LET and x-rays [124]. Shao *et al.* reported that a higher LET carbon ion irradiation was more efficient in inducing the bystander effect (increasing PE of unirradiated cells) than a lower LET carbon ion irradiation. An LET-dependency could not be measured in this thesis. Both cell combinations of unirradiated IEC-6 cells with irradiated RAT-1 cells as well as unirradiated RAT-1 cells with irradiated IEC-6 cells, did not show a LET-dependent increase of PE, independent of the used serum batch.

Anzenberg *et al.* studied the co-culture effect of x-ray or α-particle irradiated human

prostate cancer cells, DU-145, with unirradiated human fibroblasts, AG01522 [3]. They showed that the survival of unirradiated fibroblasts decreased when the cells were combined with x-ray irradiated but not with α-particle irradiated prostate cancer cells. The negative effect on the fibroblast survival could be blocked by the nitric oxide (NO) specific scavenger PTIO, which indicates the involvement of NO in the bystander effect [3]. Furthermore, Wang *et al.* reported for the same prostate cancer cells, DU-145, a bystander effect (micronuclei formation) after α-particle irradiation in unirradiated DU-145 cells which involves a short life radical but another than NO [142].
In co-culture survival experiments, performed in this thesis, the x-ray or carbon ion irradiated RAT-1 cells induced a decrease in survival of co-cultured unirradiated IEC-6 cells. If the decreasing survival of the IEC-6 cells was induced by radicals, the effect should be more pronounced when higher doses were applied because higher doses of x-rays or carbon ions produce more radicals than lower doses. But the negative effect on the IEC-6 cell survival was not longer present with increasing delivered dose to RAT-1 cells (see figure 3.26). Therefore, it is implausible to consider radicals as the only molecule inducing the effect on the survival of IEC-6 cells. It is possible that the effect of radicals is superimposed by other mechanisms which become relevant at higher doses.
Gaugler *et al.* irradiated primary human lung endothelial cells with 15 Gy of 6 MV x-rays and combined the cells with unirradiated human colon epithelial cells. The induced bystander effects in epithelial cells were decreasing cell numbers and mitotic cells as well as increased apoptotic cells. The three effects in epithelial cells correspond in general to reduced survival rate and were enhanced when both cell lines were irradiated [42]. The detected effects in Gaugler *et al.* were contrary to the results in this work. In the irradiated sample RAT-1 cells and IEC-6 cells a dose-dependent increase in survival rate was induced in IEC-6 cells while the RAT-1 cells were not affected (figure 3.29).
In conclusion, these results indicate that not only a cell type specific response to irradiation but also the combination of cell type are responsible for the induced bystander effect.

4.3.4 Cytokines

Based on the detected effect in the survival experiments (see subsection 3.5.1) substances were chosen for analysis in medium supernatants which could be the affecting mediator. It was expected to find an inflammatory response after irradiation and that the involved molecules could be inflammatory cytokines. As mentioned under subsection 4.3.3 at least three factors could induce the effects whereas one factor is independent of irradiation and two were irradiation dependent.

TGFβ

TGFβ could be measured in the performed experiments and the measured TGFβ amount was adjusted for the medium TGFβ level as well as for the cell number which produced the TGFβ. In all carried out experiments no additional TGFβ secretion was found through the irradiation or the co-culturing. It seems that the cells kept the level of TGFβ in the medium constant to the cell number. Furthermore, no active TGFβ was found in proliferating cultures. Active TGFβ could only be measured in confluent cell cultures at which the medium pH was shifted to lower values, which might have activated TGFβ.
The decision to analyze TGFβ was made on the following working hypothesis. The number of publications is limited which deal in general with *in vitro* RAT-1 cell experiments and in particular with cytokine or cytokine receptor production. But it was reported that the RAT-1 cell line expressed *in vitro* elevated TGFβ1, TGFβRI, and TGFβRII mRNA levels [145]. The effect of TGFβ on RAT-1 cells is unknown. Since the RAT-1 tumor cell line is anaplastic, the originating cell type can not be identified (e.g. basal, luminal, stromal, glandular, epithelium, smooth muscle cells of the prostate). Therefore, direct conclusions on the TGFβ effect on RAT-1 cells are not possible based on the different prostate cell types. TGFβ secretion can be induced by irradiation [2] so that the RAT-1 cells could be stimulated by irradiation to produce and secret the cytokine as well. In co-culture with IEC-6 cells, the medium mediating TGFβ, secreted by the RAT-1 cells, could induce effects in the IEC-6 cells. Podolsky reported that TGFβ negatively affects the proliferation of IEC-6 cells [102]. By Ko *et al.* it was shown that TGFβ arrests the IEC-6 cells in G_1-phase by blocking the induction of cyclin D1 [75]. In summary, the irradiation should induce TGFβ secretion by the RAT-1 cells and this medium mediated TGFβ should reduce or affect the survival rate of co-cultured unirradiated IEC-6 cells. With this hypothesis the reduced survival rate of unirradiated IEC-6 cell in co-culture with irradiated RAT-1 cells should be explained. But in the performed experiments no additional TGFβ was found so that the hypothesis was disproved.

TNFα and IL-2

The motivation to measure both cytokinesTNFα and IL-2 was based on the paper by Lyu *et al.* which demonstrated that IEC-6 cells are able to secret TNFα and IL-2 after LPS stimulation [87]. For a long time, IL-2 and TNFα were thought to be only produced and secreted by cells of the immune system. But several publications showed that also other normal cells or tumors cells are capable of IL-2 [110] and TNFα [107] production as well as secretion. IL-2 has been detected in normal tissues like endothelial and intestinal

epithelium to stimulate the proliferation [5] which was also published by Shigematsu *et al.* for the IEC-6 cells [126]. For TNFα an effect on cell proliferation, differentiation, and induction of other cytokines in epithelial cells was reported [107]. In agreement with these results TNFα induced in IEC-6 cells DNA synthesis and increased cell proliferation [149]. The IEC-6 cells were combined with the prostate cancer cell line RAT-1. In highly proliferating tumors like prostate tumors increased expression of IL-2 and IL-2R has been reported [41]. On RAT-1 cells IL-2 has *in vivo* an inhibitory growth effect [70, 54]. TNFα induced slower tumor growth *in vivo* in some Dunning sub-lines [125]. This result was not reproduced in *in vitro* experiments with the same sub-lines [135]. Until now the effect of TNFα on RAT-1 cells was not investigated, which means that a negative effect on proliferation can but do not necessarily have to appear.
The working hypothesis for TNFα and IL-2 measurements was as followed. In the co-culture survival experiments a negative growth effect on the RAT-1 colonies and a positive growth effect on the IEC-6 colony formation concomitant with increased colony size were detected (see section 3.5.1). IL-2 and TNFα could mediate the detected effects since IL-2 and TNFα induced proliferation and DNA synthesis in IEC-6 cells as well as the cytokines promoted growth inhibition *in vivo* in RAT-1 cells at which IL-2 *in vitro* also inhibit the RAT-1 cell growth. But in the performed experiments neither TNFα nor IL-2 could be detected. It might be that the sensitivity of the used ELISA was not high enough. The detection limit of both used ELISA kits was 62.5 pg/ml. Human serum e.g. contains a IL-2 level of 5-15 pg/ml [6]. The used fetal calf serum was not tested for IL-2 and TNFα levels but the manufacturer assumes that low amount of both cytokines are present in the serum [11].
In summary, in the analyzed cell system only TGFβ could be detected while IL-2 and TNFα were not secreted by the cell line or below the detection limit of the assay. Since the whole TGFβ amount in the supernatant was determined, the origin cell line could not be named.

The three analyzed cytokines TNFα, TGFβ, and IL-2 can not represent the huge and complicated signaling system which is induced in cells after irradiation. Other interesting cytokines for analysis in co-culture would be IL-1α, IL-1β, and IL-6. IEC-6 cells have large intracellular IL-1α pools which the cells do not secret. Stadnyk *et al.* suggested that IL-1α pools might be released from damaged cells and might act on neighboring cells [129]. It might be that the secretion can be induced with ionizing radiation.
Beside IL-1α detection it would be interesting to analyze the interplay between IL-1β, TGFβ and IL-6 which could partly explain the results of the co-culture survival experiments. IL-1β and TGFβ strongly modulate the IL-6 section by IEC-6 cells [90]. IL-6

itself modulates the intestine cell population. In addition, IL-1β enhance epithelial cell restitution and enhance the production of active TGFβ [102].

A further result of the co-culture was the increasing PE of IEC-6 cells in co-culture with unirradiated RAT-1 cells (see figure 3.26). An increasing PE can be caused by enhanced cell adhesion or proliferation. The adhesion-mediating molecules between cells or cells and matrix are integrins. Integrins regulates the adhesion in G_1-phase and the entry in S-phase of the cell cycle. In addition, integrins are connected to the actin cytoskeleton and control proliferation as well as migration [60]. A second group of adhesion molecules are cadherins. The major expressed cadherin in epithelium is E-cadherin which is important in cell-cell contacts [49].
Independent of the co-culture the IEC-6 cell line underwent huge changes in PE, cell doubling time, and radio-resistance (see sections 3.2 and 3.4). An integrin which is is involved in all three processes is integrin β1. Integrin β1 mediates cell-matrix interactions (proliferation) and is associated with malignant progression (migration). Furthermore, it is mediating pro-survival signaling as well as resistance to radiation [24]. It would be interesting to analyze the integrin profile with special regard to integrin β1 and the E-cadherin appearance in mono-cultures and co-cultures of IEC-6 cells to see a) if the mono-culture modify the expression integrin β1 with age, which could explain the detected changes in IEC-6 mass cultures and b) if the co-culture induced changes in the adhesion molecule expression, which could stimulate the adhesion or the proliferation of IEC-6 cells.

4.4 Hypoxia chamber - measurement of the oxygen effect

To analyze the radiation response of cells under hypoxic conditions the container in which the irradiation takes place has to fulfill several criteria which were mentioned in section 2.5. No suitable application was found to be commercially available. For example Billups-Rothberg Inc. (San Diego, CA, USA) and Biopherix Ltd. (Lacona, NY, USA) offered hypoxia chambers made of plastic and stainless steel. Both containers are comparable to an incubation with an additional influx for gas mixtures (see figure 4.4) and do not allow sample irradiation.

To determine the oxygen effect, RAT-1 cells were irradiated in the hypoxia chamber which was developed for the irradiation with x-rays and ions under oxic and hypoxic conditions. Therefore, the cells were seeded on bioFolie 25 instead of in Petri dishes or in culture flasks. Details on construction and sample handling are given in section 2.5 while in sec-

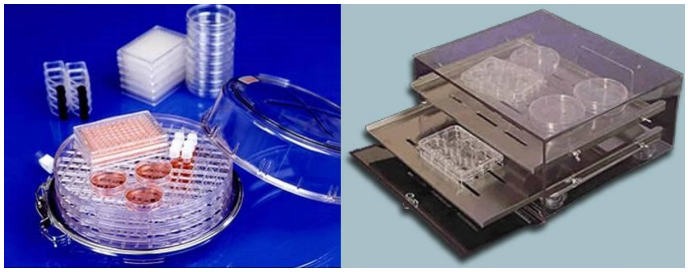

Figure 4.4: Cell culture system for hypoxic conditions. Left panel: Hypoxia chamber from Billups-Rothberg Inc., right panel: Hypoxia Chamber from Biopherix Ltd.

tion 3.6 the obtained results are presented.

4.4.1 OER for x-ray irradiation

The incubation at room temperature did not further affect the PE of cells growing on bioFolie 25 at which in general the PE on bioFolie 25 was lower than the PE in culture flasks. In 250 kVp x-ray experiments performed under oxic conditions the standard deviations of survival increased continuously from 12% to 65% (0 Gy to 10 Gy, $r^2 = 0.96$) while the standard deviation for hypoxic survival experiments was $29 \pm 9\%$. The detected errors in the hypoxia chamber were higher for oxic experiments than the error of experiments performed under oxic conditions in culture flasks. Here the standard deviation increased continuously from 10% to 51% (0 Gy to 10 Gy, $r^2 = 0.87$). But the survival data under oxic conditions obtained in culture flasks or in sample rings were comparable as shown in figure 4.5. It seems that the survival under oxic conditions is more strongely influenced than the survival under hypoxic conditions since the oxic experiments had higher error values independent of the growth support. It might be that the oxic survival is affected more by sub-lethal damages because of the damage fixation with oxygen than the hypoxic survival. Under hypoxia the purely lethal damages were measured.

The stronger increase of the error at higher doses indicates different radio-sensitivities in the cell culture. A reason for the different radio-resistance may be the different situation during the gassing time. Whereas the hypoxic samples where gassed for 2 h with a mixture of nitrogen and 5% CO_2 at room temperature, the oxic chambers stayed for the same time at room temperature but without additional CO_2. During the 2 h at room temperature the pH of the oxic samples changed to alkaline values optically evaluated by color change of pH indicator phenol red from light red into deep red. It might be that the slightly enhanced pH influenced the radio-sensitivity of the cells. Jayanth *et al.* demonstrated that

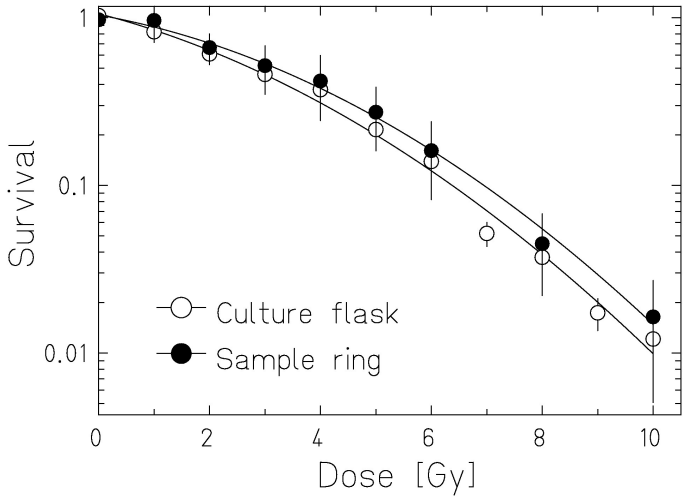

Figure 4.5: RAT-1 cells: Comparison of cell survival after 250 kVp x-ray irradiation under oxic conditions in culture flasks and sample rings.

cell survival after x-ray irradiation is reduced when the cells are cultured in medium with a pH beyond the optimum (6.6) whereas a lower medium pH (6.0) affect the survival more than the higher medium pH (7.6) [69]. In future experiments the oxic sample will be aerated with a gas mixture composed of synthesized air with 5% CO_2 to avoid possible errors.

A second reason for the changing radio-sensitivity may be that differences in cell cycle phases are expressed more under oxic than under hypoxic conditions. Hypoxia, with oxygen levels under 0.5%, induces an arrest in S-phase while oxygen levels above 0.5% have little effects on cell proliferation [8]. With the used system oxygen levels below 0.5% are achieved after $\approx$ 70 min of gassing. Since the total gassing time is 2 h, in the additional 50 min a partial synchronization of the cells in S-phase can appear. The reoxygenation after hypoxia activates ATM which induces G_2-phase arrest [8]. I showed that RAT-1 cells underwent G_2/M-phase arrest after irradiation independent of the reoxygenation after irradiation. The induced G_2/M-phase arrest after reoxygenation, is therefore of minor importance in the performed experiments.
As mentioned previously, the medium pH of oxic samples in hypoxia chamber shifted toward alkaline values within 2 h. Musgrove *et al.* demonstrated that the intracellular pH has an influence on the cell cycle phase [94]. Higher pH is associated with enrichment of cells in S-, G_2-, and M-phase. If the extracellular pH of the medium influence the intracellular pH within 2 h, is not known. But the possible cell cycle shift in the oxic samples would be comparable to that of the hypoxic samples.

The OER_{10}, calculated with the cumulative curves, for x-ray irradiation was 2.35 $\pm$ 0.13

in this thesis. But a dose dependent change of the OER was detected. For higher survival levels the OER decreased to 2.18 (90% survival). This has also been reported by Freyer *et al.* which analyzed the OER as a function of cell cycle [36]. The OER was higher for cells in S-phase (2.8-2.9) compared to cells in G_2-phase (2.6-2.7) or G_1-phase (2.3-2.4). They concluded that the OER of cells in one cell cycle phase is a purely dose-modifying effect. In asynchronous proliferating cells increased the OER with dosage because of the changing radio-resistance of the cells in different cell cycle phases. The changing OER in this thesis demonstrated that no partly synchronization took place through the hypoxia or the pH shift in the oxic samples. The oxic survival curves fluctuated more than the hypoxic survival curves which is indicated by higher standard deviations (see three paragraphs above). With the most sensitive and the most resistant oxic survival curve as well as the cumulative hypoxic survival curve a minimum OER_{10} of 2.01 and an maximum OER_{10} of 2.84 was calculated.
A comparison of the determined OER values with literature data is presented in table 4.1. The OER for x-rays is in agreement with the values determined in Zölzer and Streffer [151] while Hirayama *et al.* measured a higher OER [56]. The differences may be explained by the used cell lines. In the case of this work as well as in Zölzer and Streffer study tumor cells were used [151] while Hirayama *et al.* worked with normal cells [56]. Furthermore, the irradiation modalities in this work were more similar to Zölzer and Streffer [151] than to Hirayama *et al.* [56]. But concerning the hypoxic gassing Hirayama *et al.* performed their experiments using a comparable set-up [56]. In the itemized literature (see table 4.1) the oxic samples were gassed with air/ 5% CO_2 which was not done in this work. As mentioned above in future experiments the oxic samples will be gassed as well. As expected, OER values obtained in model calculation of the clinical data on prostate cancer patients are lower, as 100% hypoxia will not be reached in tumors or otherwise leads to necrotic tissue.

4.4.2 OER for carbon ion irradiation

The RBE values of carbon ion experiments determined under oxic conditions in the hypoxia chamber can be compared with RBE values determined in culture flasks under the same irradiation conditions. Figure 4.6 presents the comparison. For RAT-1 cells growing on bioFolie 25 the $RBE_{10,\,oxic}$ was 2.5 while the $RBE_{\alpha,\,oxic}$ was 6.0. In figure 4.6 it is shown that the $RBE_{10,\,oxic}$ value fits perfectly to the RBE values determined in culture flasks while the $RBE_{\alpha,\,oxic}$ is higher. The deviation might be due to the fact that the underlying fit parameter α of the survival curves is very sensitive to fluctuations especially

Table 4.1: Comparison of OER values found in literature (Lit) and OER values determined in this work.

Lit	Gassing	Cell line	Irradiation	OER
This work	95% N_2+5% CO_2 /air	RAT-1 tumor, rat	250 kVp x-ray	2.2 ± 0.1
[151]	95% N_2+5% CO_2 /air+5% CO_2, 3 h under hypoxic condition	Be11 tumor, human MeWo tumor, human 4197 tumor, human 4451 tumor, human	240 kVpx-ray	2.1 ± 0.5 2.1 ± 0.3 2.3 ± 0.1 2.5 ± 0.7
[56]	95% N_2+5% CO_2 / air+5% CO_2	CHO normal, hamster	200 kVp x-ray	2.8 ± 0.2
This work	95% N_2+5% CO_2 /air	RAT-1 tumor, rat	carbon ion, $\overline{LET}$ 100 keV/μm	1.5
[40]	95% N_2+5% CO_2 / air+5% CO_2	salivary gland tumor, human V79 normal, hamster	carbon ion, $\overline{LET}$ 100 keV/μm	≈ 2 ≈ 2
[56]	95% N_2+5% CO_2 / air+5% CO_2	CHO normal, hamster	carbon ion, $\overline{LET}$ 80 keV/μm	1.8 ± 0.0
[141]	clinical data, prostate cancer patients, model calculation			1.4 (CI 1.2-1.8)

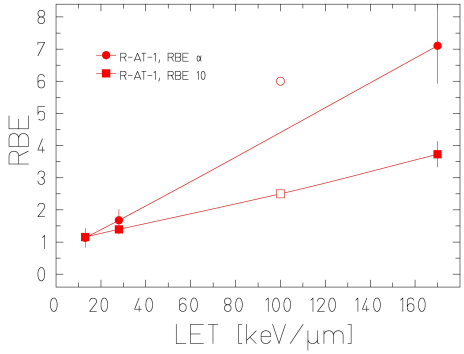

Figure 4.6: RBE_{α} (circle) and RBE_{10} (square) determined with RAT-1 cells in culture flasks (closed symbols) compared with RAT-1 cells on bioFolie 25 in the hypoxia chamber (open symbols) plotted against the LET.

in the case of low statistics like that for survival curves irradiated with carbon ions (oxic: n=2) in the hypoxia chamber. In principle, the measured RBE values indicates that the cell survival rate was not affected through the cell growth on bioFolie 25 and the sample preparation method.

The OER obtained for carbon irradiation with a SOBP and a $\overline{LET}$ of 100 kev/μm was 1.5. This value is compared to literature data in table 3.11 as well. Despite the low statistics of carbon ion experiments performed in hypoxia chamber (oxic: n=2, hypoxic: n=1) the obtained OER value was in agreement with published data. Additional experiments will be performed and determine a more precise value.

4.4.3 Gassing modalities: acute or chronic hypoxia

It was demonstrated that the developed hypoxia chamber is suitable for x-ray and carbon ion irradiation under hypoxic and oxic conditions. The hypoxia was achieved by gassing with 200 ml/min over 2 h with 95% N_2/5% CO_2 as measured with the optical O_2-sensor and the thermal mass flow meter.
The normal oxygen supply in tissue is ranging from atmospheric levels of nearly 21% O_2 (159 mm Hg) to 2-8% O_2 (15-60 mm Hg) [84]. Tumor tissue often is characterized by a partial lower oxygen pressure of $\approx$ 10 mm Hg (1.32% O_2) [14] which causes altered gene expression and radio-resistance [18]. This lower tissue supply occurs when the supporting blood vessel is more than 100-150 μm away from the cells. Studies show that hypoxia is a very dynamic process in tissue. An acute hypoxic status *in vivo* is resolved within 20 min while chronic hypoxia can retain for hours or even days [14]. With this definition the performed experiments were done under chronic hypoxia. To measure cells under acute hypoxia, the chamber has to be deoxygenated, irradiated and reoxygenated within 20 min.

This is technically not possible with the existing chamber and sample ring. It is difficult to evaluate if the hypoxia definitions made *in vivo* should be adapted to *in vitro* experiments. There are publications in which hypoxia is achieved in 1 h [40, 56] but shorter time periods to reach hypoxia through gassing could not be found in scientific literature. To develop new strategies for deoxygenating, the oxygen content in the chamber was calculated. The hypoxia chamber sample ring has a capacity of 1.4 ml medium. The oxygen content in 1.4 ml medium can be calculated with the assumption that the oxygen amount solved in medium is equal to that solved in water. The room temperature is assumed to be 25°C which corresponds to 8 mg/l solved oxygen in water. The molecular weight of O_2 is 32 g/mol. Taken together in 1.4 ml water, respectively medium, **0.35** μ**mol** of oxygen is solved. The oxygen exchange is proceed via the whole surface of the bioFolie 25 (6.3 μmol/cm^{2}h) which is in contact to medium (7.6 cm^2). During the 2 h of gassing an exchange of $\approx$ **95** μ**mol** O_2 is possible. This means that the permeability of bioFolie 25 for oxygen does not limit the time for reaching hypoxia. The deoxygenating process of the medium can be modulated through the gassing as shown under subsection 2.5.3. The higher influx enhances the gas cross-flow along the medium/membrane-interface and ensures a consequently low oxygen level along the membrane-interface. This might have had an influence on the oxygen concentration gradient in the medium. In addition, the oxygen consumption of cells growing on the membrane is important for the rapid decrease of the O_2. Typical O_2 uptake ratio for CHO cells, which were grown for 48 h in culture, were determined to be $1.8 \cdot 10^{-13}$ mol O_2/h·cell [27]. Assuming that one RAT-1 cell has a similar O_2 uptake ratio and that $2x10^5$ RAT-1 cells were grown on the membrane, these cells would consume **0.128** μ**mol** O_2 within 2 h of gassing. It seems that the diffusion of oxygen molecules from deeper medium layers to the medium/membrane-interface define the time for achieving hypoxia conditions. In 1955 Wilke and Chang developed a correlation for diffusion coefficient in liquids [146] which is based on Stockes-Einstein equation.

$$D_{O_2-H_2O} = 7.4 \cdot 10^{-8} \frac{T \cdot (\Psi_{H_2O} \cdot M_{H_2O})^{0.5}}{\eta \cdot V_{O_2}^{0.6}} \tag{4.1}$$

With Eq. 4.1 the diffusion coefficient for oxygen in water $D_{O_2-H_2O}$ [cm^2/s] was calculated to be **2.26** $\cdot 10^{-5}$ **cm^2/s** where T is the absolute temperature [25°C = 298.15 K], Ψ_{H_2O} an association parameter for the solvent water [2.26; [111]], M_{H_2O} the molecular weight of water [18 g/mol], η the viscosity of water [0,8904 cP = g/cm·s·10^{-2}; [143]], and V_{O_2} the molar volume of oxygen [25.6 cm^3/mol; [144]]. During 2 h of gassing an O_2 molecule can diffuse through 0.163 cm^2. This time is the minimum needed for an O_2 molecule to diffuse from the center of the medium layer over the membrane when assuming that the

molecule moves with a directed motion to the membrane caused by the oxygen concentration gradient in the medium. To measure cells under acute hypoxia the amount medium and the amount of O_2 has to be decreased. This is only feasible with reduced thickness of the sample ring from 3 mm to lower values.

4.4.4 Hypoxia chamber: outlook

Beside the gassing procedure there are other steps which need to be optimized. The silicon paste for connecting the foils with the ring is a time consuming method and is not suitable for high sample numbers. Tests with different glues are in progress to simplify the technique, reduce the preparation time, and provide opportunities for the sterilization process. For upcoming research the question of the irradiation of several samples in one chamber is of interest to measure e.g. a complete depth dose profile under hypoxic conditions. With regard to simulating a tumor with its surrounding tissue a chamber will be developed in which samples with different oxygen status can be measured.

The cooperation with Dr. P. Peschke from the DKFZ allows an *in vivo*/*in vitro* comparison of all data. Concerning hypoxia, a direct comparison does not seem to be possible. Halin *et al.* exposed RAT-1 cells in a Billups-Rothberg Inc. chamber over 24 h to a hypoxic gas mixture (1% O_2, 5% CO_2, 94% N_2) and analyzed the status of angiogenetic factors and chemokines afterward. The *in vitro* data were compared to *in vivo* experiments. The authors reported that no major differences between *in vitro* RAT-1 cells under hypoxic or normoxic conditions were detected but the comparison to the *in vivo* data showed large differences to the *in vitro* data. They concluded that the changed expression profile between the RAT-1 tumors and the RAT-1 cells was due to the surrounding tumor host cells [51].

Bibliography

[1] B. Alberts, D. Bray, A. Johnson, J. Lewis, M. Raff, K. Roberts, and P. Walter. *Lehrbuch der Molekularen Zellbiologie, 2. korrigierte Auflage*. Wiley-VCH Verlag GmbH, Weinheim, Germany, 2001.

[2] K. L. Andarawewa, J. Paupert, A. Pal, and M. H. Barcellos-Hoff. New rationales for using TGFbeta inhibitors in radiotherapy. *International Journal of Radiation Biology*, 83(11-12):803–811, Dec. 2007. PMID: 18058368.

[3] V. Anzenberg, S. Chandiramani, and J. A. Coderre. LET-dependent bystander effects caused by irradiation of human prostate carcinoma cells with x rays or alpha particles. *Radiation Research*, 170(4):467–476, Oct. 2008. PMID: 19024654.

[4] ATCC. E-mail communication:. IEC-6 cell line, September 2007.

[5] B. Azzarone, C. Pottin-Clemenceau, P. Krief, E. Rubinstein, C. Jasmin, M. Scudeletti, and F. Indiveri. Are interleukin-2 and interleukin-15 tumor promoting factors for human non-hematopoietic cells? *European Cytokine Network*, 7(1):27–36, Mar. 1996. PMID: 8704093.

[6] M. Balasoiu, A. Turculeanu, C. Avramescu, V. Comanescu, C. Simionescu, and L. Mogoanta. Cytokines levels in prostate adenocarcinomas. *Romanian Journal of Morphology and Embryology = Revue Roumaine De Morphologie Et Embryologie*, 46(3):179–182, 2005. PMID: 16444302.

[7] P. L. Beck, I. M. Rosenberg, R. J. Xavier, T. Koh, J. F. Wong, and D. K. Podolsky. Transforming growth factor-beta mediates intestinal healing and susceptibility to injury in vitro and in vivo through epithelial cells. *The American Journal of Pathology*, 162(2):597–608, Feb. 2003. PMID: 12547717.

[8] Z. Bencokova, M. R. Kaufmann, I. M. Pires, P. S. Lecane, A. J. Giaccia, and E. M. Hammond. ATM activation and signaling under hypoxic conditions. *Molecular and Cellular Biology*, 29(2):526–537, 2009. PMID: 18981219.

[9] S. Bhattacharya, R. M. Ray, and L. R. Johnson. Integrin beta3-mediated src activation regulates apoptosis in IEC-6 cells via akt and STAT3. *The Biochemical Journal*, 397(3):437–447, Aug. 2006. PMID: 16669788.

[10] K. Bühling. *Intensivkurs - Allgemeine und spezielle Pathologie, 3. Auflage*. Urban & Fischer, 2004.

[11] BiochromAG. Telefone communication:. about cell culture serum, 2009.

[12] V. A. Bourke, D. Zhao, J. Gilio, C. Chang, L. Jiang, E. W. Hahn, and R. P. Mason. Correlation of radiation response with tumor oxygenation in the dunning prostate R3327-AT1 tumor. *International Journal of Radiation Oncology, Biology, Physics*, 67(4):1179–1186, Mar. 2007. PMID: 17336219.

[13] S. Brons. Private communication:. alpha/ beta ratio for prostate cancer treatment, 2009.

[14] J. M. Brown. Tumor microenvironment and the response to anticancer therapy. *Cancer Biology & Therapy*, 1(5):453–458, Oct. 2002. PMID: 12496469.

[15] A. Buwe, C. Steinlein, M. R. Koehler, I. Bar-Am, N. Katzin, and M. Schmid. Multicolor spectral karyotyping of rat chromosomes. *Cytogenetic and Genome Research*, 103(1-2):163–168, 2003. PMID: 15004481.

[16] D. J. Carlson, R. D. Stewart, X. A. Li, K. Jennings, J. Z. Wang, and M. Guerrero. Comparison of in vitro and in vivo alpha/beta ratios for prostate cancer. *Physics in Medicine and Biology*, 49(19):4477–4491, Oct. 2004. PMID: 15552412.

[17] C. Cepko, E. Ryder, D. M. Fekete, and S. Bruhn. *Detection of ß-galactosidase and aljaline phosphatase actiities in tissue*, 2009.

[18] N. Chan, M. Milosevic, and R. G. Bristow. Tumor hypoxia, DNA repair and prostate cancer progression: new targets and new therapies. *Future Oncology (London, England)*, 3(3):329–341, June 2007. PMID: 17547528.

[19] A. D. Christ and R. S. Blumberg. The intestinal epithelial cell: immunological aspects. *Springer Seminars in Immunopathology*, 18(4):449–61, 1997. PMID: 9144864.

[20] R. J. Cohen, T. M. Wheeler, H. Bonkhoff, and M. A. Rubin. A proposal on the identification, histologic reporting, and implications of intraductal prostatic carcinoma. *Archives of Pathology & Laboratory Medicine*, 131(7):1103–1109, July 2007. PMID: 17616999.

[21] S. E. Combs, A. Nikoghosyan, O. Jaekel, C. P. Karger, T. Haberer, M. W. Münter, P. E. Huber, J. Debus, and D. Schulz-Ertner. Carbon ion radiotherapy for

pediatric patients and young adults treated for tumors of the skull base. *Cancer*, 115(6):1348–1355, Mar. 2009. PMID: 19156905.

[22] D. B. Cooke, V. E. Quarmby, D. D. Mickey, J. T. Isaacs, and F. S. French. Oncogene expression in prostate cancer: Dunning r3327 rat dorsal prostatic adenocarcinoma system. *The Prostate*, 13(4):263–272, 1988. PMID: 3217275.

[23] H. Corban-Wilhelm, W. E. Hull, G. Becker, U. Bauder-Wüst, D. Greulich, and J. Debus. Cytosine deaminase and thymidine kinase gene therapy in a dunning rat prostate tumour model: absence of bystander effects and characterisation of 5-fluorocytosine metabolism with 19F-NMR spectroscopy. *Gene Therapy*, 9(23):1564–1575, Dec. 2002. PMID: 12424609.

[24] N. Cordes and C. C. Park. ß-1 integrin as a molecular therapeutic target. *International Journal of Radiation Biology*, 83(11-12):753–760, Dec. 2007. PMID: 18058364.

[25] D. Danielpour. Functions and regulation of transforming growth factor-ß in the prostate. *European Journal of Cancer (Oxford, England: 1990)*, 41(6):846–57, Apr. 2005. PMID: 15808954.

[26] D. Danielpour, K. Kadomatsu, M. A. Anzano, J. M. Smith, and M. B. Sporn. Development and characterization of nontumorigenic and tumorigenic epithelial cell lines from rat dorsal-lateral prostate. *Cancer Research*, 54(13):3413–3421, July 1994. PMID: 8012960.

[27] R. R. Deshpande and E. Heinzle. On-line oxygen uptake rate and culture viability measurement of animal cell culture using microplates with integrated oxygen sensors. *Biotechnology Letters*, 26(9):763–767, May 2004. PMID: 15195979.

[28] G. P. Dimri and J. Campisi. Molecular and cell biology of replicative senescence. *Cold Spring Harbor Symposia on Quantitative Biology*, 59:67–73, 1994. PMID: 7587128.

[29] M. Durante, K. George, and F. A. Cucinotta. Chromosomes lacking telomeres are present in the progeny of human lymphocytes exposed to heavy ions. *Radiation Research*, 165(1):51–8, 2006. PMID: 16392962.

[30] R. Eckert, D. Randall, W. Burggren, and K. French. *Tierphysiologie*. George Thieme Verlag Stuttgart, 2002.

[31] T. Elsässer. Private communication:. Local effect model, 2009.

[32] T. Elsässer, M. Krämer, and M. Scholz. Accuracy of the local effect model for the prediction of biologic effects of carbon ion beams in vitro and in vivo. *International Journal of Radiation Oncology, Biology, Physics*, 71(3):866–872, July 2008. PMID: 18430521.

[33] T. Elsässer and M. Scholz. Cluster effects within the local effect model. *Radiation Research*, 167(3):319–29, Mar. 2007. PMID: 17316069.

[34] P. Erbar. *Onkologie, 4. Auflage*. Schattauer Stuttgart, 2002.

[35] C. A. Feghali and T. M. Wright. Cytokines in acute and chronic inflammation. *Frontiers in Bioscience: A Journal and Virtual Library*, 2:d12–26, 1997. PMID: 9159205.

[36] J. P. Freyer, K. Jarrett, S. Carpenter, and M. R. Raju. Oxygen enhancement ratio as a function of dose and cell cycle phase for radiation-resistant and sensitive CHO cells. *Radiation Research*, 127(3):297–307, Sept. 1991. PMID: 1886986.

[37] K. Fu, P. Rui-yun, G. Ya-bing, W. De-wen, L. Qing-liang, D. Bo, and M. Jun-jie. Effect of il-2 on the growth and apoptosis of intestinal epithelial cells radiated by neutron and mechanisms of il-2 on the injured iec-6. *Chinese Journal of Cellular and Molecular Immunology*, 23(8):723–726, Aug. 2007. PMID: 17618564.

[38] K. Fu, R. yun Peng, Y. bing Gao, D. wen Wang, Q. liang Luo, Y. Yang, and B. Dong. An experimental study of the effect of il-2 on the growth of irradiated intestinal epithelial cells. *Chinese Journal of Cellular and Molecular Immunology*, 21(2):250–253, Mar. 2005. PMID: 15766418.

[39] K. Fukutsu, T. Kanai, Y. Furusawa, and K. Ando. Response of mouse intestine after single and fractionated irradiation with accelerated carbon ions with a spread-out bragg peak. *Radiation Research*, 148(2):168–174, Aug. 1997. PMID: 9254736.

[40] Y. Furusawa, K. Fukutsu, M. Aoki, H. Itsukaichi, K. Eguchi-Kasai, H. Ohara, F. Yatagai, T. Kanai, and K. Ando. Inactivation of aerobic and hypoxic cells from three different cell lines by accelerated (3)He-, (12)C- and (20)Ne-ion beams. *Radiation Research*, 154(5):485–496, Nov. 2000. PMID: 11025645.

[41] I. García-Tuñón, M. Ricote, A. Ruiz, B. Fraile, R. Paniagua, and M. Royuela. Interleukin-2 and its receptor complex alpha, beta and gamma chains in in situ and infiltrative human breast cancer: an immunohistochemical comparative study. *Breast Cancer Research: BCR*, 6(1):R1–7, 2004. PMID: 14680494.

[42] M. Gaugler, M. Neunlist, S. Bonnaud, P. Aubert, M. Benderitter, and F. Paris. Intestinal epithelial cell dysfunction is mediated by an endothelial-specific radiation-induced bystander effect. *Radiation Research*, 167(2):185–193, Feb. 2007. PMID: 17390726.

[43] A. A. Geldof, M. A. B. D. Plaizier, I. Duivenvoorden, M. Ringelberg, R. T. Versteegh, D. W. W. Newling, and G. J. J. Teule. Cell cycle perturbations and radiosensitization effects in a human prostate cancer cell line. *Journal of Cancer Research and Clinical Oncology*, 129(3):175–182, Mar. 2003. PMID: 12684891.

[44] E. Giovannucci. Insulin and colon cancer. *Cancer Causes & Control: CCC*, 6(2):164–179, Mar. 1995. PMID: 7749056.

[45] V. C. Gray-Schopfer, S. C. Cheong, H. Chong, J. Chow, T. Moss, Z. A. Abdel-Malek, R. Marais, D. Wynford-Thomas, and D. C. Bennett. Cellular senescence in naevi and immortalisation in melanoma: a role for p16? *British Journal of Cancer*, 95(4):496–505, Aug. 2006. PMID: 16880792.

[46] V. C. Gray-Schopfer, J. K. Soo, and D. C. Bennett. Comment on: Absence of senescence-associated ß-galactosidase activity in human melanocytic nevi in vivo. *J Invest Dermatol*, 128(6):1581, 2008.

[47] A. Grishin, H. Ford, J. Wang, H. Li, V. Salvador-Recatala, E. S. Levitan, and E. Zaks-Makhina. Attenuation of apoptosis in enterocytes by blockade of potassium channels. *American Journal of Physiology. Gastrointestinal and Liver Physiology*, 289(5):G815–821, Nov. 2005. PMID: 16020659.

[48] A. V. Grishin, J. Wang, D. A. Potoka, D. J. Hackam, J. S. Upperman, P. Boyle, R. Zamora, and H. R. Ford. Lipopolysaccharide induces cyclooxygenase-2 in intestinal epithelium via a noncanonical p38 MAPK pathway. *Journal of Immunology (Baltimore, Md.: 1950)*, 176(1):580–588, 2006. PMID: 16365453.

[49] X. Guo, J. N. Rao, L. Liu, T. Zou, D. J. Turner, B. L. Bass, and J. Wang. Regulation of adherens junctions and epithelial paracellular permeability: a novel function for polyamines. *American Journal of Physiology. Cell Physiology*, 285(5):C1174–1187, Nov. 2003. PMID: 12853285.

[50] T. Haberer, W. Becher, D. Schardt, and G. Kraft. Magnetic scanning system for heavy ion therapy. *Nuclear Instruments and Methods*, A330:296–365, 1993.

[51] S. Halin, S. H. Rudolfsson, N. V. Rooijen, and A. Bergh. Extratumoral macrophages promote tumor and vascular growth in an orthotopic rat prostate

tumor model. *Neoplasia (New York, N.Y.)*, 11(2):177–186, Feb. 2009. PMID: 19177202.

[52] E. J. Hall. *Radiobiology for the radiologist, Third Edition*. JB Lippincott Company, Philadelphia, USA, 1988.

[53] S. Hautmann, E. Huland, A. Wullbrand, M. Friedrich, and H. Huland. Treatment of metastatic hormone-refractory prostate adenocarcinoma (MatLyLu) in copenhagen rats with micro-osmotic interleukin-2 pumps. *Anticancer Research*, 20(6B):4495–4498, Dec. 2000. PMID: 11205294.

[54] S. H. Hautmann, E. Huland, and H. Huland. Local intratumor immunotherapy of prostate cancer with interleukin-2 reduces tumor growth. *Anticancer Research*, 19(4A)(4A):2661–3, 1999. PMID: 10470215.

[55] R. Henriksson, A. Widmark, A. Bergh, and J. E. Damber. Interleukin-2-induced growth inhibition of prostatic adenocarcinoma dunning R3327 in rats. *Urological Research*, 20(3):189–91, 1992. PMID: 1615579.

[56] R. Hirayama, Y. Furusawa, T. Fukawa, and K. Ando. Repair kinetics of DNA-DSB induced by x-rays or carbon ions under oxic and hypoxic conditions. *Journal of Radiation Research*, 46(3):325–332, Sept. 2005. PMID: 16210789.

[57] N. M. Hoosein. Neuroendocrine and immune mediators in prostate cancer progression. *Frontiers in Bioscience: A Journal and Virtual Library*, 3:D1274–1279, Dec. 1998. PMID: 9851913.

[58] J. S. Horoszewicz, S. S. Leong, T. M. Chu, Z. L. Wajsman, M. Friedman, L. Papsidero, U. Kim, L. S. Chai, S. Kakati, S. K. Arya, and A. A. Sandberg. The LNCaP cell line–a new model for studies on human prostatic carcinoma. *Progress in Clinical and Biological Research*, 37:115–132, 1980. PMID: 7384082.

[59] C. J. Hunter, V. K. Singamsetty, N. K. Chokshi, P. Boyle, V. Camerini, A. V. Grishin, J. S. Upperman, H. R. Ford, and N. V. Prasadarao. Enterobacter sakazakii enhances epithelial cell injury by inducing apoptosis in a rat model of necrotizing enterocolitis. *The Journal of Infectious Diseases*, 198(4):586–593, Aug. 2008. PMID: 18588483.

[60] S. Huveneers, H. Truong, and H. J. Danen. Integrins: signaling, disease, and therapy. *International Journal of Radiation Biology*, 83(11-12):743–751, Dec. 2007. PMID: 17852562.

[61] IAEA. *Cytogenetic analysis for radiation dose assessment.* International Atomic Energy Agency., a manual tech. rep. 405 edition, 2001.

[62] M. Iizuka, K. Sasaki, Y. Hirai, K. Shindo, S. Konno, H. Itou, S. Ohshima, Y. Horie, and S. Watanabe. Morphogenic protein epimorphin protects intestinal epithelial cells from oxidative stress by the activation of EGF receptor and MEK/ERK, PI3 kinase/Akt signals. *American Journal of Physiology. Gastrointestinal and Liver Physiology*, 292(1):G39–52, 2007. PMID: 16891298.

[63] J. T. Isaacs, W. D. Heston, R. M. Weissman, and D. S. Coffey. Animal models of the hormone-sensitive and -insensitive prostatic adenocarcinomas, dunning R-3327-H, R-3327-HI, and R-3327-AT. *Cancer Research*, 38(11 Pt 2):4353–4359, Nov. 1978. PMID: 698976.

[64] J. T. Isaacs and B. Hukku. Nonrandom involvement of chromosome 4 in the progression of rat prostatic cancer. *The Prostate*, 13(2):165–188, 1988. PMID: 3174494.

[65] J. T. Isaacs, W. B. Isaacs, W. F. Feitz, and J. Scheres. Establishment and characterization of seven dunning rat prostatic cancer cell lines and their use in developing methods for predicting metastatic abilities of prostatic cancers. *The Prostate*, 9(3):261–81, 1986. PMID: 3774632.

[66] H. Ishikawa, H. Tsuji, T. Kamada, N. Hirasawa, T. Yanagi, J. Mizoe, K. Akakura, H. Suzuki, J. Shimazaki, and H. Tsujii. Risk factors of late rectal bleeding after carbon ion therapy for prostate cancer. *International Journal of Radiation Oncology, Biology, Physics*, 66(4):1084–1091, Nov. 2006. PMID: 16979840.

[67] K. Itahana, J. Campisi, and G. P. Dimri. Methods to detect biomarkers of cellular senescence: the senescence-associated ß-galactosidase assay. *Methods in Molecular Biology (Clifton, N.J.)*, 371:21–31, 2007. PMID: 17634571.

[68] C. Janeway, P. Travers, M. Walport, and M. Shlomchik. *Immunologie, 5. Auflage*. Spektrum Akademischer Verlag GmbH, Heidelberg, Germany, 2002.

[69] V. R. Jayanth, M. T. Bayne, and M. E. Varnes. Effects of extracellular and intracellular pH on repair of potentially lethal damage, chromosome aberrations and DNA double-strand breaks in irradiated plateau-phase a549 cells. *Radiation Research*, 139(2):152–162, Aug. 1994. PMID: 8052690.

[70] S. Johansson, M. Landström, K. Hellstrand, and R. Henriksson. The response of dunning R3327 prostatic adenocarcinoma to IL-2, histamine and radiation. *British Journal of Cancer*, 77(8):1213–9, Apr. 1998. PMID: 9579825.

[71] S. Johansson, M. Landström, and R. Henriksson. Alterations of tumour cells, stroma and apoptosis in rat prostatic adenocarcinoma following treatment with histamine, interleukin-2 and irradiation. *Anticancer Research*, 19(3A):1961–1969, June 1999. PMID: 10470141.

[72] M. E. Kaighn, K. S. Narayan, Y. Ohnuki, J. F. Lechner, and L. W. Jones. Establishment and characterization of a human prostatic carcinoma cell line (PC-3). *Investigative Urology*, 17(1):16–23, July 1979. PMID: 447482.

[73] K. Kimura, C. Bowen, S. Spiegel, and E. P. Gelmann. Tumor necrosis factor-alpha sensitizes prostate cancer cells to gamma-irradiation-induced apoptosis. *Cancer Research*, 59(7):1606–1614, Apr. 1999. PMID: 10197636.

[74] K. Kitagawa and Y. Niikura. Caspase-independent mitotic death (CIMD). *Cell Cycle (Georgetown, Tex.)*, 7(8):1001–1005, Apr. 2008. PMID: 18414023.

[75] T. C. Ko, W. Yu, T. Sakai, H. Sheng, J. Shao, R. D. Beauchamp, and E. A. Thompson. TGF-beta1 effects on proliferation of rat intestinal epithelial cells are due to inhibition of cyclin d1 expression. *Oncogene*, 16(26):3445–3454, July 1998. PMID: 9692552.

[76] G. Kraft, H. Daues, B. Fischer, U. Kopf, H. Leibold, D. Quis, H. Stelzer, J. Kiefer, R. Schoepper, E. Schneider, U. Weber, H. Wulf, and H. Dertinger. Irradiation chamber and sample changes for biological samples. *Nuclear Instruments and Methods*, 168:175–179, 1980.

[77] A. Krempler, D. Deckbar, P. A. Jeggo, and M. Löbrich. An imperfect G2M checkpoint contributes to chromosome instability following irradiation of S and G2 phase cells. *Cell Cycle (Georgetown, Tex.)*, 6(14):1682–1686, July 2007. PMID: 17637566.

[78] M. Krämer, O. Jäkel, T. Haberer, G. Kraft, D. Schardt, and U. Weber. Treatment planning for heavy-ion radiotherapy: physical beam model and dose optimization. *Physics in Medicine and Biology*, 45(11):3299–317, Nov. 2000. PMID: 11098905.

[79] D. J. Kuhn and Q. P. Dou. The role of interleukin-2 receptor alpha in cancer. *Frontiers in Bioscience: A Journal and Virtual Library*, 10:1462–74, 2005. PMID: 15769637.

[80] D. J. Kurz, S. Decary, Y. Hong, and J. D. Erusalimsky. Senescence-associated (beta)-galactosidase reflects an increase in lysosomal mass during replicative ageing of human endothelial cells. *Journal of Cell Science*, 113 (Pt 20):3613–3622, Oct. 2000. PMID: 11017877.

[81] M. Löbrich and P. A. Jeggo. The impact of a negligent G2/M checkpoint on genomic instability and cancer induction. *Nature Reviews. Cancer*, 7(11):861–869, Nov. 2007. PMID: 17943134.

[82] B. Y. Lee, J. A. Han, J. S. Im, A. Morrone, K. Johung, E. C. Goodwin, W. J. Kleijer, D. DiMaio, and E. S. Hwang. Senescence-associated beta-galactosidase is lysosomal beta-galactosidase. *Aging Cell*, 5(2):187–195, Apr. 2006. PMID: 16626397.

[83] C. Lee, S. M. Sintich, E. P. Mathews, A. H. Shah, S. D. Kundu, K. T. Perry, J. S. Cho, K. Y. Ilio, M. V. Cronauer, L. Janulis, and J. A. Sensibar. Transforming growth factor-beta in benign and malignant prostate. *The Prostate*, 39(4):285–90, June 1999. PMID: 10344218.

[84] A. S. E. Ljungkvist, J. Bussink, J. H. A. M. Kaanders, and A. J. van der Kogel. Dynamics of tumor hypoxia measured with bioreductive hypoxic cell markers. *Radiation Research*, 167(2):127–145, Feb. 2007. PMID: 17390721.

[85] R. Lüllmann-Rauch. *Histologie*. Thieme Verlag Stuttgart, 2003.

[86] A. Luch. Cell cycle control and cell division: implications for chemically induced carcinogenesis. *Chembiochem: A European Journal of Chemical Biology*, 3(6):506–516, June 2002. PMID: 12325006.

[87] S. Lyu and W. Park. Mistletoe lectin modulates intestinal epithelial cell-derived cytokines and b cell IgA secretion. *Archives of Pharmacal Research*, 32(3):443–451, Mar. 2009. PMID: 19387590.

[88] B. S. Marasa, L. Xiao, J. N. Rao, T. Zou, L. Liu, J. Wang, E. Bellavance, D. J. Turner, and J. Wang. Induced TRPC1 expression increases protein phosphatase 2A sensitizing intestinal epithelial cells to apoptosis through inhibition of NF-kappaB activation. *American Journal of Physiology. Cell Physiology*, 294(5):C1277–1287, May 2008. PMID: 18322138.

[89] L. Marignol, M. Coffey, M. Lawler, and D. Hollywood. Hypoxia in prostate cancer: a powerful shield against tumour destruction? *Cancer Treatment Reviews*, 34(4):313–27, June 2008. PMID: 18334284.

[90] D. W. McGee, T. Bamberg, S. J. Vitkus, and J. R. McGhee. A synergistic relationship between TNF-alpha, IL-1 beta, and TGF-beta 1 on IL-6 secretion by the IEC-6 intestinal epithelial cell line. *Immunology*, 86(1):6–11, Sept. 1995. PMID: 7590883.

[91] J. E. McNeal. The zonal anatomy of the prostate. *The Prostate*, 2(1):35–49, 1981. PMID: 7279811.

[92] C. Michaloglou, M. S. Soengas, W. J. Mooi, and D. S. Peeper. Comment on "Absence of senescence-associated beta-galactosidase activity in human melanocytic nevi in vivo". *The Journal of Investigative Dermatology*, 128(6):1582–1583; author reply 1583–1584, June 2008. PMID: 18478016.

[93] T. R. Munro. The relative radiosensitivity of the nucleus and cytoplasm of chinese hamster fibroblasts. *Radiation Research*, 42(3):451–70, June 1970. PMID: 5463516.

[94] E. Musgrove, M. Seaman, and D. Hedley. Relationship between cytoplasmic pH and proliferation during exponential growth and cellular quiescence. *Experimental Cell Research*, 172(1):65–75, Sept. 1987. PMID: 3653258.

[95] A. E. Nahum, B. Movsas, E. M. Horwitz, C. C. Stobbe, and J. D. Chapman. Incorporating clinical measurements of hypoxia into tumor local control modeling of prostate cancer: implications for the alpha/beta ratio. *International Journal of Radiation Oncology, Biology, Physics*, 57(2):391–401, Oct. 2003. PMID: 12957250.

[96] R. Négrel, P. Rampal, J. L. Nano, C. Cavenel, and G. Ailhaud. Establishment and characterization of an epithelial intestinal cell line from rat fetus. *Experimental Cell Research*, 143(2):427–437, Feb. 1983. PMID: 6131830.

[97] A. Nikoghosyan, D. Schulz-Ertner, B. Didinger, O. Jäkel, I. Zuna, A. Höss, M. Wannenmacher, and J. Debus. Evaluation of therapeutic potential of heavy ion therapy for patients with locally advanced prostate cancer. *International Journal of Radiation Oncology, Biology, Physics*, 58(1):89–97, 2004. PMID: 14697425.

[98] D. Padua and J. Massagué. Roles of TGFbeta in metastasis. *Cell Research*, 19(1):89–102, 2009. PMID: 19050696.

[99] A. R. Patel, J. Li, B. L. Bass, and J. Y. Wang. Expression of the transforming growth factor-beta gene during growth inhibition following polyamine depletion. *The American Journal of Physiology*, 275(2 Pt 1):C590–598, Aug. 1998. PMID: 9688614.

[100] P. Peschke. Private communication:. Dunning prostate carcinoma cell system, 2009.

[101] P. Peschke, S. Heimburg, G. Wolber, I. Zuna, and E. W. Hahn. Improved therapeutic response by distinct timing of multiple heat treatments during interstitial radiation in the dunning R3327 prostate tumor model. *Journal of Cancer Research and Clinical Oncology*, 124(3-4):172–178, 1998. PMID: 9619743.

[102] D. K. Podolsky. Review article: healing after inflammatory injury–coordination of a regulatory peptide network. *Alimentary Pharmacology & Therapeutics*, 14 Suppl 1:87–93, Apr. 2000. PMID: 10807409.

[103] K. M. Prise and J. M. O'Sullivan. Radiation-induced bystander signalling in cancer therapy. *Nature Reviews. Cancer*, 9(5):351–360, May 2009. PMID: 19377507.

[104] T. T. Puck and P. I. Marcus. A rapid method for viable cell titration and clone production with hela cells in tissue culture: The use of x-irradiated cells to supply conditioning factors. *Proceedings of the National Academy of Sciences of the United States of America*, 41(7):432–7, July 1955. PMID: 16589695.

[105] A. Quaroni and K. J. Isselbacher. Cytotoxic effects and metabolism of benzo[a]pyrene and 7,12-dimethylbenz[a]anthracene in duodenal and ileal epithelial cell cultures. *Journal of the National Cancer Institute*, 67(6):1353–1362, Dec. 1981. PMID: 6273638.

[106] A. Quaroni, J. Wands, R. L. Trelstad, and K. J. Isselbacher. Epithelioid cell cultures from rat small intestine. Characterization by morphologic and immunologic criteria. *The Journal of Cell Biology*, 80(2):248–65, Feb. 1979. PMID: 88453.

[107] M. M. Rahman and G. McFadden. Modulation of tumor necrosis factor by microbial pathogens. *PLoS Pathogens*, 2(2):e4, Feb. 2006. PMID: 16518473.

[108] J. N. Rao, O. Platoshyn, L. Li, X. Guo, V. A. Golovina, J. X. Yuan, and J. Wang. Activation of K(+) channels and increased migration of differentiated intestinal epithelial cells after wounding. *American Journal of Physiology. Cell Physiology*, 282(4):C885–898, Apr. 2002. PMID: 11880277.

[109] N. N. Raveendran, K. Silver, L. C. Freeman, D. Narvaez, K. Weng, S. Ganta, and J. D. Lillich. Drug-induced alterations to gene and protein expression in intestinal epithelial cell 6 cells suggest a role for calpains in the gastrointestinal toxicity of nonsteroidal anti-inflammatory agents. *The Journal of Pharmacology and Experimental Therapeutics*, 325(2):389–399, May 2008. PMID: 18281595.

[110] T. E. Reichert, S. Nagashima, Y. Kashii, J. Stanson, G. Gao, Q. P. Dou, and T. L. Whiteside. Interleukin-2 expression in human carcinoma cell lines and its role in cell cycle progression. *Oncogene*, 19(4):514–525, 2000. PMID: 10698521.

[111] R. Reid, J. Praunsnitz, and T. Sherwood. *The Properties of Gases and Liquieds, Third Edition*. McGraw-Hill, New York, 1977.

[112] A. R. Reynolds and N. Kyprianou. Growth factor signalling in prostatic growth: significance in tumour development and therapeutic targeting. *British Journal of Pharmacology*, 147 Suppl 2:S144–52, Feb. 2006. PMID: 16465179.

[113] V. Rohde, A. Katalinic, and J. Wasern. *Gesundheitsberichtserstattung des Bundes "Prostataerkrankungen", Heft 36*. Robert Koch-Institut, 2007.

[114] M. Royuela, M. P. D. Miguel, F. R. Bethencourt, B. Fraile, M. I. Arenas, and R. Paniagua. IL-2, its receptors, and bcl-2 and bax genes in normal, hyperplastic and carcinomatous human prostates: immunohistochemical comparative analysis. *Growth Factors (Chur, Switzerland)*, 18(2):135–146, 2000. PMID: 11019784.

[115] M. Royuela, G. Rodríguez-Berriguete, B. Fraile, and R. Paniagua. TNF-alpha/IL-1/NF-kappaB transduction pathway in human cancer prostate. *Histology and Histopathology*, 23(10):1279–90, Oct. 2008. PMID: 18712680.

[116] Y. Sambuy and I. D. Angelis. Formation of organoid structures and extracellular matrix production in an intestinal epithelial cell line during long-term in vitro culture. *Cell Differentiation*, 19(2):139–147, Sept. 1986. PMID: 3757038.

[117] C. Schicker. Entwicklung eines Systems zur Simulation hypoxischer Tumore für die Bestrahlungsplanung mit variabler biologischer Wirksamkeit. Master's thesis, Hochschule Darmstadt, Fachbereich Chemie- und Biotechnologie, 2007.

[118] C. Schicker, C. von Neubeck, U. Kopf, and W. Kraft-Weyrather. Patent: De 10 2008 010 918.5, Zellkultur-Bestrahlungskammer, 2008.

[119] C. Schicker, C. von Neubeck, U. Kopf, and W. Kraft-Weyrather. Patent: Ep 09 002 402.7, Zellkultur-Bestrahlungskammer, 2009.

[120] M. Scholz, A. M. Kellerer, W. Kraft-Weyrather, and G. Kraft. Computation of cell survival in heavy ion beams for therapy. the model and its approximation. *Radiation and Environmental Biophysics*, 36(1):59–66, Feb. 1997. PMID: 9128899.

[121] B. W. Schuller, A. B. Rogers, K. S. Cormier, K. J. Riley, P. J. Binns, R. Julius, M. F. Hawthorne, and J. A. Coderre. No significant endothelial apoptosis in the radiation-induced gastrointestinal syndrome. *International Journal of Radiation Oncology, Biology, Physics*, 68(1):205–210, May 2007. PMID: 17448874.

[122] D. Schulz-Ertner, C. P. Karger, A. Feuerhake, A. Nikoghosyan, S. E. Combs, O. Jäkel, L. Edler, M. Scholz, and J. Debus. Effectiveness of carbon ion radiotherapy in the treatment of skull-base chordomas. *International Journal of Radiation Oncology, Biology, Physics*, 68(2):449–457, June 2007. PMID: 17363188.

[123] D. Schulz-Ertner, A. Nikoghosyan, H. Hof, B. Didinger, S. E. Combs, O. Jäkel, C. P. Karger, L. Edler, and J. Debus. Carbon ion radiotherapy of skull base chondrosarcomas. *International Journal of Radiation Oncology, Biology, Physics*, 67(1):171–177, 2007. PMID: 17056193.

[124] C. Shao, M. Aoki, and Y. Furusawa. Medium-mediated bystander effects on HSG cells co-cultivated with cells irradiated by x-rays or a 290 MeV/u carbon beam. *Journal of Radiation Research*, 42(3):305–316, Sept. 2001. PMID: 11840647.

[125] M. W. Shaw, P. D. Guinan, A. Dubin, C. F. McKiel, and M. Rubenstein. Administration of recombinant tumor necrosis factor to rats bearing the dunning r3327 MAT-LyLu prostatic adenocarcinoma. *Clinical Physiology and Biochemistry*, 5(6):315–319, 1987. PMID: 3446431.

[126] T. Shigematsu, S. Miura, M. Hirokawa, R. Hokari, H. Higuchi, N. Watanabe, Y. Tsuzuki, H. Kimura, S. Tada, R. C. Nakatsumi, H. Saito, and H. Ishii. Induction of endothelin-1 synthesis by IL-2 and its modulation of rat intestinal epithelial cell growth. *The American Journal of Physiology*, 275(3 Pt 1):G556–563, Sept. 1998. PMID: 9724269.

[127] D. H. Smith and J. J. DeCosse. Radiation damage to the small intestine. *World Journal of Surgery*, 10(2):189–94, Apr. 1986. PMID: 3705603.

[128] K. Song, S. C. Cornelius, and D. Danielpour. Development and characterization of DP-153, a nontumorigenic prostatic cell line that undergoes malignant transformation by expression of dominant-negative transforming growth factor beta receptor type II. *Cancer Research*, 63(15):4358–4367, Aug. 2003. PMID: 12907605.

[129] A. W. Stadnyk, G. R. Sisson, and C. C. Waterhouse. IL-1 alpha is constitutively expressed in the rat intestinal epithelial cell line IEC-6. *Experimental Cell Research*, 220(2):298–303, Oct. 1995. PMID: 7556437.

[130] K. R. Stone, D. D. Mickey, H. Wunderli, G. H. Mickey, and D. F. Paulson. Isolation of a human prostate carcinoma cell line (DU 145). *International Journal of Cancer. Journal International Du Cancer*, 21(3):274–281, Mar. 1978. PMID: 631930.

[131] J. L. Tatum, G. J. Kelloff, R. J. Gillies, J. M. Arbeit, J. M. Brown, K. S. C. Chao, J. D. Chapman, W. C. Eckelman, A. W. Fyles, A. J. Giaccia, R. P. Hill, C. J. Koch, M. C. Krishna, K. A. Krohn, J. S. Lewis, R. P. Mason, G. Melillo, A. R. Padhani, G. Powis, J. G. Rajendran, R. Reba, S. P. Robinson, G. L. Semenza, H. M. Swartz, P. Vaupel, D. Yang, B. Croft, J. Hoffman, G. Liu, H. Stone, and D. Sullivan. Hypoxia: importance in tumor biology, noninvasive measurement by imaging, and value of its measurement in the management of cancer therapy. *International Journal of Radiation Biology*, 82(10):699–757, Oct. 2006. PMID: 17118889.

[132] C. Thomas and P. S. Oates. IEC-6 cells are an appropriate model of intestinal iron absorption in rats. *The Journal of Nutrition*, 132(4):680–687, Apr. 2002. PMID: 11925460.

[133] D. C. Tomlinson, S. H. Freestone, O. C. Grace, and A. A. Thomson. Differential effects of transforming growth factor-beta1 on cellular proliferation in the developing prostate. *Endocrinology*, 145(9):4292–300, Sept. 2004. PMID: 15192047.

[134] H. Tsujii, T. Kamada, M. Baba, H. Tsuji, H. Kato, S. Kato, S. Yamada, S. Yasuda, T. Yanagi, H. Kato, R. Hara, Naotakayamamoto, and J. Mizoe. Clinical advantages of carbon-ion radiotherapy. *New Journal of Physics*, 10:075009(16pp), 2008.

[135] R. J. van Moorselaar, B. T. Hendriks, P. van Stratum, P. H. van der Meide, F. M. Debruyne, and J. A. Schalken. Synergistic antitumor effects of rat gamma-interferon and human tumor necrosis factor alpha against androgen-dependent and -independent rat prostatic tumors. *Cancer Research*, 51(9):2329–2334, May 1991. PMID: 1901759.

[136] C. von Neubeck and T. Friedrich. Report on error calculation. Technical report, GSI, 2009.

[137] M. Wakatsuki, H. Tsuji, H. Ishikawa, T. Yanagi, T. Kamada, T. Nakano, H. Suzuki, K. Akakura, J. Shimazaki, and H. Tsujii. Quality of life in men treated with carbon ion therapy for prostate cancer. *International Journal of Radiation Oncology, Biology, Physics*, 72(4):1010–1015, Nov. 2008. PMID: 18495370.

[138] M. F. Walsh, D. R. Ampasala, J. Hatfield, R. V. Heide, S. Suer, A. K. Rishi, and M. D. Basson. Transforming growth factor-beta stimulates intestinal epithelial focal adhesion kinase synthesis via smad- and p38-dependent mechanisms. *The American Journal of Pathology*, 173(2):385–399, Aug. 2008. PMID: 18583311.

[139] J. Y. Wang, S. A. McCormack, M. J. Viar, H. Wang, C. Y. Tzen, R. E. Scott, and L. R. Johnson. Decreased expression of protooncogenes c-fos, c-myc, and c-jun following polyamine depletion in IEC-6 cells. *The American Journal of Physiology*, 265(2 Pt 1):G331–338, Aug. 1993. PMID: 8368314.

[140] J. Z. Wang, M. Guerrero, and X. A. Li. How low is the alpha/beta ratio for prostate cancer? *International Journal of Radiation Oncology, Biology, Physics*, 55(1):194–203, 2003. PMID: 12504054.

[141] J. Z. Wang, X. A. Li, and N. A. Mayr. Dose escalation to combat hypoxia in prostate cancer: a radiobiological study on clinical data. *The British Journal of Radiology*, 79(947):905–911, Nov. 2006. PMID: 16885177.

[142] R. Wang and J. A. Coderre. A bystander effect in alpha-particle irradiations of human prostate tumor cells. *Radiation Research*, 164(6):711–722, Dec. 2005. PMID: 16296877.

[143] R. C. Weast, editor. *Handbook of Chemistry and Physics 54th Edition*. CRC Press, 1973.

[144] J. Welty, C. Wicks, and R. Wilson. *Fundamentals of Momentum, Heat, and Mass Transfer, Third Edition*. John Wiley & Sons, New York, 1984.

[145] P. Wikström, G. Lindh, A. Bergh, and J. E. Damber. Alterations of transforming growth factor beta1 and TGFbeta receptor expressions with progression in dunning rat prostatic adenocarcinoma sublines. *Urological Research*, 27(3):185–93, June 1999. PMID: 10422820.

[146] C. Wilke and P. Chang. *A.E.CH.E. Journal*, 1:264–270, 1955.

[147] R. Wróblewski, M. Jalnäs, G. V. Decker, J. Björk, J. Wroblewski, and G. M. Roomans. Effects of irradiation on intestinal cells in vivo and in vitro. *Histology and Histopathology*, 17(1):165–77, 2002. PMID: 11813866.

[148] K. Yamazaki, J. E. Lehr, J. S. Rhim, and K. J. Pienta. Establishment of immortalized copenhagen rat prostate endothelial cell lines. *In Vivo (Athens, Greece)*, 9(5):421–426, Oct. 1995. PMID: 8900918.

[149] K. Zachrisson, V. Neopikhanov, A. Samali, and A. Uribe. Interleukin-1, interleukin-8, tumour necrosis factor alpha and interferon gamma stimulate DNA synthesis but have no effect on apoptosis in small-intestinal cell lines. *European Journal of Gastroenterology & Hepatology*, 13(5):551–9, May 2001. PMID: 11396536.

[150] C. M. Zechmann, E. C. Woenne, G. Brix, N. Radzwill, M. Ilg, P. Bachert, P. Peschke, S. Kirsch, H. Kauczor, S. Delorme, W. Semmler, and F. Kiessling. Impact of stroma on the growth, microcirculation, and metabolism of experimental prostate tumors. *Neoplasia (New York, N.Y.)*, 9(1):57–67, 2007. PMID: 17325744.

[151] F. Zölzer and C. Streffer. Increased radiosensitivity with chronic hypoxia in four human tumor cell lines. *International Journal of Radiation Oncology, Biology, Physics*, 54(3):910–920, Nov. 2002. PMID: 12377345.

Acknowledgement

First, let me thank Prof. Dr. Gerhard Kraft and Prof. Dr. Gerhard Thiel who offered me the possibility for this work.
I thank Dr. Wilma K.-Weyrather for her mentoring throughout the entire doctorate and my time at GSI. She also assisted me with this doctorate with her advice as well as her actions.
I would like to express my sincere appreciation to all current and former members of the biophysics group who have contributed, directly or indirectly, to this doctorate in form of technical or other support (in alphabetic order): Daniela Becker (☺), Wolfgang Becher (technical support at UNILAC facility), Dr. Sandro Conrad (May I have one? ELISA instructor), Anna Constantinescu (Try it with 200, RT, water + five in line.), Prof. Dr. Marco Durante (Discussions: I call it freak of nature!), Dr. Thilo Elsässer (LEM calculations, beam time support at SIS facility, What do you think about... ?), Dr. Claudia Fournier (Let's talk about cytokines!), Dr. Thomas Friedrich (Must be this term! I think, I'm sure.), Eva Gehrmann (4 h?! Not bad! 15,000 in total?! Respect!), Dr. Alexander Gemmel (Should be possible to move it... Did you lost some?), Carola Hartel (Silver! May I have this recipe?), Petra Hessel (chromosomes and cocktails), Dr. Gheorghe Iancu (nightly beam time friend), Kerstin Knoop (MikTex Instructor 1), Gabriele Kragl (experimental support, wall painting), Dr. Michael Krämer (the real dude, TRiP plans), Dr. Ryonfa Lee (a negative result and grammar book), Günter Lenz (technical support at UNILAC facility and with gas bottles. Do you think that you can produce it by means of my "drawing"?!), Janina Lindemann (Final destination?), Eva Kehr (technical support in cell lab and experiments, pasta salad), Barbara Meyer (It's raining... natch!) Dr. Sylvia Ritter (chromosome world), Priv. Doz. Dr. Michael Scholz (LEM calculations, beam time support at SIS facility. Knock, knock, just some questions...), Jörn Spliter (Tomorrow - half past seven? Ey, today... here we go again!), Frank Tobias (MikTex Instructor 2), Dr. Jana Topsch (flow cytometer instructor, tea and chocolate donor).
In addition, I would like to thank my parents who consistently supported me during my years of study. They made this work possible.
Finally, I also want to thank my family and friends for their encouragement, proofreading, understanding, and patience during this work.

Eidesstattliche Erklärung

Ich erkläre hiermit an Eides Statt, dass ich die vorliegende Dissertation selbständig und nur mit den angegebenen Hilfsmitteln angefertigt habe.

Hierdurch erkläre ich an Eides Statt, dass ich bisher noch keinen Promotionsversuch unternommen habe.

Darmstadt, November 17, 2009 .....

Cläre Hanna Freiin von Neubeck

Annex

Used solutions

Soerensen buffer

- 0.067 M Na_2HPO_4 in purified water (Merck KGaA, Darmstadt, Germany)
- 0.067 M KH_2PO_4 in purified water (Merck KGaA, Darmstadt, Germany)
- mix in equal volumes
- pH 6.8

threefold methylene blue

- 300 ml Löfflers methylene blue solution (Merck KGaA, Darmstadt, Germany)
- 90 ml 0.1% potassium hydroxide in purified water
- 50 ml methanol for analysis (Merck KGaA, Darmstadt, Germany)
- 560 ml purified water

Gal buffer

- 40 mM Na_2HPO_4 x 12 H_2O
- 40 mM $C_6H_8O_7$ x H_2O
- dissolve in 1 l purified water
- adjust pH with NaOH to 6.0
- add
- 5 mM $K_3[Fe(CN)_6]$
- 5 mM $K_4[Fe(CN)_6]$
- 150 mM NaCl
- 2 mM $MgCl_2$ x 6 H_2O

X-Gal staining solution

- 5 mg X-Gal (5-bromo-4-chloro-3-indolyl-β-D-galactoside)
- 280 μl C_3H_7NO
- 720 μl X-Gal buffer
- dilute before use to 1 mg X-Gal with X-Gal buffer

List of Figures

List of Tables

List of Abbreviations

β-gal	β-galactosidase
$\overline{LET}$	dose-averaged LET
ATCC	American Tissue Culture Collection
DAPI	4',6-diamidino-2-phenylindole
DMEM	Dulbecco's modified Eagle medium
DMSO	Dimethyl sulfoxide
DNA	Deoxyribonucleic acid
EDTA	Ethylenediaminetetraacetic acid
ELISA	Enzyme-Linked ImmunoSorbent Assay
Eq.	Equation
FCS	Fetal Calf Serum
I	Inoculum
IEC-6	Intestinal Epithelial Cell line 6
IL-2	Interleukin 2
IMRT	Intensity Modulated Radiotherapy
KCl	Potassium chloride
LET	Linear Energy Transfer
method P	Co-culture set-up at which the cells were **P**re-seeded before the irradiation
method T	Co-culture set-up at which the cells were **T**rypsinized after irradiation
mFISH	Multicolor fluorescence in situ hybridization
MI	Mitotic index
N_C	Colony number/ culture flask which should grow in a colony forming assay
N_{ml}	Cell number/ ml in cell suspension
N_R	Average of resulting colony number/ sample
OER	Oxygen Enhancement Ratio
PBS^-	Phosphate Buffered Saline without calcium and magnesium ions
PE	Plating Efficiency

PE_{co} ..... Co-culture PE in co-culture experiments

PE_{mono} ..... Mono-culture PE in co-culture experiments

PFA ..... Paraformaldehyde

RAT-1 ..... Dunning R-3327-AT-1 cell line

RBE ..... Relative Biological Effectiveness

RPMI ..... Roswell Park Memorial Institute medium

S ..... Survival

SIS ..... Heavy ion synchrotron

SOBP ..... Spread Out Bragg Peak

TGFβ ..... Transforming growth factor β

TNFα ..... Tumor necrosis factor α

UNILAC ..... Universal Ion Linear Accelerator

WCN ..... Weighted chromosome number

X-Gal 5-bromo-4-chloro-3-indolyl-β-D-galactoside